VANÚCIA SCHUMACHER POGORZELSKI

CLIMATE AND MODELING GLACIER IN THE COMPLEX TERRAIN OF CHILEAN ANDES

Thesis submitted to the Applied Meteorology Graduate Program of the Universidade Federal de Viçosa in partial fulfillment of the requirements for the degree of *Doctor Scientiae*.

Advisor: Flávio Barbosa Justino

Co-advisor: Alfonso Andrés Fernández Rivera

VIÇOSA - MINAS GERAIS
2019

Ficha catalográfica preparada pela Biblioteca Central da Universidade Federal de Viçosa - Câmpus Viçosa

T
P746c
2019

Pogorzelski, Vanúcia Schumacher, 1985-
Climate and modeling glacier in the complex terrain of Chilean Andes / Vanúcia Schumacher Pogorzelski. – Viçosa, MG, 2019.
144 f. : il. (algumas color.) ; 29 cm.

Orientador: Flávio Barbosa Justino.
Tese (doutorado) - Universidade Federal de Viçosa.
Inclui bibliografia.

1. Geleiras - Andes,Cordilheira dos, Região. 2. Precipitação (Meteorologia) - Previsão. 3. Aquecimento global - Chile. I. Universidade Federal de Viçosa. Departamento de Engenharia Agrícola. Programa de Pós-Graduação em Meteorologia Aplicada. II. Título.

CDD 22. ed. 630.2515

VANÚCIA SCHUMACHER POGORZELSKI

CLIMATE AND MODELING GLACIER IN THE COMPLEX TERRAIN OF CHILEAN ANDES

Thesis submitted to the Applied Meteorology Graduate Program of the Universidade Federal de Viçosa in partial fulfillment of the requirements for the degree of *Doctor Scientiae*.

APPROVED: August 30, 2019.

Vanúcia Schumacher Pogorzelski
Author

Flávio Barbosa Justino
Adviser

Selma (in memoriam).

ACKNOWLEDGEMENTS

This PhD study was financed in part by the Coordenação de Aperfeitçoamento de Pessoal de Nível Superior - Brazil (CAPES) - Finance Code 001. I would like to thank to the Universidade Federal de Viçosa and the Agricultural Engineering Department for the support to conduct my research.

I am very grateful for the support and motivation throughout this research for my advisors, Dr. Flávio Justino and Dr. Alfonso Fernández. For friendship, patience, availability for questions and for all learning shared during this trajectory. Thank you very much!

I also want to acknowledge the Department of Geography and Mountain GeoScience Group from Universidad de Concepción in Chile, for welcoming me very well for three months. I appreciate the opportunity to participate in the fieldwork at the Universidad Glacier. It was one of the most amazing experiences I have had during these almost 10 years of science research.

I appreciate the support of the Diretoria de Tecnologia da Informação (DTI-UFV) for the availability of running the WRF model on the supercomputer.

I would like to thank the NCAR Command Language (NCL) support team, especially Dennis Shea, Mary Haley, David Allured, Adam Phillips, and Rick Brownrigg for collaboration and attention to all my questions about NCL.

I would like to say many thanks to all team of the Research Group in Ocean-Atmosphere-Biosphere-Criosphere, Alex, Noele, Alcimoni, Rafael, Gurjão, Álvaro, Cristian, Gabriela, and Paola. We support each other when we have challenges in the researcher's life! I will miss our barbecues and political talk.

To Graça Freitas, secretary of the Post-Graduate Program in Applied Meteorology, for friendship, availability and all help anytime.

To all who directly or indirectly contributed to the accomplishment of this research.

I want to thank the constant support of my family, even with the distance they always encouraged me.

And in these final words, not least, I want to thank my husband Denison and son Kurt. My sincere thanks for your patience all these years, all the help, for believing in my ability and motivating me not to give up. I cannot complete my PhD work without their support.

To you my son, I dedicate all the learning I had opportunity to build. The best legacy I can leave to you is the motivation for the pursuit of knowledge!

ABSTRACT

POGORZELSKI, Vanúcia Schumacher, D. Sc., Universidade Federal de Viçosa, August, 2019. **Climate and modeling glacier in the complex terrain of Chilean Andes**. Advisor: Flávio Barbosa Justino. Co-advisor: Alfonso Andrés Fernández Rivera.

Glacier fluctuations are an important source of water for the semi-arid in Central of Chile, especially during the dry season, ensuring the resources related to hydropower, agriculture, industry, tourism and mainly for domestic consumption. However, the retraction of Andean glaciers caused by local climate variability and global warming may impact future water resources. Glacier changes might also affect the economic growth and development of large cities in Chile as well as livelihoods of local communities living in the Andean mountains. With ongoing global climate change, water resources are vulnerable and should lead to mass migrations in the near future. Additionally, there are many gaps in the understanding of the Andean climate and glaciers, specially in terms of mass balance. In particular, the Andes of Chile have received little attention due to scarcity of surface stations to allow climate research in this region. The main objective of this study is to analyze main characteristics associated with precipitation and temperature along Chile, and application of a glacier mass balance model in the complex terrain of Chilean Andes employing high resolution modeling. There is a significant reduction of precipitation and warming trends in the high Chilean Andes, especially in Central Chile during the winter season, as well as an increase of the consecutive number of dry days. In addition, we simulated a mass loss of -82 cm w.e.yr^{-1} averaged between 1996 and 2015 over the Universidad Glacier, in Central Andes, with a negative trend of -2.2 cm w.e.yr^{-1}. The interannual variability is controlled mainly by summer melt. The sublimation accounts about 10% of ablation while evaporation is a smaller component, corresponding to 6%. Furthermore, the high-resolution simulations of glacier mass balance developed in this study will be support future analyses of these glaciers at unprecedented detail, providing

a deeper understanding of climate-glacier feedback, and provide new insights into glaciers mass balance in the Central Andes.

Keywords: Glaciers in Central Andes. WRF. Precipitation and Temperature.

RESUMO

POGORZELSKI, Vanúcia Schumacher, D. Sc., Universidade Federal de Viçosa, agosto de 2019. **Clima e modelagem de geleira em terreno complexo dos Andes Chileno**. Orientador: Flávio Barbosa Justino. Coorientador: Alfonso Andrés Fernández Rivera.

As flutuações das geleiras são uma fonte importante de água para o semi-árido no Chile Central, especialmente durante a estação seca, garantindo os recursos relacionados à energia de hidrelétricas, agricultura, indústria, turismo e principalmente ao consumo doméstico. No entanto, a retração das geleiras Andinas causada pela variabilidade climática local e o aquecimento global podem afetar o futuro dos recursos hídricos. As mudanças nas geleiras também deve afetar o crescimento econômico e o desenvolvimento das grandes cidades no Chile, bem como os meios de subsistência das comunidades locais que vivem nas montanhas Andinas. Com a mudança climática global em curso, os recursos hídricos são vulneráveis e devem levar à migrações em massa no futuro. Além disso, existem muitas lacunas na compreensão das geleiras nos Andes, especificamente em termos de balanço de massa. Em particular, os Andes do Chile Central têm recebido pouca atenção devido à escassez de estações de superfície para viabilizar pesquisas climáticas nesta região. O principal objetivo deste estudo é analisar as principais características associadas à precipitação e temperatura no Chile e a aplicação de um modelo de balanço de massa glacial em terreno complexo dos Andes chileno, utilizando um modelo de alta resolução. Há uma redução significativa da precipitação e tendência de aquecimento nos Andes chilenos, especialmente na região central do Chile durante o inverno, assim como um aumento do número consecutivo de dias secos. Além do mais, simulações mostram uma perda média de massa de -82 cm w.e. yr^{-1} entre 1996 e 2015 sobre a geleira Universidad, localizada nos Andes Central, com uma tendência negativa de -2,2 cm w.e. yr^{-1}. A variabilidade interanual é controlada principalmente pelo derretimento durante o verão. A sublimação representa cerca de 10% do processo de ablação enquanto a evaporação é o menor componente, correspondendo a 6%. As simulações

de alta resolução do balanço de massa desenvolvido neste estudo permitirá análises futuras com detalhes sem precedentes, proporcionando uma compreensão mais profunda do feedback entre as geleiras e o clima, além de fornecer novos conhecimentos sobre o balanço de massa das geleiras no Chile Central.

Palavras-chave: Geleiras nos Andes Central. WRF. Precipitação e Temperatura.

LIST OF ILLUSTRATION

LIST OF TABLE

SUMMARY

Chapter 1

General introduction

Importance of snow on past, present and future climate conditions

Snow cover is an important component of cryosphere and plays a fundamental role in the Earth's climate system. Snow cover is a key point in surface energy balance, which snow albedo reflects most solar radiation back into space, contributing to regulate the surface temperature of the Earth (Cohen and Rind, 1991). Seasonal variation of snow also has an important hydrological contribution, such as nourishing the regime of rivers and freshwater storage in several regions of the world. For instance, in semi-arid regions such as Andes, central Asia and western North America are highly dependent of melting of mountain glaciers for water resources. In these regions, snow accumulation as well as snowmelt is fundamental to water consumption and economic activities, such as irrigation, hydro-electrical generation, industry and tourism (Masiokas et al., 2016).

Snow cover and glaciers fluctuation are important as indicators of climate change due to high sensitivity to minor variations in the climate system, providing visible evidence of changes in temperature and precipitation patterns (IPCC, 2013; Kaser et al., 2010). The reduction of snow cover contributes to increase climate sensitivity through feedback processes, which it also exerts an influence on the climate. When snow and ice cover retreat or disappears, it implies a decrease in the albedo, which increase the absorption of the solar radiation, thus increasing the temperature and reducing snow and ice cover even more. This effect can be amplified by the permafrost thaw releasing methane into the atmosphere. In this way, decreasing snow cover means more energy absorbed at the Earth's surface, amplifying the global

warming (Barry and Gan, 2011; Armstrong and Brun, 2013).

The importance of snow cover as well as ice is also related to the preservation and reconstruction of the history of the climate in different geological eras. Past climate variations can provide relevant information for understanding climate change and its potential impacts. Through these reconstructions of the past climate it is possible to obtain indicators of climate changes by human activity. Changes in snow cover and melting of mountain glaciers should affect livelihoods worldwide, with several impacts on the natural and human systems (Mark and Fernández, 2017). Therefore, understanding the importance of snow cover under climate conditions is essential to define adaptation strategies and policies related to changes in the ecosystem, biodiversity and water resources under the modified climatic conditions for polar and mountain regions.

How may the Andes be affected by global warming?

Glaciers worldwide have been losing mass significantly in the last decades, in response to increasing temperature and higher precipitation variability (IPCC, 2013). The widespread retreat of glaciers is also happening across the Andes (Braun et al., 2019; Barcaza et al., 2017; Masiokas et al., 2016). There is evidence that the Andean glaciers shrinking has been occuring since the Litle Ice Age (17th-19th centuries). However, the magnitude of melting rate is not comparable with the unprecedented rate that has been happening throughout 20th century (Vuille et al., 2008a).

For instance, the total glacierized area in the tropical Andes has decreased by about 15% since 1970. This fast recession is related to temperature and air humidity increase (Kaser and Georges, 1999; Kaser and Osmaston, 2002). In addition, Rabatel et al. (2013b) also showed that the recession of tropical glaciers can be explained by the increase of temperature up to 0.10ºC/decade accompanied by higher frequency of

the El Niño events in the last 70 years.

Venezuela it is the Andean country with the smallest ice coverage (less than 3 km² in 1952). Morris et al. (2006) showed through satelite images that glacier surface area shrink about 86% between 1952 and 2003. The disappearance of glaciers in Venezuela is discussed by Braun and Bezada (2013). Colombian glaciers have lost 50% or more of their area in the past 50 years, with strong tendency to lose completely the remaining glaciated area in a few years (Ceballos et al., 2006). An uptodate the glacier inventory of Colombia is made available by Rabatel et al. (2017) using satelite images, they showed a reduction of 62% and 90% since the last century and Litle Ice Age, respectively.

In Ecuador, the ice caps on three volcanoes are also rapidly losing glacier coverage, about 57% on Chimborazo since 1962, 37% and 33% for Cotopaxi and Antisana, respectively in relation to 1979 and 2007 (Rabatel et al., 2013a). Bolivian glacier extent at Nevado Illimani reduced 35% from 1963 to 2009 (Da Rocha Ribeiro et al., 2013), while glacial volume in the Cordillera Real decreased by about 43% between 1963 and 2006, and 48% between 1975 and 2006 (Soruco et al., 2009).

Peruvian glaciers account 70% of all tropical glaciers and have lost about 30% of surface area from 1985 to 2006, mainly due to the increase in surface temperature (Salzmann et al., 2013). The Cordillera Blanca hosts about a quarter of all tropical glaciers in Peru, several studies point to important changes in the shrinkage in this mountain in the last decades. Georges (2004) estimated a decreased from 800-850 km² in 1930 to only 600 km² at the end of the 20th century. Silverio and Jaquet (2017) pointed a reduction of 46% of glacier cover in the Cordillera Blanca from 1930 to 2016.

In central Andes of Chile, glacier has decreased 20% on average since 1955

(Bown et al., 2008). The Patagonian glaciers also have show a marked loss of glacier volume related to increase in temperature and reduction in precipitation during the 20th century (Masiokas et al., 2009a).

In parallel with the glacier retreat, temperature and precipitation also has changed in the long Andes over the past 50-60 years, where temperature has increased by 0.1ºC/decade since 1961 to 1990 while precipitation has increased in the inner tropics and decreased in the outer tropics in the second half of the 20th century (Vuille et al., 2008b).

This glacier's imbalance in current climate implies that glaciers will continue to shrink in the future, even if the temperature remains stable (IPCC, 2013; Zemp et al., 2015). The accelerated retreat affects mainly small glaciers at low altitudes, which may disappear in the next decades, such as the disappearance of the Chacaltaya glacier in Bolivia, known for hosting a world's highest skiing station (Ramírez et al., 2001; Coudrain et al., 2005; Rabatel et al., 2013a).

Projections for the 21st century along the Andes indicate a continued warming, precipitation is expected to increase, but uncertainties are large (IPCC, 2013). The increase and acceleration in the warming rate along the Andes mountain range is consensual in both emissions scenarios in the future. For instance, projected temperature increase over Argentina for the next decades is greater than the observed warming of the last 60 years (Barros et al., 2015).

In the subtropical Central Andes of Argentina and Chile is expected a 5ºC warming at high elevations and a decrease in winter precipitation in the period 2075-2100 (Zazulie et al., 2017). In the Andes of Colombia is projected an increase in the precipitation by 2071-2100 (Palomino-lemus et al., 2015). On the other hand,

southern Patagonian Andes is expected a decrease precipitation about 15% and 10% in summer and winter, respectively, while in northern Patagonia an increase of 30% in precipitation to both summer and winter is projected in the period 2081-2090.

The climate change observed and projected during the 20th-21st century linked to unprecedented reduction in glacier area as well as volume implies severe consequences in regard to runoff, which it is of great importance for water supply in many regions of the Andes. The speed glaciers retreat implies reduces the ability of the glaciers in storing water seasonally (Mark et al., 2005).

For instance, projections indicate the disappearance in some catchments in the Cordillera Blanca until 2080, which is may affect the runoff necessary for water consuming (Juen et al., 2007; Vuille et al., 2008a). In Central Andes of Chile also is projected a significant decrease in more than 90% in total annual runoff (Ragettli et al., 2016). In addition to the water crisis, the projected precipitation reduction over the Central Andes may also be expected severe consequences in future hydropower production (Kronenberg et al., 2016).

These alterations in the Andean glaciers caused by changes associated with the increase in air temperature and its feedback in the climate result in several consequences besides the impact on water resources, such as increase of natural hazard risk, landscape alterations, tourism activities, food supply, socioeconomic, biogeochemical processes, biodiversity and sea level rise (Herzog et al., 2012; Mark et al., 2015).

Characteristics of accumulation and ablation process along in Chile

In general terms, the mass balance is the response associated with gain and loss of ice in glacial systems, which is determined by the difference between the accumulation and ablation processes. The accumulation is mainly dependent on snowfall, while ablation is mostly controlled by near surface temperature when exceeds the melting point. However, these processes are led by other important factors related to glacier-climate interactions, such as local and regional climate and topographic conditions (Benn and Evans, 2014).

The Andean glaciers experience several climatic conditions along the latitudinal-longitudinal profile imposed by cordillera and atmospheric circulation, dictates by a large range of precipitation and temperature features, with west-east climatic contrasts (Garreaud, 2009). The Andes acts as a continental barrier against circulation, leading to strong zonal gradients of moisture related climate features such as precipitation, cloudiness and latent heat flux (evaporation), which can affect glacier mass balance regimes (Kaser, 2002).

In the semi-arid Chile, the climate is characterized by wet and cold winters (April-September) with snow accumulated at high elevations, in contrast with warm and dry summers (October-March) with almost zero precipitation, low relative humidity, and intense solar radiation. This region is also commonly referred to as a Mediterranean-type climate (32ºS-38ºS) (Pellicciotti et al., 2008, 2014; Bravo et al., 2017; Bown et al., 2008).

These climate features are mainly associated with the northward-southward displacement of the high-pressure on the Pacific Ocean, which generally inhibits pre-

cipitation during the warm season, but allows the passage of westerlies and a higher occurrence of frontal precipitation during the cold season (Masiokas et al., 2009b). From longitudinal profile along the 33ºS the annual average precipitation ranges from 459 mm in Valparaiso (33.02ºS, 71.63ºW, 41 m) to 356 mm in Santiago (33.45ºS, 70.70ºW, 520 m) on the Chilean side and 180 mm in Mendoza (32.89ºS, 68.83ºW, 769 m) on the Argentinean side (Corripio and Purves, 2005).

Snow accumulation in the semi-arid Chile occurs mostly during winter while ablation predominantly in summer, which ablation energy is consumed mainly by melting compared to sublimation. The high melting regime is attributed to the low cloud cover that allows high insolation on the surface (Bravo et al., 2017). For instance, at Universidad glacier (34ºS) sublimation rates are represented by only a small fraction of ablation (3-6% in 2012/2014), where ablation occurred mainly by melting (Kinnard et al. 2018). At Juncal Norte glacier (33ºS) sublimation contribution is smaller, about 1% of total ablation at the glacier tongue, which is more important at higher elevations (Pellicciotti et al., 2008). Indeed, above 5500 m surface sublimation represent more than 75% of total ablation at Juncal Norte (Ayala et al., 2017).

Therefore, sublimation also plays an important role in the semi-arid Andes due to the combination of high elevation and warm and dry atmosphere (Ayala et al., 2017), wherein the sublimation accounts for a significant part in the total ablation in contrast to temperate environments with wet climate conditions, such as Patagonia and Tierra del Fuego, where melt dominates and sublimation is unimportant.

In southernmost South America, temperate glaciers in the Patagonia and Tierra del Fuego usually terminate with calving fronts into fjords on the western side, and into lakes on the eastern side, in which it strongly influences ablation rates

(Warren and Aniya, 1999; Casassa et al., 2006). For instance, mass losses due to calving in the Northern Patagonia as well as in the Southern Patagonia have increased in the recent decades, with higher rates than surface melting (Schaefer et al., 2013, 2015).

Patagonian glaciers are marked by constant influence from the westerlies, where the frequency and intensity increase with the latitude, inducing more abundant rainfall towards the south. This north-south precipitation gradient allows dividing the glaciers into Northern Patagonia Icefield (NPI; north of 42ºS; 4440 km^2) and Southern Patagonia Icefield (SPI; 42-49ºS; 13.500 km^2) (Barry and Gan, 2011; Sagredo and Lowell, 2012).

Moreover, western Patagonian glaciers (Chilean) presents temperate climate features with very wet conditions, while on the eastern Patagonian glaciers (Argentinean) semiarid conditions are present, spanning a strong west-east longitudinal profile of precipitation regime associated with orographic effect (Garreaud et al., 2013). From a transect along 53ºS, Schneider et al. (2003) showed the variation of annual precipitation with a higher amount on the western slopes Andean (6000-7000 mm), decreasing to 1000 mm on the eastern slopes, until 430 mm at Punta Arenas (53.2ºS, 70.9ºW). Annual thermal amplitude across the longitudinal profile in both the NPI and SPI depends on the altitude and proximity to the ocean, which is more accentuated on the Argentinean side than on the Chilean side (Villalba et al., 2003).

In contrast to glaciers in the Central Andes, Patagonian glaciers are located at lower altitudes with high accumulation and ablation throughout the year. Patagonian glaciers present highest accumulation rates due to frequent cyclonic weather systems and orographic uplift. Accumulation rates reach up to 14 m $year^{-1}$ from direct snowfall in some parts of the Patagonian icefields (Benn and Evans, 2014). In the

Patagonia appreciable part of precipitation, also occur as rain, unlike in the semi-arid Chile.

Positive mass balance is favored when high accumulation coincides with low ablation, associated with the high cloudiness in which it reduces incident solar radiation, and additional accumulated snow takes longer to melt, increasing the albedo (Schaefer et al., 2013). The west-east gradient is also observed in the mass balance on the Patagonia, where the eastern side presents minimum values of net balance compared to the western side of the Andean cordillera. For example, the Cerro Gorra Blanca glacier (49.13ºS – 73.05ºW) on the Argentinean side has been recorded 31 cm w.e. (metres water equivalent per year) while 1540 cm w.e. on the Glaciar Tyndall (50.98ºS – 73.52ºW) located on the Chilean side, with 2300 m and 1756 m altitude, respectively (Casassa et al., 2006).

The variation of the glacial area in the SPI has shown significant losses, around 93 km^2, that represents 62% of total loss for the SPI (489 km^2) between 1986 and 2000. The Pio XI glacier is the only with areal gain in the SPI, attributed to a surge or geothermal activity (Casassa et al., 2006). The modeled surface mass balance in the SPI between 1975 to 2011 presented accumulation of 67.7 $km^3\ yr^{-1}$, in which the ablation was of 36.5 $km^3\ yr^{-1}$ due to surface melt, and 44.4 $km^3\ yr^{-1}$ (1979 to 2000) and 61.3 $km^3\ yr^{-1}$ (2000 to 2011) due to calving (Schaefer et al., 2015). More recent, Malz et al. (2018) showed a mass loss of 3.3 Gt. yr^{-1} in the SPI considering an area of 12573 km^2 in the period 2000 to 2016 by remote sensing. This equals a specific glacier mass balance of 0.941 m w.e. yr^{-1} for the whole SPI.

High-latitude glaciers in the Tierra del Fuego also presents temperate climate conditions, cold and wet features, with uniform distribution of the precipita-

tion and temperature throughout the year on the western side, subsequently affected by continuous frontal and cyclonic activity, with average annual wind speed of 12 ms^{-1} (Sagredo and Lowell 2012; Bown et al. 2014). However, around northern and eastern of Cordillera Darwin (54° S, 69.6° W; 2605 km^2) is characterized by drier and warmer conditions, with low precipitation, humidity and cloudiness, contrasting with the greater snowfall on southern and western glaciers (Strelin and Iturraspe, 2007; Buttstädt et al., 2009). This contrast of precipitation together with the variation of altitude from west to east, induce a reduction of the glaciated area (Masiokas et al., 2009a).

Strelin and Iturraspe (2007) showed that wet and cool conditions, especially in summer season, induces positive net balance, otherwise dry and warm features determines negative net balance on the Martial Este glacier – Tierra del Fuego. In addition, they projected the vanishing of most of these glaciers for the next 100 years. Continuous surface mass balance in the Martial Este glacier for the period 1960 until 2099 show negative mass balance from 1960 until 2006, -772 mm w.e. yr^{-1}, whereas the mean annual loss in the period 2000 until 2006 is about 533 mm w.e. yr^{-1} (Buttstädt et al., 2009). This is interesting to note that retreating has been more marked from the last years.

The Cordillera Darwin icefield lost mass at an average rate of -3.9 Gt. yr^{-1} between 2000 and 2011 (Melkonian et al., 2013). The majority of the glaciers in Tierra del Fuego have shown a retreat in the last decades, except for two glaciers located at the southern of Cordillera Darwin (Glaciar Garibaldi) and another glacier calving into Bahia Pia. These advancing glaciers have been associated to calving and not necessarily to negative trend of precipitation (Bown et al., 2014).

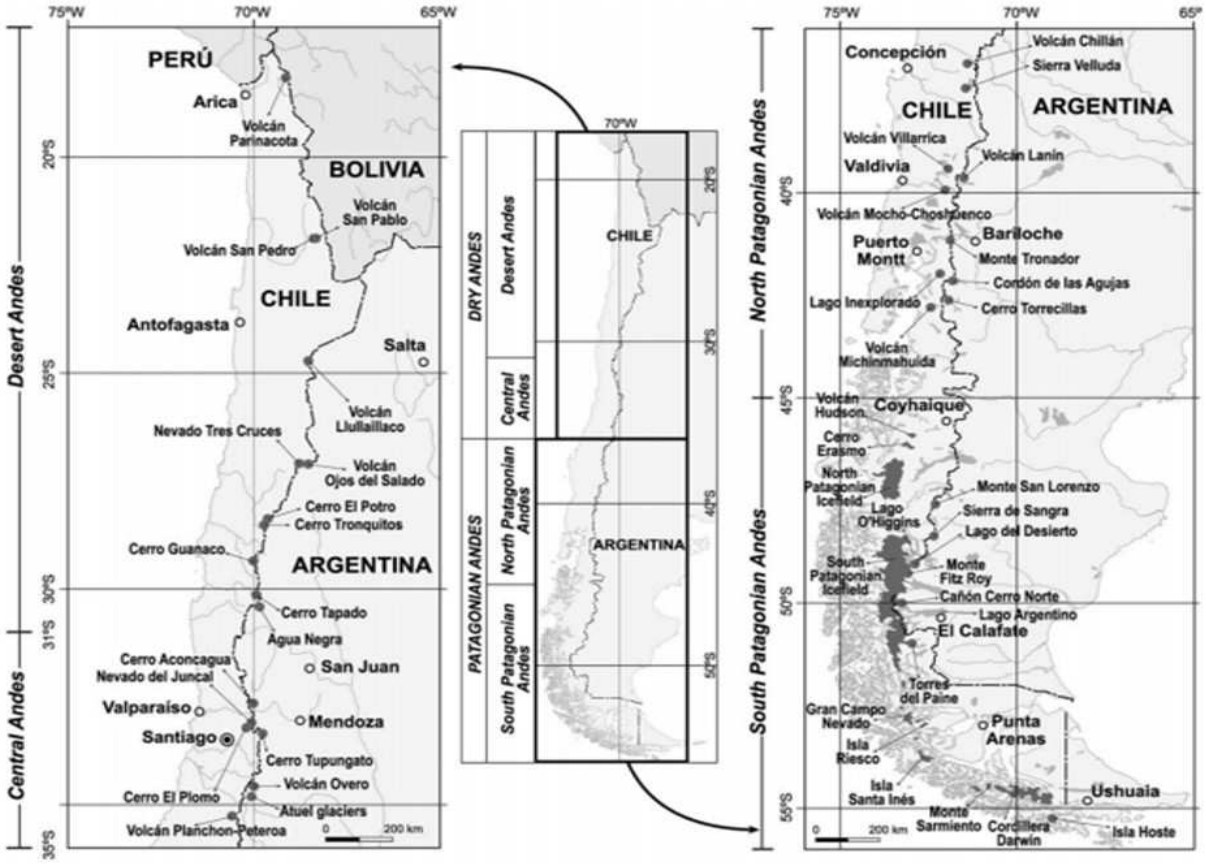

Figure 1.1: Map of the Chilean Andes showing the regional subdivisions (Desert Andes, Central Chilean–Argentinean Andes, and the North and South Patagonian Andes) and the location of the glacier sites mentioned in the text, from Masiokas et al. (2009a)

In summary, glaciers features along Chile exhibit several regional differences in relation to the longitudinal and latitudinal profile of the Andean Cordillera. This overview shows that the sensitivity of the glaciers mass balance is not only related to the regional and local climate, but also the distribution and topographical effect.

Objective

To analyze precipitation and temperature characteristics in the Chilean Andes and modeling application of the glacier surface mass balance in the Central Andes.

Specific objectives

1)To analyze precipitation and temperature features along Chilean Andes;

2)Evaluation of precipitation from dynamically downscaled at present climate focused on complex terrain;

3)To simulate recent glacier surface mass balance behavior at high spatio-temporal on the Chilean Andes.

Structure and organization of the thesis

This thesis consists of four chapters, encompassing from the climatic characteristics throughout Andes Chilean to the application of a mass balance model and its implications. The Chapter 1 deals with this general introduction. The Chapter 2, entitled “Comparison between observations and gridded datasets over complex terrain in the Chilean Andes: precipitation and temperature", submitted and pre-accepted in the *International Journal of Climatology*. The Chapter 3 is entitled “WRF high resolution dynamical downscaling of precipitation for Central Andes". Chapter 4, entitled as Modeling glacier surface mass balance in complex terrain on Chilean Central Andes shows the uncertainties about mass balance model and main features about the mass balance in the present-day conditions over the Universidad Glacier, in Central Andes.

References

Armstrong, R. L. and Brun, E. (2013). *Snow and climate: physical processes, surface energy exchange and modeling*, volume 46. Cambridge University Press.

Ayala, A., Pellicciotti, F., Peleg, N., and Burlando, P. (2017). Melt and surface sublimation across a glacier in a dry environment: Distributed energy-balance modelling of Juncal Norte Glacier, Chile. *Journal of Glaciology*, 63(241):803–822.

Barcaza, G., Nussbaumer, S. U., Tapia, G., Valdés, J., García, J. L., Videla, Y., Albornoz, A., and Arias, V. (2017). Glacier inventory and recent glacier variations in the Andes of Chile, South America. *Annals of Glaciology*, 58(75):166–180.

Barros, V. R., Boninsegna, J. A., Camilloni, I. A., Chidiak, M., Magrín, G. O., and Rusticucci, M. (2015). Climate change in Argentina: Trends, projections, impacts and adaptation. *Wiley Interdisciplinary Reviews: Climate Change*, 6(2):151–169.

Barry, R. G. and Gan, T. Y. (2011). *The global cryosphere: Past, present, and future*. Cambridge University Press.

Benn, D. and Evans, D. J. (2014). *Glaciers and Glaciation*, volume 36. Routledge.

Bown, F., Rivera, A., and Acuña, C. (2008). Recent glacier variations at the Aconcagua basin, central Chilean Andes. *Annals of Glaciology*, 48:43–48.

Bown, F., Rivera, A., Zenteno, P., Bravo, C., and Cawkwell, F. (2014). First Glacier Inventory and Recent Glacier Variation on Isla Grande de Tierra Del Fuego and Adjacent Islands in Southern Chile. *Global Land Ice Measurements from Space*, pages 661–674.

Braun, C. and Bezada, M. (2013). The History and Disappearance of Glaciers in Venezuela. *Journal of Latin American Geography*, 12(2):85–124.

Braun, M. H., Malz, P., Sommer, C., Farías-Barahona, D., Sauter, T., Casassa, G., Soruco, A., Skvarca, P., and Seehaus, T. C. (2019). Constraining glacier elevation and mass changes in South America. *Nature Climate Change*, 9(2):130–136.

Bravo, C., Loriaux, T., Rivera, A., and Brock, B. W. (2017). Assessing glacier melt contribution to streamflow at Universidad Glacier, central Andes of Chile. *Hydrology and Earth System Sciences*, 21(7):3249–3266.

Buttstädt, M., Möller, M., Iturraspe, R., and Schneider, C. (2009). Mass balance evolution of Martial Este Glacier, Tierra del Fuego (Argentina) for the period 1960-2099. *Advances in Geosciences*, 22(1995):117–124.

Casassa, G., Rivera, A., and Schwikowski, M. (2006). Glacier Mass-Balance data for Southern South America (30S-56S). In *In: Knight, P.G. (Ed.), Glacier Science and Environmental Change*, pages 239–241. Blackwell, Oxford,UK.

Ceballos, J. L., Euscátegui, C., Ramírez, J., Cañon, M., Huggel, C., Haeberli, W., and Machguth, H. (2006). Fast shrinkage of tropical glaciers in Colombia. *Annals of Glaciology*, 43:194–201.

Cohen, J. and Rind, D. (1991). The effect of snow Cover on the Climate.

Corripio, J. G. and Purves, R. S. (2005). *Surface Energy Balance of High Altitude Glaciers in the Central Andes: the Effect of Snow Penitentes*. Wiley \& Sons: London.

Coudrain, A., Francou, B., and Kundzewicz, Z. W. (2005). Glacier shrinkage in the Andes and consequences for water resources - Editorial. *Hydrological Sciences Journal*, 50(6):925–932.

Da Rocha Ribeiro, R., Ramirez, E., Simões, J. C., and Machaca, A. (2013). 46 years of environmental records from the Nevado Illimani glacier group, Bolivia, using digital photogrammetry. *Annals of Glaciology*, 54(63):272–278.

Garreaud, R., Minvielle, M., and Rojas, M. (2013). Large-Scale Control on the Patagonian Climate. *Journal of Climate*, 26:215–231.

Garreaud, R. D. (2009). The Andes climate and weather. *Advances in Geosciences*, 22:3–11.

Georges, C. (2004). 20th-Century Glacier Fluctuations in the Tropical Cordillera Blanca, Perú. *Arctic, Antarctic, and Alpine Research*, 36(1):100–107.

Herzog, S. K., Martínez, R., Jørgensen, P. M., and Tiessen, H. (2012). Climate Change and Biodiversity in the Tropical Andes. *Mountain Research and Development*, 32(2):348.

IPCC (2013). Climate Change 2013: The Physical Science Basis. *Contribution of working group I to the Fourth Assessment Report of the Intergovernmental Panel on Climate Change*, page 1535.

Juen, I., Kaser, G., and Georges, C. (2007). Modelling observed and future runoff from a glacierized tropical catchment (Cordillera Blanca, Perú). *Global and Planetary Change*, 59(1-4):37–48.

Kaser, G. (2002). Glacier Mass Balance and Climate in the South American Andes. In *The Patagonian Icefields*, pages 89–99. Springer.

Kaser, G. and Georges, C. (1999). on the Mass Balance of Low Latitude Glaciers With Particular Consideration of. *Physical Geography*, 81(4):643–651.

Kaser, G., Grosshauser, M., and Marzeion, B. (2010). Contribution potential of glaciers to water availability in different climate regimes. *Proceedings of the National Academy of Sciences*, 107(47):20223–20227.

Kaser, G. and Osmaston, H. (2002). *Tropical glaciers*, volume 40. Cambridge University Press.

Kronenberg, M., Schauwecker, S., Huggel, C., Salzmann, N., Drenkhan, F., Frey, H., Giraáldez, C., Gurgiser, W., Kaser, G., Juen, I., Suarez, W., Hernaández, J. G., Sanmartín, J. F., Ayros, E., Perry, B., and Rohrer, M. (2016). The Projected Precipitation Reduction over the Central Andes may Severely Affect Peruvian Glaciers and Hydropower Production. *Energy Procedia*, 97:270–277.

Mark, B., Baraer, M., Fernández, A., Immerzeel, W., Moore, R., and Weingartner, R. (2015). Glaciers as water resources. In Huggel, C., Carey, M., Clague, J., and Kääb, A., editors, *The High-Mountain Cryosphere Environmental Changes and Human Risks*, chapter 11, pages 184–203. Cambridge University Press, Cambridge, 1st edition.

Mark, B. G. and Fernández, A. (2017). The significance of mountain glaciers as sentinels of climate and environmental change. *Geography Compass*, 11(6):1–16.

Mark, B. G., McKenzie, J. M., and Gómez, J. (2005). Hydrochemical evaluation of changing glacier meltwater contribution to stream discharge: Callejon de Huaylas, Peru. *Hydrological Sciences Journal*, 50(6):975–988.

Masiokas, M. H., Christie, D. A., Le Quesne, C., Pitte, P., Ruiz, L., Villalba, R., Luckman, B. H., Berthier, E., Nussbaumer, S. U., González-Reyes, Á., McPhee, J., and Barcaza, G. (2016). Reconstructing the annual mass balance of the Echaurren Norte glacier (Central Andes, 33.5° S) using local and regional hydroclimatic data. *The Cryosphere*, 10(2):927–940.

Masiokas, M. H., Rivera, A., Espizua, L. E., Villalba, R., Delgado, S., and Aravena, J. C. (2009a). Glacier fluctuations in extratropical South America during the past 1000 years. *Palaeogeography, Palaeoclimatology, Palaeoecology*, 281(3-4):242–268.

Masiokas, M. H., Rivera, A., Espizua, L. E., Villalba, R., Delgado, S., and Aravena, J. C. (2009b). Glacier fluctuations in extratropical South America during the past 1000years. *Palaeogeography, Palaeoclimatology, Palaeoecology*, 281(3-4):242–268.

Melkonian, A. K., Willis, M. J., Pritchard, M. E., Rivera, A., Bown, F., and Bernstein, S. A. (2013). Satellite-derived volume loss rates and glacier speeds for the Cordillera Darwin Icefield, Chile. *Cryosphere*, 7(3):823–839.

Morris, J. N., Poole, A. J., and Klein, A. G. (2006). Retreat of Tropical Glaciers in Colombia and Venezuela from 1984 to 2004 as Measured from ASTER and Landsat Images. *Proceedings of the 63rd Eastern Snow Conference*, pages 181–191.

Palomino-lemus, R., Córdoba-machado, S., Gámiz-fortis, S. R., Castro-díez, Y., and Esteban-parra, M. J. (2015). Summer precipitation projections over northwestern South America from CMIP5 models. *Global and Planetary Change*, 131:11–23.

Pellicciotti, F., Helbing, J., Rivera, A., Favier, V., Corripio, J., Araos, J., Sicart, J.-E., and Carenzo, M. (2008). A study of the energy balance and melt regime on Juncal Norte Glacier, semi-arid Andes of central Chile, using melt models of different complexity. *Hydrological Processes*, 22(19):3980–3997.

Pellicciotti, F., Ragettli, S., Carenzo, M., and McPhee, J. (2014). Changes of glaciers in

the Andes of Chile and priorities for future work. *The Science of the total environment*, 493C:1197–1210.

Rabatel, A., Ceballos, J. L., Micheletti, N., Jordan, E., Braitmeier, M., González, J., Mölg, N., Ménégoz, M., Huggel, C., and Zemp, M. (2017). Toward an imminent extinction of Colombian glaciers? *Geografiska Annaler, Series A: Physical Geography*, 100(1):75–95.

Rabatel, A., Francou, B., Soruco, A., Gomez, J., Caceres, B., Ceballos, J., Basantes, R., Vuille, M., Sicart, J.-E., Huggel, C., Scheel, M., Lejeune, Y., Arnaud, Y., Collet, M., Condom, T., Consoli, G., Favier, V., Jomelli, V., Galarraga, R., Ginot, P., Maisincho, L., Mendoza, J., Menegoz, M., Ramirez, E., Ribstein, P., Suarez15, W., Villacis, M., and Wagnon, P. (2013a). Current state of glaciers in the tropical Andes: a multi-century perspective on glacierevolution and climate change. *The Cryosphere*, 7(1):81–102.

Rabatel, A., Francou, B., Soruco, A., Gomez, J., C??ceres, B., Ceballos, J. L., Basantes, R., Vuille, M., Sicart, J. E., Huggel, C., Scheel, M., Lejeune, Y., Arnaud, Y., Collet, M., Condom, T., Consoli, G., Favier, V., Jomelli, V., Galarraga, R., Ginot, P., Maisincho, L., Mendoza, J., M??n??goz, M., Ramirez, E., Ribstein, P., Suarez, W., Villacis, M., and Wagnon, P. (2013b). Current state of glaciers in the tropical Andes: A multi-century perspective on glacier evolution and climate change. *Cryosphere*, 7(1):81–102.

Ragettli, S., Immerzeel, W. W., and Pellicciotti, F. (2016). Contrasting climate change impact on river flows from high-altitude catchments in the Himalayan and Andes Mountains. *Proceedings of the National Academy of Sciences*, 113(33):9222–9227.

Ramírez, E., Francou, B., Ribstein, P., Descloitres, M., Guérin, R., Mendoza, J., Gallaire, R., Pouyaud, B., and Jordan, E. (2001). Small glaciers disappearing in the Tropical Andes. A case study in Bolivia; the Chacaltaya Glacier (16° S). *Journal of Glaciology*, 47:187–194.

Sagredo, E. A. and Lowell, T. V. (2012). Climatology of Andean glaciers: A framework to understand glacier response to climate change. *Global and Planetary Change*, 86-87(August):101–109.

Salzmann, N., Huggel, C., Rohrer, M., Silverio, W., Mark, B. G., Burns, P., and Portocarrero, C. (2013). Glacier changes and climate trends derived from multiple sources in the data scarce Cordillera Vilcanota region, southern Peruvian Andes. *Cryosphere*, 7(1):103–118.

Schaefer, M., Machguth, H., Falvey, M., and Casassa, G. (2013). Modeling past and future surface mass balance of the Northern Patagonia Icefield. *Journal of Geophysical Research: Earth Surface*, 118(2):571–588.

Schaefer, M., MacHguth, H., Falvey, M., Casassa, G., and Rignot, E. (2015). Quantifying mass balance processes on the Southern Patagonia Icefield. *Cryosphere*, 9(1):25–35.

Schneider, C., Glaser, M., Kilian, R., Santana, A., and Casassa, G. (2003). Weather observations across the southern andes at 53°s. *Physical Geography,*, 24:97–119.

Silverio, W. and Jaquet, J.-m. (2017). Evaluating glacier fluctuations in Cordillera Blanca (Peru) by remote sensing between 1987 and 2016 in the context of ENSO. *ARCHIVES DES SCIENCES*, 69:145–162.

Soruco, A., Vincent, C., Francou, B., and Gonzalez, J. F. (2009). Glacier decline between 1963 and 2006 in the Cordillera Real, Bolivia. *Geophysical Research Letters*, 36(3):2–7.

Strelin, J. and Iturraspe, R. (2007). Recent evolution and mass balance of Cordón Martial glaciers, Cordillera Fueguina Oriental. *Global and Planetary Change*, 59(1-4):17–26.

Villalba, R., Lara, A., Masiokas, M., Delgado, S., Aravena, J. C., Roig, F. A., Schmelter, A., Wolodarsky, A., and Ripalta, A. (2003). Large-scale temperature changes across the southern andes: 20th-century variations in the context of the past 400 years. *Climatic Change*, 59:177–232.

Vuille, M., Francou, B., Wagnon, P., Juen, I., Kaser, G., Mark, B. G., and Bradley, R. S. (2008a). Climate change and tropical Andean glaciers: Past, present and future. *Earth-Science Reviews*, 89(3-4):79–96.

Vuille, M., Kaser, G., and Juen, I. (2008b). Glacier mass balance variability in the Cordillera Blanca, Peru and its relationship with climate and the large-scale circulation. *Global and Planetary Change*, 62(1-2):14–28.

Warren, C. and Aniya, M. (1999). The calving glaciers of southern South America. *Global and Planetary Change*, 22:59–77.

Zazulie, N., Rusticucci, M., and Raga, G. B. (2017). Regional climate of the Subtropical Central Andes using high-resolution CMIP5 models. Part II: future projections for the twenty-first century. *Climate Dynamics*, 51(7-8):2913–2925.

Zemp, M., Frey, H., Gärtner-Roer, I., Nussbaumer, S. U., Hoelzle, M., Paul, F., Haeberli, W., Denzinger, F., Ahlstrøm, A. P., Anderson, B., Bajracharya, S., Baroni, C., Braun, L. N., Càceres, B. E., Casassa, G., Cobos, G., Dàvila, L. R., Delgado Granados, H., Demuth, M. N., Espizua, L., Fischer, A., Fujita, K., Gadek, B., Ghazanfar, A., Hagen, J. O., Holmlund, P., Karimi, N., Li, Z., Pelto, M., Pitte, P., Popovnin, V. V., Portocarrero, C. A., Prinz, R., Sangewar, C. V., Severskiy, I., Sigurdsson, O., Soruco, A., Usubaliev, R., and Vincent, C. (2015). Historically unprecedented global glacier decline in the early 21st century. *Journal of Glaciology*, 61(228):745–762.

Chapter 2

Comparison between observations and gridded datasets over complex terrain in the Chilean Andes: precipitation and temperature

Schumacher, Vanúcia; Justino, Flávio.; Fernández, Alfonso.; Meseguer-Ruiz, Oliver.; Sarricolea, Pablo.; and Comin, Alcimoni., 2019. Comparison between observations and gridded datasets ove complex terrain in the Chilean Andes: precipitation and temperature. **International Journal of Climatology**. Final review process.

Introduction

Due to its complex topography and latitudinal extension, Chile exhibits different climatic zones, from tropical to extratropical featuring desertic, volcanic, lacustrine and icy landscapes that define extreme gradients, including the arid North in Atacama and the extreme precipitation in Southern Patagonia (Garreaud 2009; Sarricolea et al. 2017). Central Chile concentrates the country's population, including the densely populated Metropolitan Santiago region, as well as important sectors of the economic activity. In this region, millions depend on steady water availability to support hydropower generation, and activities associated with agriculture, industry and tourism, especially during the dry season (Masiokas et al. 2012). As water availability depends on the local climate variability, changes in temperature and precipitation may affect future water resources and availability in several regions in Chile (Bradley 2006; Sarricolea and Romero 2015; Boisier et al. 2016).

As a number of studies indicate that the behavior of glaciers and river

flows in high Andes are sensitive to warming trends and precipitation changes under ongoing climate change (Vuille et al. 2008; Urrutia and Vuille 2009; Rabatel et al. 2013; Neukom et al. 2015; Ragettli et al. 2016), it becomes evident that the characterization of these meteorological variables is crucial to understand how climate change may impact these regions. On the other hand, despite recent encouraging initiatives (Alvarez-Garreton et al. 2018), obtaining continuous and accurate weather information in the Andean mountain range is still a difficult task (Manz et al. 2016). The Andean complex orography makes it difficult to maintain and expand the network of meteorological stations and the development of reliable measurements of the spatial and long-term historical observations (Cowtan and Way 2014).

In this context, gridded datasets are useful tools to overcome the dearth of observations, allowing the development of long-term for climate analyses and monitoring (e.g. Gu and Adler 2019). Among several applications, gridded datasets are utilized for data assimilation, comparison with observations, forcing data for global and regional models, and to investigate atmospheric process and climatic variability during recent decades (Lorenz and Kunstmann 2012; Huang et al. 2016; Cortés et al. 2016; Zazulie et al. 2017; Serrano-Notivoli et al. 2018). Reanalyses products also have been widely used for statistical, dynamical, and hydric downscaling (Bieniek et al. 2016; El-Samra et al. 2017; Soares et al. 2012). These downscaled climate fields can be used as input in other climate models, especially in complex terrain of the Andes, helping to understand the physical and dynamic processes in regions of irregular topography (Fernández and Mark 2016; Comin et al. 2018).

However, the performance of these applications depends on the accuracy and ability of the gridded datasets to reproduce local climatic features. Indeed, gridded datasets have shown great performance on the global scale, but the improvements needed for these datasets to be accurate at the regional scale are important due to large uncertainties related (Angélil et al. 2016). This is more critical in mountain areas, where complex terrain induces large biases and gradients of precipitation and near surface temperature (Silva et al. 2011; Schauwecker et al. 2014; Schauwecker et al. 2017).

Some studies have evaluated temperature and precipitation changes in the Southern Hemisphere at the regional scale and using different gridded products

(e.g. Bromwich et al. 2011). Although gridded datasets have been subjected to diverse evaluations worldwide (Morice et al. 2012; Rapaić et al. 2015), there is a lack of studies focusing on the complex Chilean terrain. Nearby areas have been studied, however, such as the case of a comparison of precipitation depicted by CFSR and MERRA reanalyses and combined products over basins in Bolivia, show overestimation of precipitation over the Altiplano basin (Blacutt et al. 2015).

This paper aims to presents the results of the performance of five widely used global gridded datasets in reproducing precipitation and surface temperature along the Chilean Andes between (17ºS to 40ºS for the period 1980-2015). This study also includes an analysis of climate indices associated with precipitation using the observational and gridded datasets, as well as the relationship of the gridded products with climate modes of variability that are known to be important in this region. Section 2 describes the data and methods utilized. Section 3 presents results of the performance of the gridded datasets a) mean annual, b) seasonal value, and c) spatio-temporal trends of precipitation and near surface temperature relative to instrumental observations. Finally, in Section 4 we draw conclusions of our findings.

Data and Methods

Observational datasets

Observed monthly mean precipitation and surface temperature were used to evaluate gridded datasets. These measurements are maintained by the Chilen Water Directorate (Dirección General de Aguas, DGA) and the Chilean Weather Directorate (Dirección Meteorológica de Chile, DMC), and are available trhough the Climate Explorer of the Center for Climate and Resilence (CR2, http://explorador.cr2.cl). In this study, high Chilean Andes climatology with complex topography is represented by all weather stations above 500 m a.s.l. To achieve the most representative and consistent data for verification, we selected only data with less than 10% of missing data in each monthly series for the period. Individual records were considered outliers and discarded when monthly totals exceeded four times the standard deviation above the mean. No interpolation method was attempted to fill gaps. Beyond these considerations, we believe that these datasets are a good representation of Chilean observations

without interference by interpolation and data filling.

Given that the distribution of data in Andes is very sparse for a long-term climatic assessment, measurements were selected considering two periods from 1980 to 2015 and from 1990 to 2015, since little stations span between 1980-2015 interval. The observations consist of a total of 116 (34) stations for precipitation (near-surface temperature), 44 (5) located in North, 55 (21) in Central and 17 (7) in South Chile (see Fig. 1). From Figure 1 we detected two relatively large strips where no instrumental records exist. The first, approximately between latitudes 24ºS and 27ºS and a second between 34ºS and 35ºS (34ºS to 36ºS for temperature). For the sake of clarity in the description of results, we therefore used those spatial gaps to define a Northern region (17ºS-24ºS), a Central region (27ºS-34ºS), and a Southern region (35ºS-40ºS). Maximum elevations of the records of precipitation and temperature are, respectively 4576 m and 3010 m in the North. For Central, the highest altitude is 3160 m and 1043 m in the Southern region.

Gridded datasets

Five gridded datasets were used - namely: (i) The Global Precipitation Climatology Project (GPCP) monthly analysis (New Version 2.3) provided by the NOAA/OAR/ESRL PSD (https://www.esrl.noaa.gov/psd/). The GPCP is a merger of various satellite-based rainfall estimates over both ocean and land, combined with the precipitation gauge analyses over land (Adler et al. 2003). (ii) The Global Precipitation Climatology Centre (GPCC) Full Data Monthly Product Version 2018 (V8) available at https://www.esrl.noaa.gov/
psd/. The GPCC product is based on observations in-situ data from rain gauges in order to provide gridded high quality and high-resolution land surface precipitation analyses (Schneider et al. 2018). (iii) Climatic Research Unit (CRU) Time series (TS) version 4.01 available at http://badc.nerc.ac.uk/data/cru/. The CRU provides monthly mean precipitation and surface air temperature, and merges observations at meteorological stations across land areas using angular distance weighting interpolation (Harris et al. 2014). (iv) Re-Analysis Interim Project (ERA-I), which is a global atmospheric reanalysis produced by the European Centre for Medium-Range Weather Forecasts (ECMWF) that can be accessed from https://apps.ecmwf.int/datasets/.

The ERA-I is produced using a sequential 4D-VAR data assimilation scheme (Dee et al. 2011), and (v) Modern-Era Retrospective analysis for Research and Applications Version2 (MERRA2). The MERRA2 is the newest reanalysis product from the NASA Global Modeling and Assimilation Office (GMAO), generated using the Goddard Earth Observing System Model, Version 5 (GEOS5) data assimilation system (DAS) (Bosilovich et al. 2017) available at https://gmao.gsfc.nasa.gov. Additional information of the gridded datasets is presented in Table 1. Further details about data assimilation techniques and physical processes represented in these datasets are summarized in Fujiwara et al. (2017).

As a result of the different spatial resolutions, these gridded datasets reproduce the complex Andean topography with different detail (Fig. 1c). To exemplify these differences, we interpolate the ETOPO data at 1 arc minute global digital elevation model (https://www.ngdc.noaa.gov/mgg/global/) for the resolution corresponding to each gridded dataset, given that most of these data do not present topographic variables. For GPCP the comparison evidences limitation in reproducing topographic gradients especially at 30ºS. More reasonable patterns show up in CRU and MERRA2 (Fig. 1c). As discussed by Justino et al. (2011) and Van den Broeke et al. (2005), misrepresentation of regions with steep slopes modifies the wind pattern, changing the temperature and consequently resulting in unrealistic seasonal contrast.

Table 2.1: Spatial horizontal resolution of the gridded datasets used in this study. P indicates precipitation and T temperature.

Gridded Data	Variables	Resolution	Description	Reference
GPCP	P	2.5º x 2.5º	Centre: GSFC NASA	Adler et al. (2003)
GPCC	P	1º x 1º	Centre: DWD	Schneider et al. 2018
CRU	P and T	0.5º x 0.5º	Centre: UEA	Harris et al. (2014)
ERA-I	P and T	0.75º x 0.75º	Centre: ECMWF	Dee et al. (2011)
MERRA2	P and T	0.5º x 0.625º	Centre: NASA GMAO	Bosilovich et al. (2017)

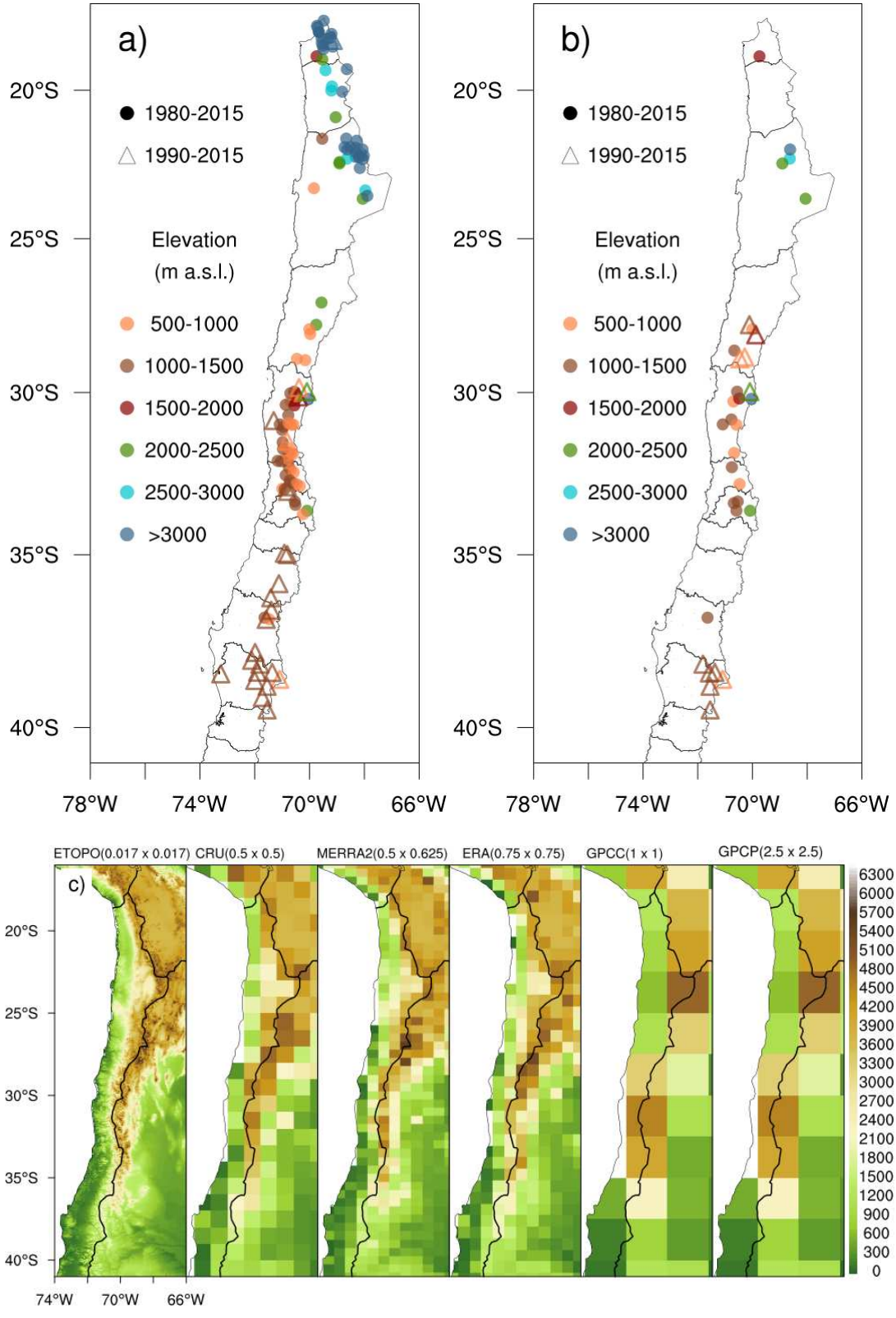

Figure 2.1: Location of the selected meteorological stations including time span (years) and its corresponding elevation for a) precipitation and b) temperature. (c) Differences topographic based on interpolation of elevation model (ETOPO1) for each corresponding spatial resolution of the gridded datasets.

Methods

To compare the gridded datasets with observations, we interpolated the datasets (with simple bilinear interpolation) to the station location, to overcome the mismatch scale between coarse gridded datasets and observations. The bilinear interpolation method uses the distance-weighted average of the four nearest grid values to give an estimate at a point of interest. This grid-to-point methodology has been applied satisfactorily in previous studies (e.g. Bromwich and Fogt 2004; Bao and Zhang 2013; Ebrahimi et al. 2017; Mayor et al 2017; Meher and Das 2019). The bilinear interpolation has been chosen due to its more realistic local interpretation instead of using the coarse grid value. This simplified method with two-dimensional interpolation allows to assess improvements and uncertainties (Uddim et al. 2008; Caroletti et al. 2019). An attempt of interpolation of the observations would involve large uncertainties given the lack of high-density weather stations database along the complex terrain (Rivera et al. 2018).

The evaluation of the gridded datasets to represent annual and seasonal features associated with precipitation and surface temperature over high Chilean Andes, included computation of several validation statistics: difference (bias), root mean square error (RMSE), the Pearson correlation coefficient (CC), and Willmott index of agreement (Skill). The positive values of bias indicate an overestimation of the precipitation or temperature of the gridded datasets in relation to observed, whereas negative values indicate underestimation. The RMSE provides information on the standard metric for gridded datasets errors, where 0 is the best score. The CC indicates whether is linear relationship between the gridded datasets and observations, where 1 is the perfect match. Willmott's index is a standardized measure of the degree of dataset temporal-prediction error and varies between 0 and 1, where value of 1 indicates a perfect match, and 0 indicates no agreement.

The Sen Slope and the Mann-Kendall test are used to estimate annual and seasonal trends in time-series. Trends are considered to be statistically significant at the 10% significance level. A more detailed description of these methods can be found

in Mann (1975); Kendall (1975); Wilks (2006). The gridded datasets were compared for annual, summer (December-February, DJF) and winter (June-August, JJA) periods.

In order to explore the influence of climate indices onto precipitation and temperature variability, Pearson's correlation was performed between climate indices and the time series of observations and gridded datasets. The indices are: Niño 1.2 (0-10ºS; 90ºW-80ºW) and Niño 3.4 (5ºN-5ºS; 170ºW-120ºW), the Pacific Decadal Oscillation (PDO), and the Antarctic Oscillation (AAO). The time-series of the climate indices are provided by the National Oceanic and Atmospheric Administration website (NOAA; https://www.esrl.noaa.gov
/psd/data/climateindices).

To further illustrate the representation of long-term trends associated to some precipitation extremes in the high Chilean Andes, daily precipitation data from observed stations and gridded datasets (GPCP, GPCC, ERA-I and MERRA2) for annual and seasonal scales are used to analyze spatio temporal trends of precipitation. For this, two precipitation-related indices were used: the maximum number of consecutive wet days (CWD) and consecutive dry days (CDD). The CWD is defined by the maximum length of wet spell (daily rainfall $\geq$ 1 mm) whereas CDD by the maximum length of dry spell (daily rainfall $<$ 1 mm), both expressed in days.

Results and Discussion

Annual and Seasonal precipitation analyses

The annual precipitation regime is characterized by a contrast among the three regions in Chile (Fig. 2a). In the North, some records near the coast show annual precipitation lower than 10 mm/year. These values contrast with increasing precipitation to the east, where the highest values are observed in the elevated areas (> 3000 m) (Fig. 1c,2a). This zonal gradient highlights the orographic precipitation over the windward slope (Garreaud et al. 2017).

There is also a clear latitudinal pattern of gradual increase of precipita-

tion, with maximum annual mean precipitation concentrated southward to 35ºS, with values above 1000 mm. During summer, precipitation increases in Northern and decreases in Central region, whereas in winter, precipitation decreases in Northern and an increase in Central region (Fig. 2b,c). The summer season is responsible for up to 80% of the rainfall occurring in the Northern region, in contrasts with the Central and the South regions, where about 40 to 80% of precipitation falls during the winter season.

Figures 3 and 4 are boxplots that summarize the overall performance of the gridded datasets in reproducing the annual and seasonal precipitation through the calculation of bias, RMSE, CC and Skill. In Northern Chile, positive biases in GPCP and ERA-I indicate overestimate precipitation, whereas for GPCC, CRU and MERRA2 a median close to zero bias, although MERRA2 is slightly more negative. In Central region, GPCC shows an improvement by lower median and quartile values. Southward 35ºS all datasets underestimate precipitation in relation to observations. It is worth mentioning that MERRA2 tends to be drier across the whole study area (Fig. 3a-c).

All gridded datasets show smaller RMSE in Northern and Central Chile, on the other hand, a larger RMSE is noted in Southern Chile (Fig. 3d-f). In general, GPCC and CRU match observations in the North, with median and quartile values smaller than 10 mm/yr., while GPCC and ERA-I performs better in the South, with median values smaller than 100 mm/yr. The datasets do a good job in Central region, with smaller bias as well as RMSE values. Most of the datasets show a high correlation, with CC values greater than 0.8, particularly in Central region. MERRA2 shows poor agreement compared to other datasets due to extreme negative bias values. The good agreement in Central Chile is also shown by the Skill index between gridded datasets and observations, particularly by CRU in North and Central Chile (Fig. 3j,k). On the other hand, lower Skill index is reported for all datasets in the South. Both North and Central regions have relatively low biases, however in the arid North, the agreement with observations by CC and Skill are generally low; this might be related

to the inherent dynamics of precipitation in the region: rainfall usually occurs as a few extreme events (e.g. Pendergrass and Knutti, 2018; Meseguer-Ruiz et al. 2019), which are more difficult to reproduce.

Figure 4 depicts seasonal precipitation statistics between gridded datasets and observations for summer and winter. In summer, gridded datasets reproduce similar annual bias variability in North and Southern Chile, however, biases are higher in the Northern region and lower in the South. Differences between datasets are noted in Central region, where all datasets appear to be positively biased relative to observations. GPCP and ERA-I overestimate precipitation with maximum values above 15 mm, whereas GPCC, CRU and MERRA2 show smaller bias (Fig. 4b). Concerning winter precipitation bias, once again GPCC, CRU and MERRA2 close match with observations, depict smaller biases in Northern Chile. In Central region, variability of gridded datasets is similarto what already seen for annual bias, with ERA-I and GPCP overestimating precipitation (Fig. 4n), and, southward 35ºS all gridded datasets underestimate observed precipitation (Fig. 4c-o).

For RMSE, larger values are found in Northern and Southern regions during summer, while in winter large disagreement occurs over Central and the Southern region (Fig. 4e,f,q,r). In Northern, GPCC and CRU (GPCC and MERRA2) have a smaller RMSE, < 30 mm/yr. (< 5 mm/yr, quartile and median values) in summer (winter). In general, the errors associated with each gridded dataset are accompanied by the magnitude of bias; the larger (lower) the bias, the greater (lower) the error in relation to the observations. In terms of the bias and RMSE values, GPCC and CRU shows the best performance.

The values of CC and Skill index show a better agreement between gridded datasets and observations in Northern Chile during summer, less spread, except to MERRA2. Maximum CC values are delivered by CRU in all regions. For Central Chile, GPCC and CRU have a good agreement, and GPCC and ERA-I for Southern (Fig. 4g-l). In winter, the CC and Skill show that all datasets provide a good agreement to observed precipitation over Central region. Conversely, poor performances

are delivered in Southern Chile in line with strong negative bias (Fig. 4u,z).

Analysis of the performance of gridded datasets reproducing the annual and seasonal precipitation shows that GPCP and ERA-I overestimate observations in the North, while MERRA2 underestimates the annual as well as seasonal precipitation. Better match is given in Central Chile (27ºS to 34ºS) with higher CC, Skill and smaller bias. It can be argued that in Northern region, differences among the datasets are related to orographic forcing processes, whereas changes in the South (35ºS to 40ºS) may be induced by differences in meso-scale processes, such as the maritime advection of water vapor, as well as the capability of the individual data to reproduce the strength and frequency of cold frontal systems (Barrett et al. 2009).

It can be argued that GPCC and CRU reasonably reproduce the annual and seasonal mean precipitation in most parts of the studied region, as they are based on in situ rainfall observation data. The CRU data are interpolated directly from station observations, including algorithms that account for the effect of elevation (New et al. 2000). Conversely, GPCP is less skilled reproducing instrumental precipitation over steep terrain and high elevation due to its relatively coarse resolution, despite merging observation and satellite data. These differences between gridded products suggest that higher horizontal resolution results in more accurate representation in this complex Andean terrain (Fig. 1c). However, it is important to note that these datasets may perform better when compared with observations in flatter terrain below our 500 m altitude criteria.

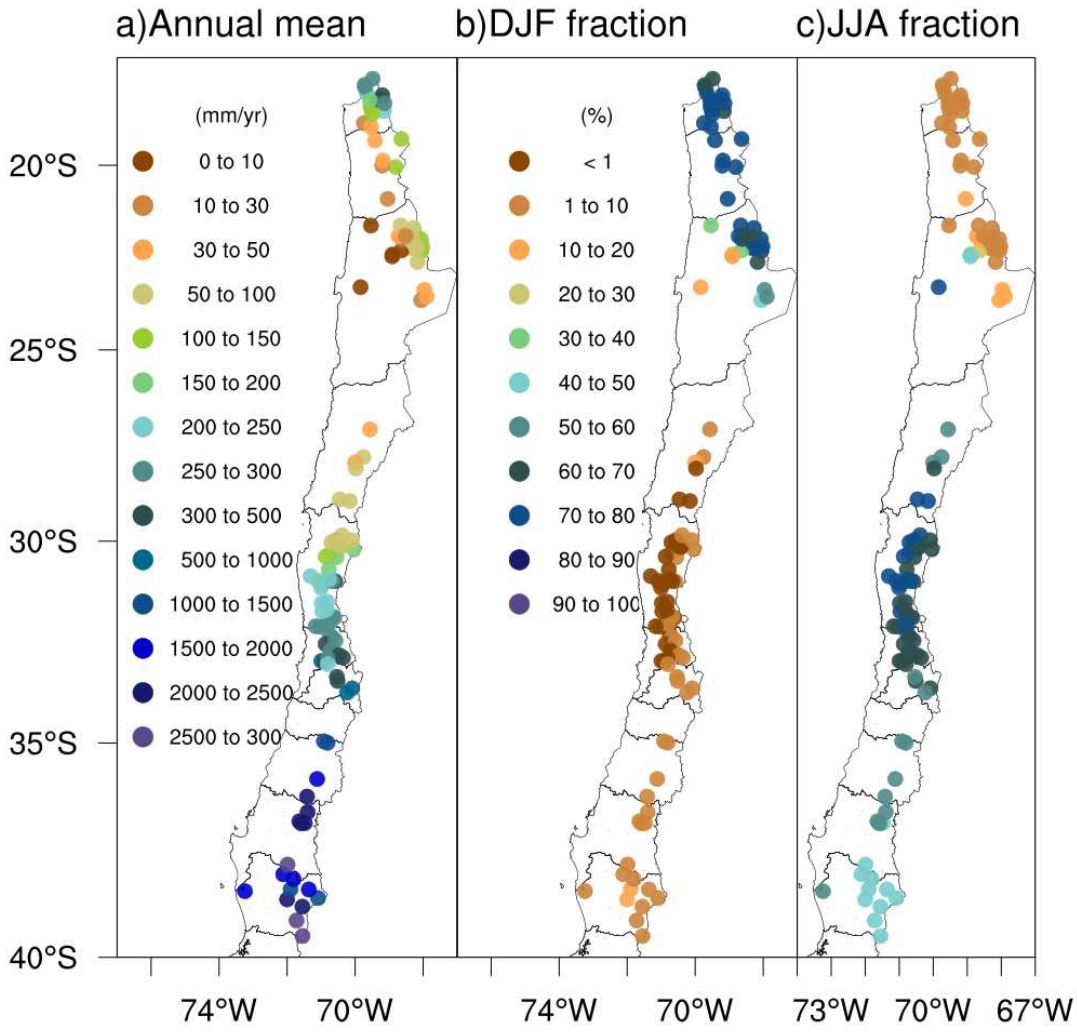

Figure 2.2: a) Spatial distribution of the annual mean accumulation of precipitation. b) Summer (DJF) fraction of the annual total and c) winter (JJA) fraction of the annual total.

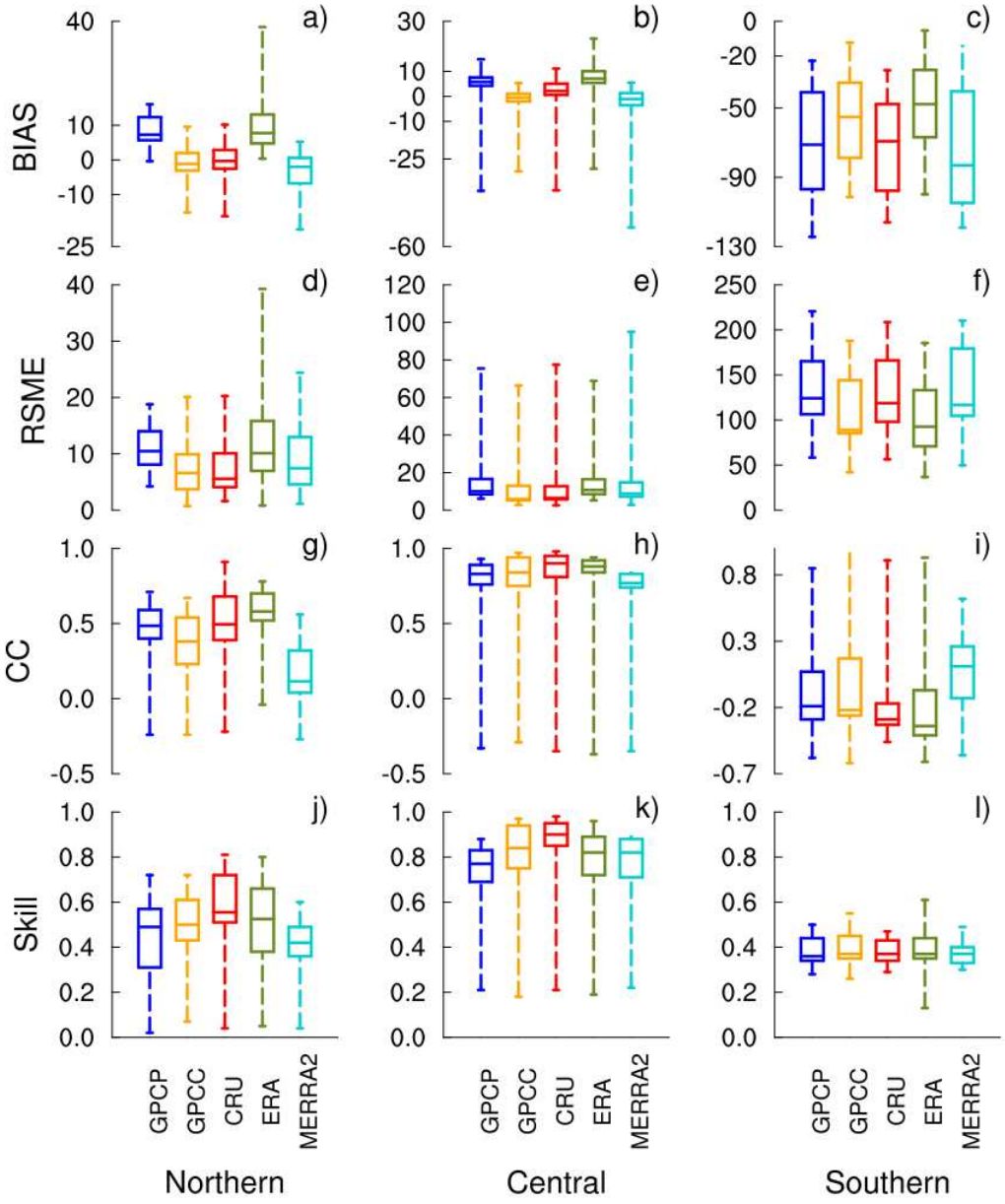

Figure 2.3: Distribution of bias (a-c), RMSE (d-f), CC (g-i) and Willmott's index of agreement (Skill) (j-l) of annual accumulation precipitation. The line in the Box represents the median (50%), the bottom and top of the Box represent the 1st (25%) and 3st (75%) quartiles, the whiskers indicate variability outside the lower and upper quartiles. Note that axis range for bias and RSME differs in each panel.

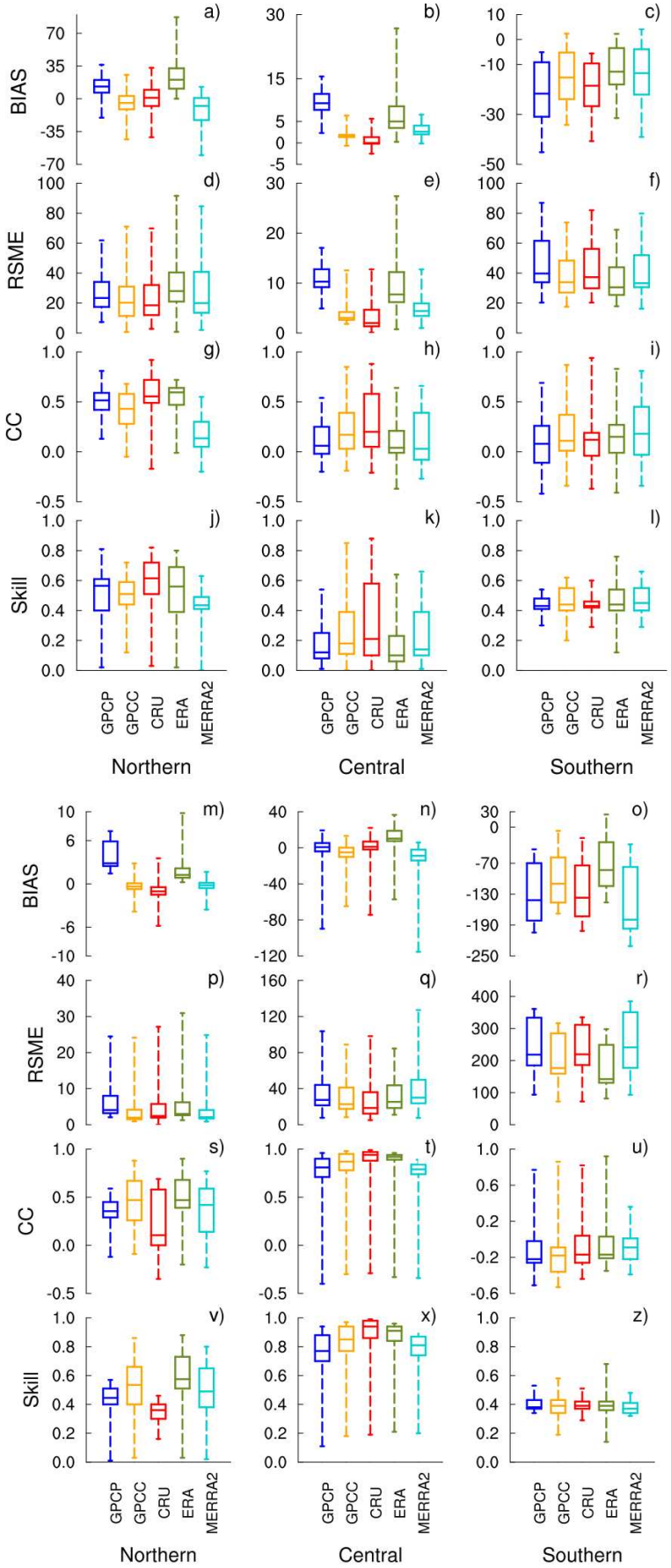

Figure 2.4: As Figure 3, but for summer (DJF) (a-l) and winter (JJA) (m-z) precipitation.

Annual and seasonal precipitation trends

Observational datasets show that negative trends in annual total precipitation are widespread in the North and Central Chile (Fig. 5a). This is consistent with earlier findings of Quintana (2012). Few exceptions are observed in Northern Chile, with negative trends in high altitudes and positive or no trends in low altitudes, which 20% of trends are statistically significant and 59.5% non-significant. The greatest magnitude of significant negative trends is observed in Central Chile (34º59'56"S – 70º48'41"W), with -728 mm/decade.

The number of observations that have no trends are dominant between 21ºS and 34ºS in the summer season, and during winter northward to 25ºS (Fig. 5f,k). Non-significant positive trends are observed, northward to 21ºS and southward to 36ºS during the summer season, whereas in winter there are positive trends southward to 35ºS. These positive trends for summer and winter may be associated with the increase of extreme rainfall events (Pfahl et al. 2017). However, observed negative trend signal during winter corresponds to 53% of the stations, which 14% are significant (Fig. 5m). This is consistent with previous drought linked to decreasing frequency of winter precipitation in this region and in the most Mediterranean climates (Boisier et al. 2016; Garreaud et al. 2017; Polade et al. 2017).

Annual precipitation trends delivered by gridded datasets shows good agreement with the observed pattern, with frequent negative trends throughout the region (Fig. 5b-f). Southward 25ºS, all datasets indicate reduction in precipitation. A slightly less coherent pattern is detected in Northern, where GPCP, GPCC and CRU present some locations with positive trends, opposite to the corresponding instrumental observations. This likely from the effect of precipitation trends delivered by both datasets for summer (Fig. 5k,l). Between 27ºS and 35ºS the annual trend is a response to winter conditions because no trends are detected in summer from observations and also delivered by CRU. In the southernmost part of the region, there is no dominant season (DJF, JJA) in the annual trend. It is important to note that the dry bias delivered by MERRA2 results to a negative trend in both summer and winter conditions

(Fig. 5l,r).

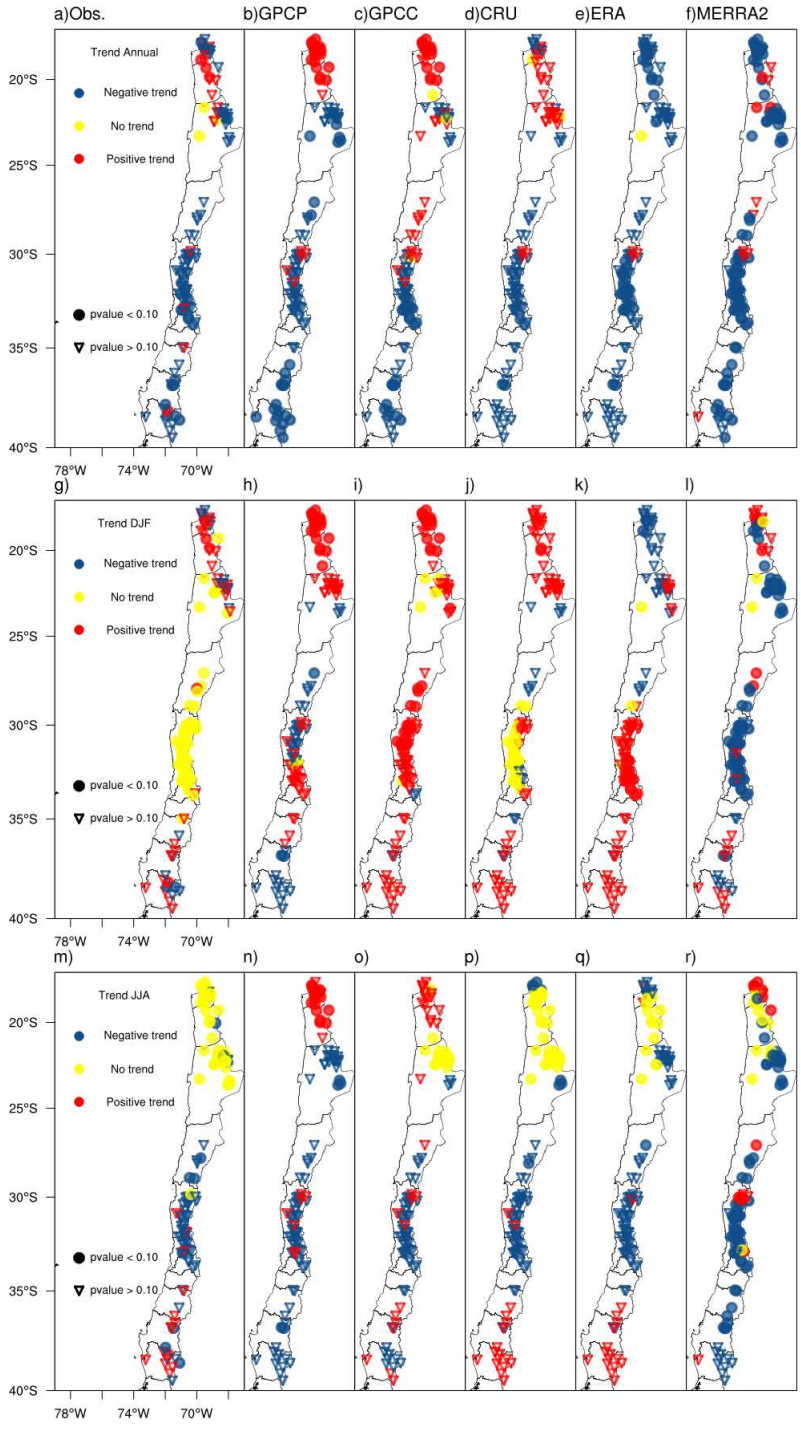

Figure 2.5: Annual and seasonal trend of precipitation from stations observations and gridded data. The filled circles are related to statistically significant trends at the 10% level.

Relationship of precipitation and climate modes

Observed precipitation time series show significant positive correlations with El Niño 1.2 and El Niño 3.4 indices, particularly in Central region, in both seasons (Table 2). The precipitation pattern in Northern Chile is not affected by ENSO at the annual scale. On the other hand, seasonal precipitation presents a strong relationship with ENSO in Northern Chile, with negative (positive) significant correlation in summer (winter). A similar response is also detected in the Southern region in relation to Niño 3.4. It is well known that El Niño events induce wet (dry) conditions in Central Chile in winter (summer), associated with northward migration (southern permanency) of subtropical anticyclone (Montecinos and Aceituno 2003; Valdés-Pineda et al. 2015).

Observations are more closely related to the El Niño 3.4 index, with statistically significant higher correlations ranging from to 0.33 to 0.60. The influence of the PDO and AAO is less noticeable, except for annual and winter precipitation. The AAO index is significant in the South region with correlation by up to 0.48 during summer.

The correlation based on gridded datasets shows a different pattern for both indices as compared to observations. The main differences between gridded datasets and observations are link to the signal of the correlation. For ENSO indices, GPCC, CRU and ERA-I are able to mimic the correlation signal described based on instrumental observations, although CRU and ERA-I do not show significant values during summer and winter in the North, unlike the pattern for Niño 1.2. The MERRA2 and GPCP show negative and positive correlations during summer in Central and Southern Chile, with both ENSO indices. In contrast to observed data, gridded datasets do not show any significant correlations between summer precipitation and ENSO indices over Central Chile.

Regarding the PDO and AAO, CRU reproduces well the significant correlations found for the instrumental observations. In general, gridded datasets tend to correlate higher with PDO and AAO relative to observational data, in particular

GPCP, GPCC, CRU and ERA-I with AAO in Southern region.

Table 2.2: Correlation coefficients between time-series of annual and seasonal precipitation from observed and gridded datasets with climate indices. Columns are organized according to Northern (N) Central (C) and Southern (S) regions. Bold numbers indicate statistically significant correlations at the 5% level and bold with asteriscs are significant at the 10% level.

Data	**Season**	**Niño1.2**			**Niño3.4**			**PDO**			**AAO**		
		N	C	S	N	C	S	N	C	S	N	C	S
Obs.	Annual	-0.11	**0.49**	0.13	-0.17	**0.53**	**0.46**	-0.15	**0.30***	0.12	0.10	-0.19	-0.23
	DJF	**-0.29**	**0.35**	-0.15	**-0.49**	**0.33**	**-0.45**	-0.15	-0.02	**-0.27***	-0.20	0.14	**0.48**
	JJA	**0.34**	**0.45**	0.19	**0.42**	**0.60**	**0.34**	**0.36**	0.26	0.11	0.13	-0.09	-0.26
GPCP	Annual	-0.11	**0.40**	0.18	-0.18	**0.44***	**0.45**	-0.01	0.23	**0.37**	0.08	-0.25	**-0.45***
	DJF	**-0.39**	0.14	-0.09	**-0.40**	0.12	0.12	0.11	0.13	-0.07	0.11	-0.39	**-0.33**
	JJA	**0.32***	**0.35**	0.13	**0.39**	**0.53**	**0.30***	0.22	0.16	**0.39**	0.16	-0.08	-0.02
GPCC	Annual	-0.18	**0.44**	0.19	-0.26	0.49	0.44	-0.09	0.29*	0.27*	0.19	-0.28*	-0.40
	DJF	**-0.36**	-0.04	-0.18	-0.45	-0.09	-0.01	0.05	-0.30*	-0.24	0.08	0.13	-0.13
	JJA	**0.25**	**0.40**	0.14	0.46	0.57	0.24	0.24	0.22	0.28*	0.15	-0.08	0.01
CRU	Annual	-0.12	**0.47**	0.21	-0.09	**0.49**	**0.47**	-0.15	**0.29***	0.18	0.03	-0.25	**-0.33**
	DJF	-0.27	0.23	-0.18	**-0.40**	0.14	-0.02	-0.15	0.16	**-0.27***	0.14	-0.26	**-0.18**
	JJA	**0.41**	**0.46**	0.26	**0.51**	**0.60**	**0.31***	0.07	0.25	0.19	0.02	-0.08	-0.01
ERA	Annual	-0.08	**0.44**	0.13	-0.03	**0.46**	**0.38**	0.02	**0.32***	0.25	0.08	-0.26	**-0.40**
	DJF	**-0.35**	-0.05	-0.06	**-0.44**	-0.20	0.08	0.03	-0.33	-0.19	0.06	-0.06	**-0.06**
	JJA	0.23	**0.42**	0.15	**0.41**	**0.53**	0.21	**0.28***	**0.32***	0.22	0.06	-0.05	0.01
MERRA2	Annual	-0.09	**0.35**	0.13	0.06	**0.46**	**0.34**	0.13	**0.30***	**0.33**	-0.25	**-0.34**	**-0.32***
	DJF	-0.16	-0.01	-0.19	-0.13	-0.05	-0.04	0.14	-0.14	-0.25	**0.37**	**0.34**	**-0.13**
	JJA	**0.28***	**0.29***	0.17	**0.37**	**0.54**	0.20	0.17	0.27	**0.36**	-0.06	-0.12	0.01

Extreme precipitation indices

Neither instrumental observations nor gridded datasets show consistent trends in CWD for annual and seasonal level (Fig. 6), except for some significant positive trends over Northern Chile in the annual scale. Conversely, MERRA2 presents some negative trends in several locations. Turning to annual CDD shows general significant positive trends over the entire study area (Fig. 7). This pattern is well reproduced by GPCP and ERA-I, while GPCC and MERRA2 are slightly more negative. Observations deliver by about 81% of the stations have positive trends, with 28.5% statistically significant. Insofar as gridded dataset is concerned, GPCP shows 75% of positive trends, GPCC with 59%, ERA-I 84%, and MERRA2 with 54%.

On the other hand, CDD during summer conditions show negative trends in Northern Chile, standing out as the only region with some detectable trends (22.5%) (Fig. 7f). GPCP delivers a widespread negative trend whereas MERRA2 shows positive trends in most locations during the summer season. In winter, observations and almost all gridded datasets show no change of precipitation in Northern region, conversely, positive trend is found in Central Chile, except for GPCC. About 83% of stations deliver positive trends (8% statistically significant), followed by GPCP with 87%, 54% for GPCC, 94% ERA-I and MERRA2 with 77%.

It is important to note that these results agree with the observational precipitation trends, particularly on the annual scale delivered by the monthly data. This is important because the increase in episodes of drought can lead to major economic losses in various locations. These changes agree with the findings of others studies with increasing of CDD in Chile (e.g. Henríquez et al. 2019).

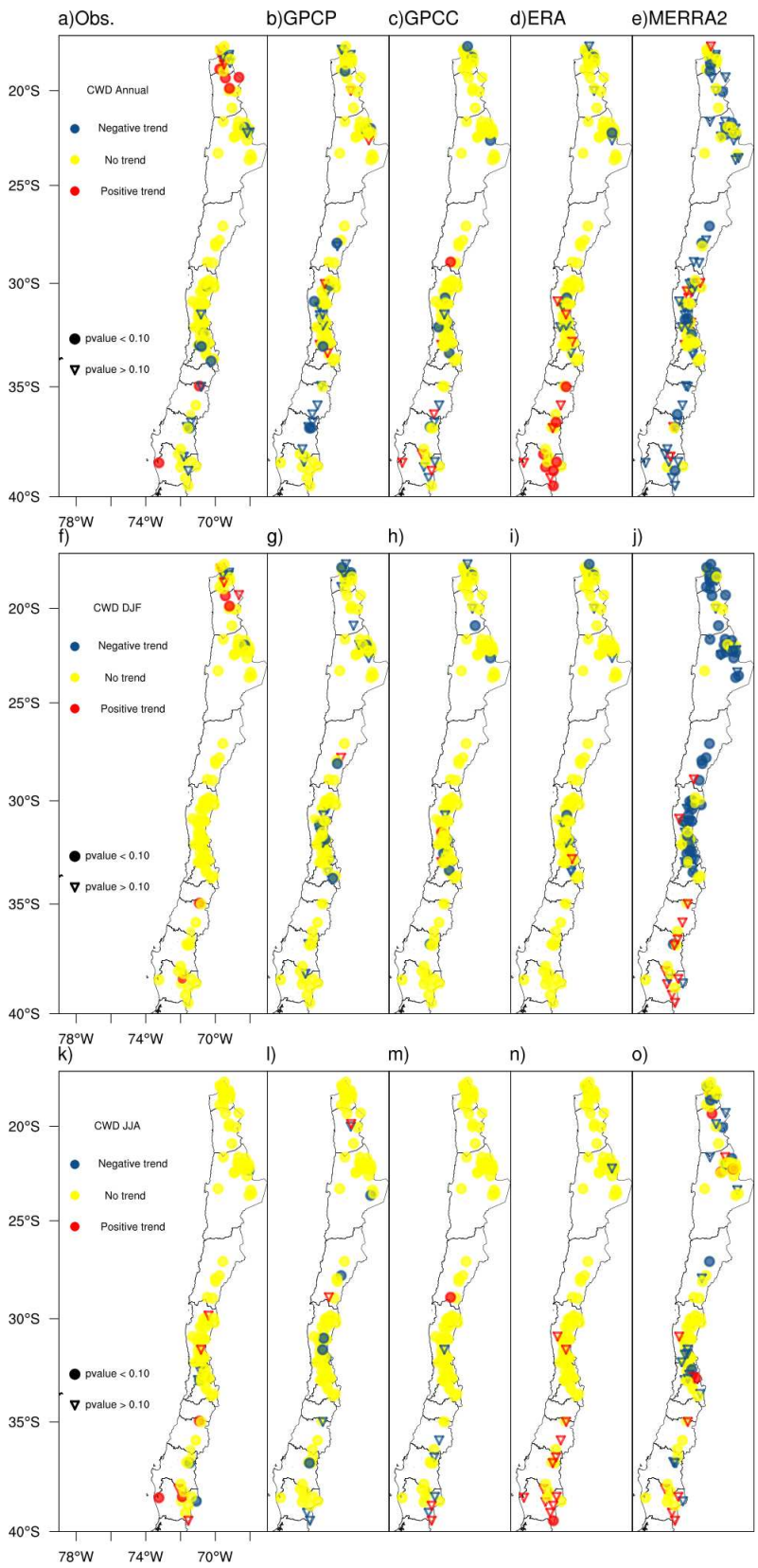

Figure 2.6: As Figure 5, but for annual and seasonal maximum number of consecutive wet days (CWD).

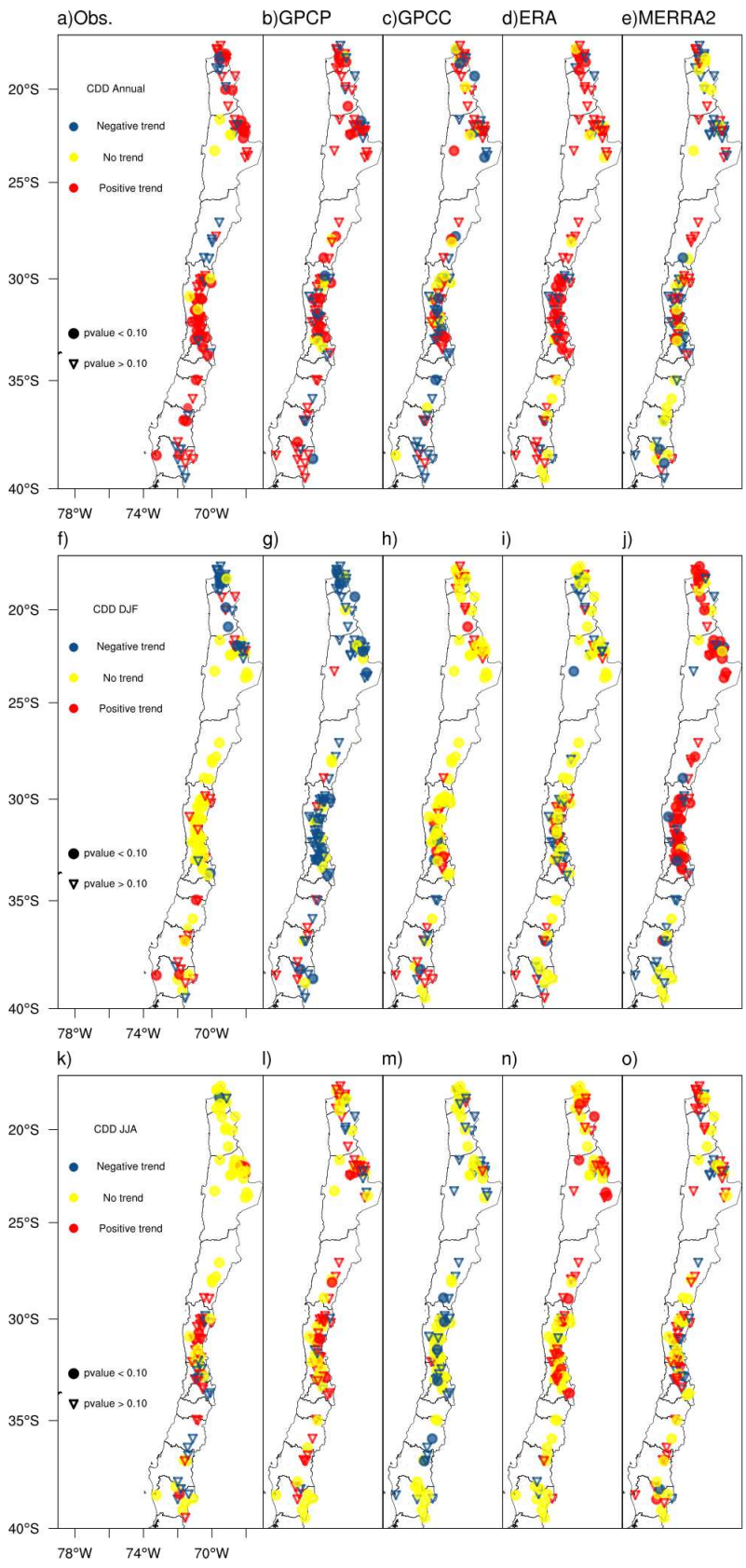

Figure 2.7: As Figure 5, but for annual and seasonal maximum number of consecutive dry days (CDD).

Annual and seasonal temperature analyses

Figure 8 shows the distribution of annual and seasonal mean surface temperature based on observations. The mean annual temperature varies between 9ºC and 19ºC. Higher temperature values occur in Central Chile, between 27ºS and 34ºS. Mean summer temperatures within the altitudinal range considered in our study can reach up to 23ºC. In winter, temperature fluctuates around 12ºC, southward to 35ºS the values are lower and range between 3ºC to 7ºC. In Northern region (17ºS to 24ºS) temperature presents lower seasonal variability, with differences between summer and winter by about 4ºC and 8 ºC, varying with altitude.

Comparison between gridded datasets and observations for annual surface temperature are shown in Figure 9. There is an overall cold bias in the whole region, but more noticeable within in Central Chile. In the North, smaller bias is depicted by MERRA2, with median values close to zero and a interquartile range between 0ºC and -2ºC (Fig. 9a). In Central Chile, MERRA2 also exhibits smaller bias followed by ERA-I and CRU. On the other hand, Southern Chile presents an inverse pattern with CRU having smaller bias and MERRA2 greater variability (Fig. 9b,c). Datasets with large biases are tend to show by high RMSE (Fig. 9d-f). Correlation analyses and the Skill index are in line with already decribed for biases and RMSE.

As in the case for annual comparisons, seasonal disaggregation indicates a cold bias in summer and winter in all gridded datasets along this high Andean region, except for CRU in Southern Chile during summer (Fig. 10a). Evaluation for RMSE shows similar values in summer as well as in winter, with large bias paired with high RMSE. The bias, RMSE, CC and Skill values show that all datasets provide a good approximation to observed surface temperature over Northern Chile during summer, and North and South regions in winter. In general, MERRA2 matches closely with observations in Northern and Central Chile, while CRU has a good performs in Southern Chile.

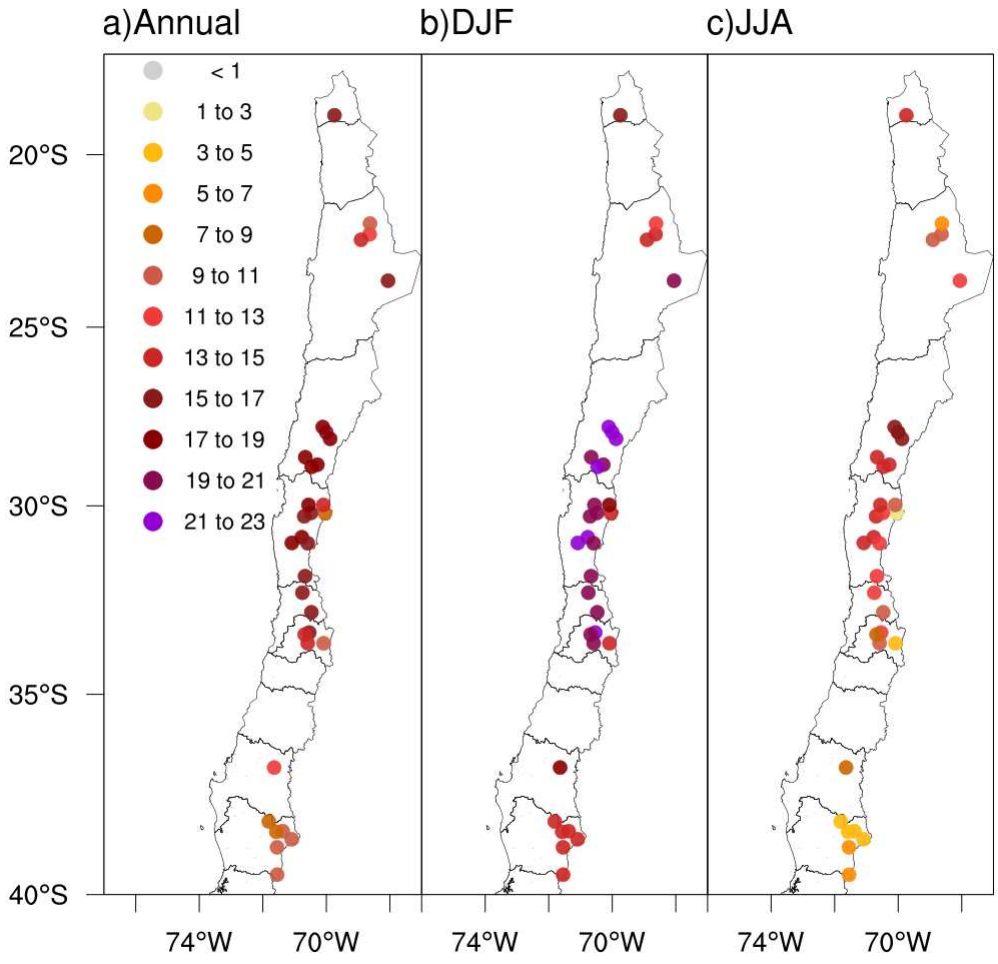

Figure 2.8: Spatial distribution of the annual and seasonal mean temperature from weather station observations.

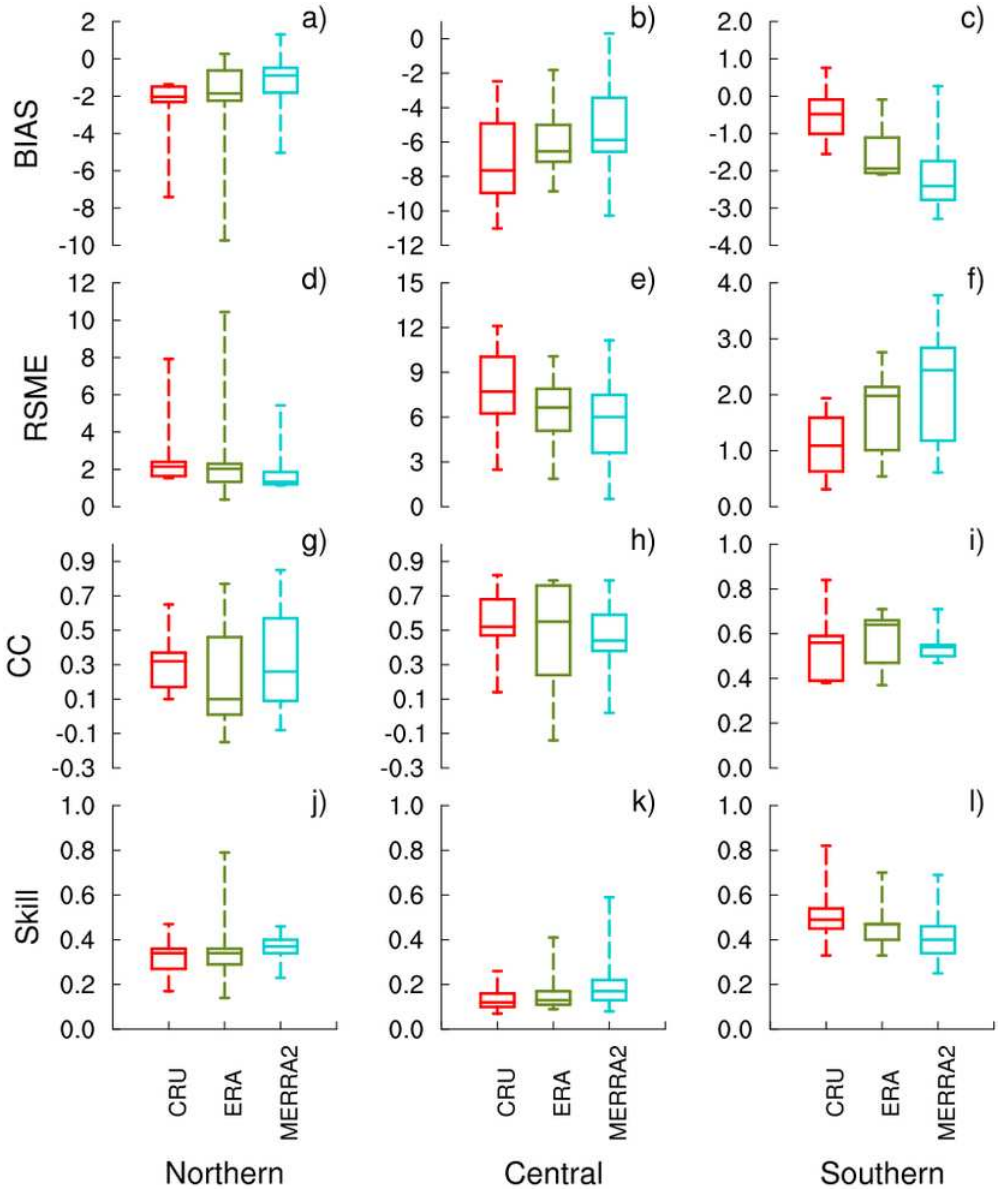

Figure 2.9: Distribution of bias (a-c), RMSE (d-f), CC (g-i) and Willmott's index of agreement (Skill) (j-l) of annual mean temperature. The line in the Box represents the median (50%), the bottom and top of the Box represent the 1st (25%) and 3st (75%) quartiles, the whiskers indicate variability outside the lower and upper quartiles. Note that axis range for bias and RSME differs in each panel.

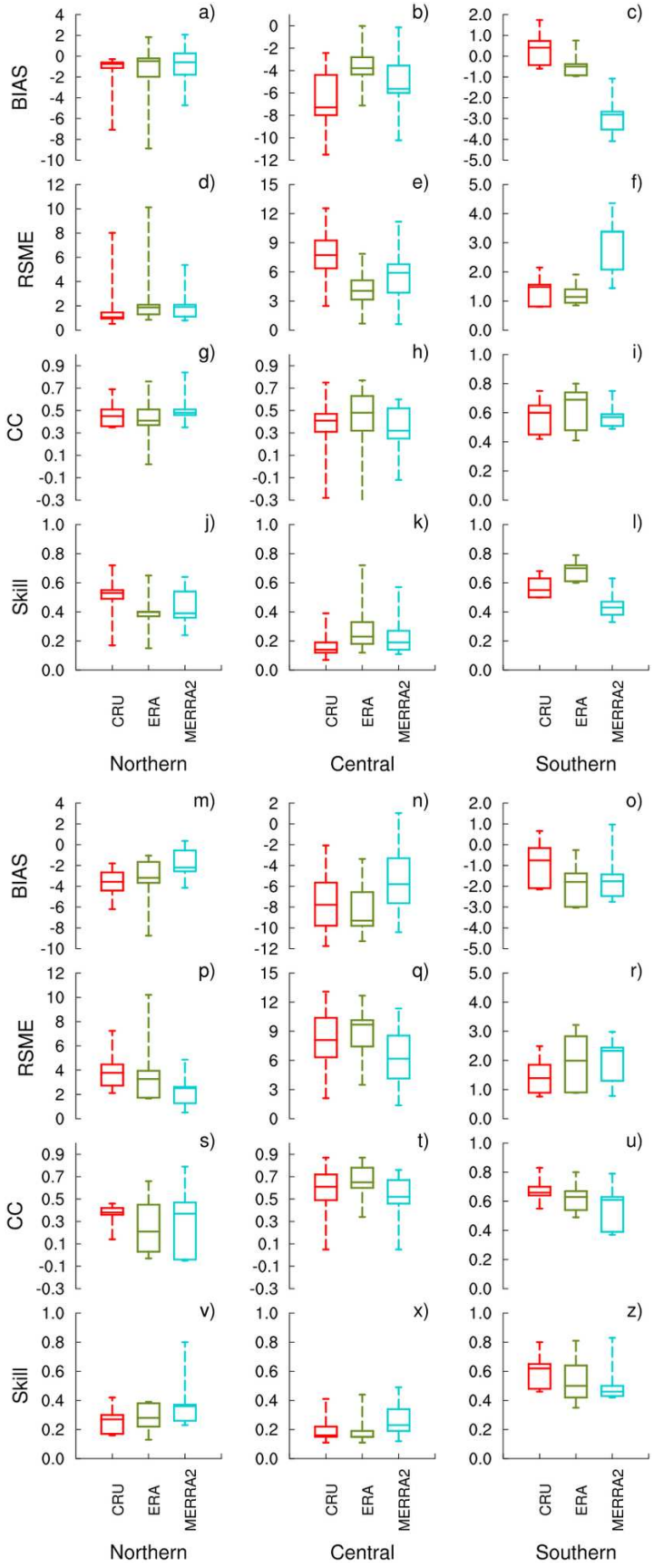

Figure 2.10: As Figure 9, but for (a-l) summer and winter (m-z) temperature.

Annual and seasonal temperature trends

Figure 11a shows that, with few exceptions, there are significant positive trends in the mean annual surface temperature. The warming trends correspond to about 79% of observations, where 38% are statistically significant, with a maximum magnitude of 0.68ºC decade-1 in Northern Chile, and 0.43ºC/decade in Central Chile. It is important to note that although 41% of the other stations do not show statistically significant changes, they are dominated by positive trends as well.

Significant warming trends are also identified in summer (71% of stations) and winter (65% of stations) with a positive trend signal. About 26.5% and 20.5% are statistically significant trends for summer and winter observations (Fig. 11e,i). This is consistent with earlier findings for Northern region (Meseguer-Ruiz et al. 2018) as well as for Central Chile (Burger et al. 2018), suggesting the end of the regional cooling trend that occurred between 1979 and 2006, related to negative phase of the Interdecadal Pacific Oscillation (IPO), allowing widespread warming trends associated with an increase of sea surface temperature.

Patterns of annual and seasonal variability from gridded datasets are similar to instrumental observations pattern, with dominance of positive trends. Annual and summer temperature trends diverge over Central part of the studied region where MERRA2 displays more stations with no trend (Fig. 11d,h). In contrast, statistically significant upward trends predominate in ERA-I. During winter season, there is an increase in the number of stations that do not experience trends, in particular CRU and MERRA2.

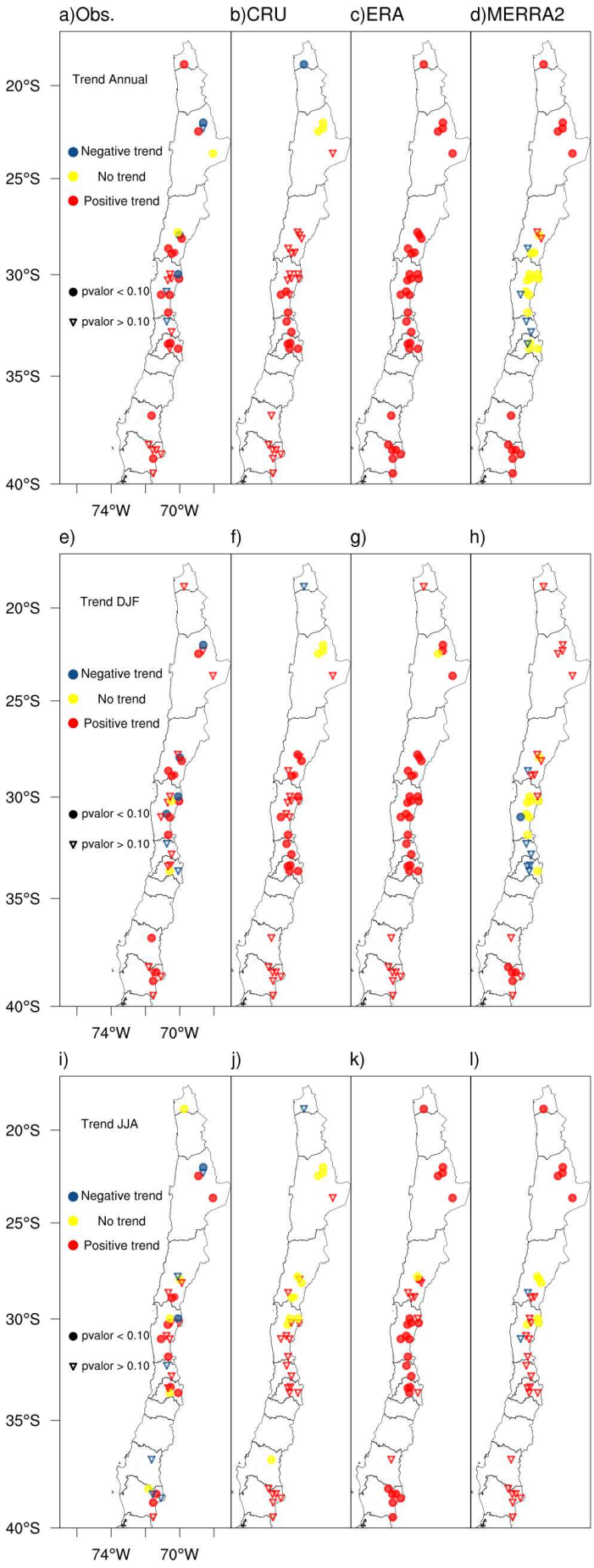

Figure 2.11: Annual and seasonal trend of temperature from stations observations and gridded data. The filled circles are related to statistically significant trends at the 10% level.

Temperature and climate modes

Table 3 shows the temporal correlation between annual and seasonal temperatures and climate indices. Changes in El Niño 1.2 lead to substantial modification in the observed annual surface temperature pattern in Northern and Southern Chile, while in Central Chile changes are more related with El Niño 3.4.

This agreement between temperature and ENSO indices in Northern region is captured by all gridded datasets, except for MERRA2 for El Niño 1.2 during winter. It should be mentioned that correlations shown by CRU in Central Chile exhibit a similar behavior as those calculated from observations. Annual and seasonal observed temperature do not correlate with neither PDO nor AAO. ERA-I replicates this behavior for these climate modes. Conversely, CRU presents a positive correlation with PDO, and MERRA2 with PDO and AAO in Northern and Central Chile.

Table 2.3: Correlation coefficients between observed and gridded datasets of annual and seasonal temperature with climate indices. Columns are organized according to Northern (N), Central (C) and Southern (S) regions. Bold numbers indicate statistically significant correlations at the 5% level and bold with asteriscs are significant at the 10% level. Negative and positive correlations are highlighted in the light blue and red cells, respectively.

Data	**Season**	**Niño1.2**			**Niño3.4**			**PDO**			**AAO**		
		N	C	S	N	C	S	N	C	S	N	C	S
Obs.	Annual	**0.45**	0.09	**0.28***	**0.56**	**0.35**	0.20	0.15	-0.04	-0.01	0.11	0.09	0.20
	DJF	**0.53**	0.13	-0.13	**0.65**	0.11	-0.22	0.23	0.11	-0.15	0.08	0.01	-0.10
	JJA	**0.35**	-0.06	0.13	**0.40**	**0.27***	0.24	0.12	-0.07	0.11	-0.04	0.02	0.20
CRU	Annual	**0.80**	**0.30***	**0.35**	**0.81**	**0.45**	0.24	**0.46**	0.21	0.01	0.09	0.23	0.19
	DJF	**0.70**	-0.01	-0.06	**0.60**	-0.03	-0.19	**0.28***	0.14	-0.22	0.09	-0.01	0.03
	JJA	**0.65**	0.21	0.16	**0.65**	**0.46**	0.27	0.43	0.15	0.12	0.05	0.03	0.17
ERA	Annual	**0.33**	0.07	0.23	**0.47**	0.21	0.13	0.03	-0.20	-0.16	0.11	0.12	0.15
	DJF	**0.65**	0.16	-0.06	**0.66**	0.15	-0.14	0.15	0.10	-0.19	0.04	-0.09	-0.03
	JJA	**0.29***	-0.06	0.10	**0.36**	0.27	0.23	-0.05	-0.06	-0.02	-0.05	0.01	0.15
MERRA2	Annual	**0.34**	-0.05	0.11	**0.52**	0.12	-0.04	0.17	0.28	0.23	**0.31***	**0.34**	0.26
	DJF	**0.70**	0.19	-0.13	**0.70**	**0.28***	-0.22	**0.28***	**0.54**	-0.06	-0.16	-0.08	-0.02
	JJA	0.18	-0.19	0.05	**0.45**	0.07	0.05	0.02	0.09	0.26	-0.03	0.05	0.14

Conclusion

In this study, we have evaluated the performance of five gridded datasets in reproducing the observed annual and seasonal mean precipitation, and surface temperature over North, Central and South over Chilean Andes. In addition, long-term trends are also analyzed with focus on high-elevated areas from observations and gridded datasets.

The ability of gridded datasets to represent the observed precipitation as well as temperature is variable, in part due to their coarse spatial resolution leading to misrepresentation of the complex topography in Chilean Andes. Weaker performance was shown by GPCP very likely related to coarsest spatial resolution compared to other datasets. However, a coarser grid cell does not always translate into good or poor performance. For instance, GPCC superior performance in precipitation is achieved with only 1° grid-cell size, contrasts with the lower skill of MERRA2 with a relatively fine spatial resolution (0.5°).

The results demonstrated that the performance of each datasets varies on the Andean regions analyzed, fluctuating on overestimating or underestimating the precipitation and temperature. It has been demonstrated that there are several differences between gridded datasets and observations. These differences are larger in Northern Chile (17ºS-24ºS) and southward 35ºS in relation to total precipitation, whereas for surface temperature disagreement is higher in Central Chile, between 27ºS and 35ºS. In general, good performance is achieved by CRU, GPCC, and ERA-I in most precipitation analyzes, whereas CRU, ERA-I, and MERRA2, respectively for temperature analyzes. Regarding reanalysis, MERRA2 tends to underestimate precipitation and temperature mainly in the central and southern regions, leading to greater mismatches with observation, and disagreement in trends analysis.

It has also been investigated correlations between climate indices with precipitation and temperature patterns. The response of precipitation to ENSO based on gridded datasets are consistent in the sense that higher significant correlations occur

in Central Chile, being related to the regions with higher number of observations. Additional to ENSO, this region is also affected by PDO, with good agreement between observed and gridded datasets. Our analysis also showed that the AAO plays a role in summer precipitation in Southern Chile. On the other hand, surface temperature depicted by observed and gridded datasets are strongly correlated with ENSO in Northern sector, while PDO and AAO indices do not seem to related with temperature, except by for CRU and MERRA2 in North and Central regions.

Our work evidences a significant reduction of annual precipitation and warming trends in the high Chilean Andes during the study period. Observations and most of gridded datasets show a decrease of winter precipitation, especially in Central Chile, as well as an increase of the consecutive number of dry days is detected in annually in all regions on this study, particularly in Central Chile during winter season. This combination of increased temperature and reduced precipitation may contribute to intensify the extreme dry events in arid areas, critically affecting the current availability water resources management in Chile. Moreover, if these changes in temperature and precipitation continue can pose a serious threat to the stability of the glaciers due to mass imbalance.

References

Adler, R.F., Huffman, G.J., Chang, A., Ferraro, R., Xie, P.-P., Janowiak, J., Rudolf, B., Schneider, U., Curtis, S., Bolvin, D., Gruber, A., Susskind, J., Arkin, P., Nelkin, E., 2003. The Version-2 Global Precipitation Climatology Project (GPCP) Monthly Precipitation Analysis (1979–Present). J Hydrometeorol.

Adler, R.F, Sapiano, M., Huffman, G.J., Wang, J. J., Gu, G., Bolvin, D., ... Xie, P., 2018. The Global Precipitation Climatology Project (GPCP) monthly analysis (new version 2.3) and a review of 2017 global precipitation. Atmosphere, 9(4), 138.

Alvarez-Garreton, C., Mendoza, P. A., Boisier, J. P., Addor, N., Galleguillos, M., Zambrano-Bigiarini, M., ... and Ayala, A., 2018. The CAMELS-CL dataset: catchment attributes and meteorology for large sample studies-Chile dataset. Hydrology and Earth System Sciences, 22(11), 5817-5846.

Angélil, O., Perkins-Kirkpatrick, S., Alexander, L. V., Stone, D., Donat, M.G., Wehner, M., Shiogama, H., Ciavarella, A., Christidis, N., 2016. Comparing regional precipitation and temperature extremes in climate model and reanalysis products. Weather Clim Extrem 13, 35–43.

Bao, X., Zhang, F., 2013. Evaluation of NCEP–CFSR, NCEP–NCAR, ERA-Interim, and ERA-40 reanalysis datasets against independent sounding observations over the Tibetan Plateau. Journal of Climate, 26 (1), 206-214.

Barrett, B.S., Garreaud, R., Falvey, M., 2009. Effect of the Andes Cordillera on Precipitation from a Midlatitude Cold Front. Mon Weather Rev 137, 3092–3109.

Bieniek, P.A., Bhatt, U.S., Walsh, J.E., Rupp, T.S., Zhang, J., Krieger, J.R., Lader, R., 2016. Full access dynamical downscaling of ERA-interim temperature and precipitation for Alaska. J Appl Meteorol Climatol 55, 635–654.

Blacutt, L.A., Herdies, D.L., de Gonçalves, L.G.G., Vila, D.A., Andrade, M., 2015. Precipitation comparison for the CFSR, MERRA, TRMM3B42 and Combined Scheme datasets in Bolivia. Atmos Res 163, 117–131.

Boisier, J.P., Rondanelli, R., Garreaud, R.D., Muñoz, F., 2016. Anthropogenic and natural contributions to the Southeast Pacific precipitation decline and recent megadrought in central Chile. Geophys Res Lett 43, 413–421.

Bosilovich, M.G., Robertson, F.R., Takacs, L., Molod, A., Mocko, D., 2017. Atmospheric water balance and variability in the MERRA-2 reanalysis. J Clim 30, 1177–1196.

Bradley, R.S., 2006. Climate Change: Threats to Water Supplies in the Tropical Andes. Science (80-) 312, 1755–1756.

Bromwich, D. H., Fogt, R. L., 2004. Strong trends in the skill of the ERA-40 and NCEP–NCAR reanalyses in the high and midlatitudes of the Southern Hemisphere, 1958–2001. Journal of Climate,17 (23), 4603-4619.

Bromwich, D.H., Nicolas, J.P., Monaghan, A.J., 2011. An Assessment of precipitation changes over Antarctica and the southern ocean since 1989 in contemporary global reanalyses. J Clim 24, 4189–4209.

Burger, F., Brock, B., Montecinos, A., 2018. Seasonal and elevational contrasts in temperature trends in Central Chile between 1979 and 2015. Glob Planet Change 162, 136–147.

Caroletti, G. N., Coscarelli, R., Caloiero, T., 2019. Validation of Satellite, Reanalysis and RCM Data of Monthly Rainfall in Calabria (Southern Italy). Remote Sensing, 11(13), 1625.

Comin, A.N., Schumacher, V., Justino, F., Fernández, A., 2018. Impact of different microphysical parameterizations on extreme snowfall events in the Southern Andes. Weather Clim Extrem 21, 65–75.

Cortés, G., Girotto, M., Margulis, S., 2016. Snow process estimation over the extratropical Andes using a data assimilation framework integrating MERRA data and Landsat imagery. Water Resour Res 52, 2582–2600.

Cowtan, K., Way, R.G., 2014. Coverage bias in the HadCRUT4 temperature series and its impact on recent temperature trends. Q J R Meteorol Soc 140, 1935–1944.

Dee, D.P., Uppala, S.M., Simmons, a. J., Berrisford, P., Poli, P., Kobayashi, S., Andrae, U., Balmaseda, M. a., Balsamo, G., Bauer, P., Bechtold, P., Beljaars, a. C.M., van de Berg, L., Bidlot, J., Bormann, N., Delsol, C., Dragani, R., Fuentes, M., Geer, a. J., Haimberger, L., Healy, S.B., Hersbach, H., Hólm, E. V., Isaksen, L., Kållberg, P., Köhler, M., Matricardi, M., Mcnally, a. P., Monge-Sanz, B.M., Morcrette, J.J., Park, B.K., Peubey, C., de Rosnay, P., Tavolato, C., Thépaut, J.N., Vitart, F., 2011. The ERA-Interim reanalysis: Configuration and performance of the data assimilation system. Q J R Meteorol Soc 137, 553–597.

Ebrahimi, S., Chen, C., Chen, Q., Zhang, Y., Ma, N., Zaman, Q., 2017. Effects of temporal scales and space mismatches on the TRMM 3B42 v7 precipitation product in a remote mountainous area. Hydrological processes, 31(24), 4315-4327.

El-Samra, R., Bou-Zeid, E., Bangalath, H.K., Stenchikov, G., El-Fadel, M., 2017. Future intensification of hydro-meteorological extremes: downscaling using the weather research and forecasting model. Clim Dyn 49, 3765–3785.

Fernández, A., Mark, B.G., 2016. Modeling modern glacier response to climate changes along the Andes Cordillera: A multiscale review. J Adv Model Earth Syst 8, 467–495.

Fujiwara, M., Wright, J.S., Manney, G.L., Gray, L.J., Anstey, J., Birner, T., Davis, S., Gerber, E.P., Lynn Harvey, V., Hegglin, M.I., Homeyer, C.R., Knox, J.A., Krüger, K., Lambert, A., Long, C.S., Martineau, P., Molod, A., Monge-Sanz, B.M., Santee, M.L., Tegtmeier, S., Chabrillat, S., Tan, D.G.H., Jackson, D.R., Polavarapu, S., Compo,

G.P., Dragani, R., Ebisuzaki, W., Harada, Y., Kobayashi, C., McCarty, W., Onogi, K., Pawson, S., Simmons, A., Wargan, K., Whitaker, J.S., Zou, C.Z., 2017. Introduction to the SPARC Reanalysis Intercomparison Project (S-RIP) and overview of the reanalysis systems. Atmos Chem Phys 17, 1417–1452.

Garreaud, R.D., 2009. The Andes climate and weather. Adv Geosci 22, 3–11.

Garreaud, R.D., Alvarez-Garreton, C., Barichivich, J., Pablo Boisier, J., Christie, D., Galleguillos, M., LeQuesne, C., McPhee, J., Zambrano-Bigiarini, M., 2017. The 2010-2015 megadrought in central Chile: Impacts on regional hydroclimate and vegetation. Hydrol Earth Syst Sci 21, 6307–6327.

Gu, G., and Adler, R. F., 2019. Precipitation, temperature, and moisture transport variations associated with two distinct ENSO flavors during 1979–2014. Climate dynamics, 52, 7249-7265.

Harris, I., Jones, P.D., Osborn, T.J., Lister, D.H., 2014. Updated high-resolution grids of monthly climatic observations - the CRU TS3.10 Dataset. Int J Climatol 34, 623–642.

Henríquez, Cristián et al., 2019. 50-Years of Climate Extreme Indices Trends and Inventory of Natural Disasters in Chilean Cities (1965–2015). In: Urban Climates in Latin America. Springer, Cham, p. 281-308.

Huang, D.Q., Zhu, J., Zhang, Y.C., Huang, Y., Kuang, X.Y., 2016. Assessment of summer monsoon precipitation derived from five reanalysis datasets over East Asia. Q J R Meteorol Soc 142, 108–119.

Justino, F., Setzer, A., Bracegirdle, T.J., Mendes, D., Grimm, A., Dechiche, G., Schaefer, C.E.G.R., 2011. Harmonic analysis of climatological temperature over Antarctica: Present day and greenhouse warming perspectives. Int J Climatol 31, 514–530.

Kendall M. 1975. Rank Correlation Methods. London: Charles Griffin

Lorenz, C., Kunstmann, H., 2012. The Hydrological Cycle in Three State-of-the-Art Reanalyses: Intercomparison and Performance Analysis. J Hydrometeorol 13, 1397–1420. Mann H. B. 1945. Nonparametric tests against trend Econometrica;13,245–59.

Manz, B., Buytaert, W., Zulkafli, Z., Lavado, W., Willems, B., Robles, L.A., Rodríguez-Sánchez, J.P., 2016. High-resolution satellite-gauge merged precipitation climatologies of the Tropical Andes. J Geophys Res Atmos 121, 1190–1207.

Masiokas, M.H., Villalba, R., Christie, D. a., Betman, E., Luckman, B.H., Le Quesne, C., Prieto, M.R., Mauget, S., 2012. Snowpack variations since AD 1150 in the Andes of Chile and Argentina (30°-37°S) inferred from rainfall, tree-ring and documentary records. J Geophys Res Atmos 117, 1–11.

Mayor, Y., Tereshchenko, I., Fonseca-Hernández, M., Pantoja, D., Montes, J., 2017. Evaluation of error in IMERG precipitation estimates under different topographic conditions and temporal scales over Mexico. Remote Sensing, 9(5), 503.

Meher, J. K., Das, L. (2019). Gridded data as a source of missing data replacement in station records. Journal of Earth System Science, 128(3), 58.

Meseguer-Ruiz, O., Ponce-Philimon, P.I., Guijarro, J.A., Sarricolea, P., 2019. Spatial distribution and trends of different precipitation variability indices based on daily data in Northern Chile between 1966 and 2015. International Journal of Climatology.

Meseguer-Ruiz, O., Ponce-Philimon, P.I., Quispe-Jofré, A.S., Guijarro, J.A., Sarricolea, P., 2018. Spatial behavior of daily observed extreme temperatures in Northern Chile (1966–2015): data quality, warming trends, and its orographic and latitudinal effects. Stoch Environ Res Risk Assess 6, 1–21.

Montecinos, A., Aceituno, P., 2003. Seasonality of the ENSO-related rainfall variability in central Chile and associated circulation anomalies. J Clim 16, 281–296.

Morice, C. P., Kennedy, J. J., Rayner, N. A., Jones, P. D., 2012. Quantifying uncertainties in global and regional temperature change using an ensemble of observational estimates: The HadCRUT4 data set. Journal of Geophysical Research: Atmospheres, 117(D8).

Neukom, R., Rohrer, M., Calanca, P., Salzmann, N., Huggel, C., Acuña, D., Christie, D.A., Morales, M.S., 2015. Facing unprecedented drying of the Central Andes? Precipitation variability over the period AD 1000–2100. Environ Res Lett 10, 084017.

New, M., Hulme, M., Jones, P., 2000. Representing twentieth-century space-time climate variability. Part II: Development of 1901-96 monthly grids of terrestrial surface climate. J Clim 13, 2217–2238.

Pendergrass, A. G., Knutti, R., 2018. The uneven nature of daily precipitation and its change. Geophysical ResearchLetters,45, 11,980–11,988.

Polade, S.D., Gershunov, A., Cayan, D.R., Dettinger, M.D., Pierce, D.W., 2017. Precipitation in a warming world: Assessing projected hydro-climate changes in Califor-

nia and other Mediterranean climate regions. Sci Rep 7, 1–10.

Quintana, J.M., 2012. Changes in the rainfall regime along the extratropical West coast 25, 1–22.

Rabatel, A., Francou, B., Soruco, A., Gomez, J., Caceres, B., Ceballos, J.L., Basantes, R., Vuille, M., Sicart, J.E., Huggel, C., Scheel, M., Lejeune, Y., Arnaud, Y., Collet, M., Condom, T., Consoli, G., Favier, V., Jomelli, V., Galarraga, R., Ginot, P., Maisincho, L., Mendoza, J., Ménégoz, M., Ramirez, E., Ribstein, P., Suarez, W., Villacis, M., Wagnon, P., 2013. Current state of glaciers in the tropical Andes: A multi-century perspective on glacier evolution and climate change. Cryosphere 7, 81–102.

Ragettli, S., Immerzeel, W.W., Pellicciotti, F., 2016. Contrasting climate change impact on river flows from high-altitude catchments in the Himalayan and Andes Mountains. Proc Natl Acad Sci 113, 9222–9227.

Rapaić, M., Brown, R., Markovic, M., Chaumont, D., 2015. An evaluation of temperature and precipitation surface-based and reanalysis datasets for the Canadian Arctic, 1950–2010. Atmosphere-Ocean, 53(3), 283-303.

Rivera, J. A., Marianetti, G., Hinrichs, S., 2018. Validation of CHIRPS precipitation dataset along the Central Andes of Argentina. Atmospheric Research, 213, 437-449.

Sarricolea, P., Romero, H., 2015. Variabilidad y cambios climáticos observados y esperados en el Altiplano del norte de Chile. Rev Geogr Norte Gd 62, 169–183.

Sarricolea, P., Herrera-ossandon, M., Meseguer-Ruiz, Ó., 2017. Climatic regionalization of continental Chile. J Maps 13, 66–73.

Sarricolea, P., Meseguer-Ruiz, Ó., Serrano-Notivolid, R., Sotoa, M.V., Martin-Vide, J., 2019. Trends of daily precipitation concentration in Central-Southern Chile. Atmos Res 85–98.

Schauwecker, S., Rohrer, M., Acuña, D., Cochachin, A., Dávila, L., Frey, H., Giráldez, C., Gómez, J., Huggel, C., Jacques-Coper, M., Loarte, E., Salzmann, N., Vuille, M., 2014. Climate trends and glacier retreat in the Cordillera Blanca, Peru, revisited. Glob Planet Change 119, 85–97.

Schauwecker, S., Rohrer, M., Huggel, C., Endries, J., Montoya, N., Neukom, R., Perry, B., Salzmann, N., Schwarb, M., Suarez, W., 2017. The freezing level in the tropical Andes, Peru: An indicator for present and future glacier extents. J Geophys Res 122, 5172–5189.

Serrano-Notivoli, R., Martín-Vide, J., Saz, M.A., Longares, L.A., Beguería, S., Sarricolea, P., Meseguer-Ruiz, O., M., de L., 2018. Spatio-temporal variability of daily precipitation concentration in Spain based on a high-resolution gridded data set. Int J Climatol 38, e518–e530.

Schneider, U., Becker, A., Finger, P., Meyer-Christoffer, A., Ziese, M., 2018. GPCC Full Data Monthly Product Version 2018 at 1.0°: Monthly LandSurface Precipitation from RainGauges built on GTSbased and Historical Data.

Silva, V.B.S., Kousky, V.E., Higgins, R.W., 2011. Daily Precipitation Statistics for South America: An Intercomparison between NCEP Reanalyses and Observations. J Hydrometeorol 12, 101–117.

Soares, P.M.M., Cardoso, R.M., Miranda, P.M.A., de Medeiros, J., Belo-Pereira, M., Espirito-Santo, F., 2012. WRF high resolution dynamical downscaling of ERA-Interim for Portugal. Clim Dyn 39, 2497–2522.

Ud din, S., A. Al-Dousari, A. Ramdan, and A. Al Ghadban, 2008. Site-specific precipitation estimate from TRMM data using bilinear weighted interpolation technique: An example from Kuwait, J. Arid Environ., 72(7), 1320–1328.

Urrutia, R., Vuille, M., 2009. Climate change projections for the tropical Andes using a regional climate model: Temperature and precipitation simulations for the end of the 21st century. J Geophys Res Atmos 114, 1–15.

Wilks D.S., 2006. Statistical Methods in the Atmospheric Sciences. 2nd ed., International Geophysics Series, vol. 91, Academic Press, 627 pp.

ValdésPineda, R., Valdes, J. B., Diaz, H. F., PizarroTapia, R., 2016. Analysis of spatiotemporal changes in annual and seasonal precipitation variability in South AmericaChile and related ocean–atmosphere circulation patterns. International Journal of Climatology, 36(8), 2979-3001.

Van den Broeke, M.R., Reijmer, C., Van As, D., Van de Wal, R., Oerlemans, J., 2005. Seasonal cycles of Antarctic surface energy balance from automatic weather stations. Ann Glaciol 41, 131–139.

Vuille, M., Francou, B., Wagnon, P., Juen, I., Kaser, G., Mark, B.G., Bradley, R.S., 2008. Climate change and tropical Andean glaciers: Past, present and future. Earth-Science Rev 89, 79–96.

Zazulie, N., Rusticucci, M., Raga, G.B., 2017. Regional climate of the subtropical

central Andes using high-resolution CMIP5 models:part I: past performance (1980-2005). Clim Dyn 0,1–21.

Chapter 3

Evaluation of WRF high resolution dynamical downscaling of precipitation in Central Andes

Introduction

The atmospheric conditions in the Central Andes of Chilean and Argentinean are associated to complex topography, lead to different precipitation scenarios with dry summers and intense winter orographic precipitation (Falvey and Garreaud, 2007; Viale and Nuñez, 2011). In fact, the natural barrier of the mountain range makes it difficult to install, maintain and expand a network of meteorological stations, leading to the lack of reliable measurements of long-term historical observations. In this way, the advance of regional climate modeling is crucial, especially in high-resolution precipitation on spatial and temporal scale, accounting for the socio-economic and water resource impacts associated with precipitation variations in this region.

In recent years, several gridded datasets like the reanalysis have been used to climate assessement on regional and global scales. However, almost all of these datasets have coarse horizontal resolutions, which leads to misrepresentation about various processes of regional and local climate variability, especially in complex terrains such as high mountainous region of the Andes (e.g. Ward et al. 2011; Soares et al. 2012).

To overcome these limitations, downscaling approaches are widely used to climate information at fine spatial resolution. Regional climate models (RCMs) have been applied for dynamical downscaling, with initial and lateral boundary conditions provided by the global climate model or reanalysis to improve resolution in the order

of a few kilometers to regional or local scales. This strategy has been frequently used in mountain regions in an attempt to reduce the scale mismatches, problem that exists between output large-scale climate and scale required at complex terrain (Mög and Kaser, 2011; Ambrizzi et al., 2019).

The Weather Research and Forecasting/Advanced Research (WRF) model is widely used by the scientific community to downscaling technique. The WRF reasonably simulates precipitation patterns and variability in several complex topography regions (Fathalli et al., 2016; Cardoso et al., 2013). Posada-Marín et al. (2019) showed that the WRF downscaling outperforms ERA-Interim reanalysis in the representation of precipitation related to a better representation of orographic effects over the tropical Cauca river valley in Colombia. However, little information is available on the performance of downscaling method in the Andean mountain region.

The aim of this study is to assess the WRF high resolution (9 and 3 km) performance in reproducing observations of precipitation along the complex terrain in Central Andes. This paper is organized as follows: Section 2 presents the study area. Section 3 the data and methods. Section 4 presents the results. The discussion of the main findings is presented in Section 5 and conclusions are summarized in Section 6.

Data and Methods

Study area

The study area covers the high-Andes of central Chile and Argentina (Figure 3.1). This region concentrates many glaciers and glacial lakes, which are the main source of water to important rivers that provide fresh water to more than 10 million people in Chile and more than 2 million in Argentina (Malmros et al., 2018). In the semi-arid Central Andes, the climate is characterized by wet and cold winters (April-September), with snow accumulation at high elevations. This contrasts with warm and dry summers (October-March) with almost zero precipitation and low relative humidity. This region is also commonly referred to as a Mediterranean-type climate (32ºS-38ºS) (Falvey and Garreaud, 2007; Pellicciotti et al., 2008; Bown et al., 2008; Bravo et al., 2017).

Those climate features are mainly associated with the northward-southward displacement of the high-pressure on the Pacific Ocean, which generally inhibits precipitation during the warm season, but allows the passage of westerlies and a the occurrence of frontal precipitation during the cold season (Masiokas et al., 2009). From longitudinal profile along the 33ºS the annual average precipitation ranges from 459 mm in Valparaiso (33.02ºS, 71.63ºW, 41 m) to 356 mm in Santiago (33.45ºS, 70.70ºW, 520 m) on the Chilean side, and 180 mm in Mendoza (32.89ºS, 68.83ºW, 769 m) on the Argentinean side (Corripio and Purves, 2005), clearly indicating the effect of topography.

WRF simulation

The model used in this study is the Weather Research and Forecasting/Advanced Research WRF (ARW) model (Skamarock et al., 2008) in its version 3.5.1. The WRF model was setup with two nested grids (Figure 1a), with high regional resolution at 9 km (WRF9km) and 3 km (WRF3km) horizontal grid spacing, using the two-way nesting technique. The both grids are centered in the Central Andes of Chile and Argentina, the coarser domain have 70 x 70 grid points, and 82 x 106 for the high-resolution inner nest. Both domains have 28 vertical levels between the surface and 50 hPa.

The WRF model run for 20 years, 1996-2015, using initial and lateral boundary conditions for the outer domain derived from the European Centre for Medium-Range Weather Forecasts (ECMWF), ERA-Interim reanalysis (ERA-I). Lateral forcing are updated every 6 h at a 0.75º horizontal resolution and 17 pressure levels. The physical parameterizations used include the WRF Single Moment 6-class (WSM6, Hong and Lim 2006). This scheme best shows performed compared to the other schemes in the high complex topography of the Andes (Comin et al., 2018). The radiation schemes of Rapid Radiative Transfer Model (RRTP, Mlawer et al. 1997) for longwave and Dudhia scheme (Dudhia, 1989) for shortwave. The MM5 similarity surface layer scheme (Paulson, 1970) are also used. The Yonsei University parameterization of the planetary Boundary Layer (Hong et al., 2006) and the Kain-Fritch scheme to atmospheric convection (Kain, 2004) are applied for outer domain but turned off for the inner domain in order to explicitly resolve the precipitation processes.

Observational datasets

Daily precipitation data in Central Chile and Argentina were used. The observations were provided by the Dirección General de Aguas (DGA) of Chile (http://snia.dga.cl/) and the Water Resources Agency of Argentina (Subsecretaría de Recursos Hídricos (SSRH); http://bdhi.hidricosargentina.gob.ar/). We select all weather stations data with at least 90% of non-missing data available within the study domain. Observations were checked for consistency and continuity, retaining 48 stations for Chile and 14 for Argentina between 1996 to 2015 (Table 4.1). Figure 3.1b presents the distribution of precipitation stations.

Table 3.1: Geographical characteristics of the selected weather stations for (WS1-WS47) Chile and (WS48-WS61) Argentina.

Indice	Name	Lat (ºS)	Lon (ºW)	Elevation (m.a.s.l)	Period
WS1	Maitenes Bocatoma	33.53	70.26	1143	1996-2015
WS2	Fundo Marruecos	33.55	70.81	430	1996-2015
WS3	Mallarauco	33.56	71.11	176	1996-2015
WS4	La Obra Recinto Emos	33.59	70.48	796	1996-2015
WS5	Cerrillos De Leyda	33.63	71.51	182	1996-2015
WS6	San Jose De Maipo Reten	33.63	70.35	943	1996-2015
WS7	Estero Puanque En Ruta78	33.66	71.34	93	1996-2015
WS8	Pirque	33.67	70.58	659	1996-2015
WS9	El Yeso Embalse	33.67	70.08	2475	1996-2015
WS10	Melipilla	33.68	71.19	168	1996-2015
WS11	El Vergel	33.69	70.92	340	1996-2015
WS12	Carmen De Las Rosas	33.75	71.15	165	1996-2015
WS13	San Gabriel	33.78	70.23	1266	1996-2015
WS14	Los Guindos	33.89	71.24	125	1996-2015
SW15	Villa Alhue	34.03	71.09	197	1996-2015

WS16	Barrera Loncha	34.08	71.18	144	1996-2015
WS17	Rancagua Cachapoal-Dcp	34.19	70.75	515	1996-2015
WS18	Cocalan	34.2	71.27	120	1996-2015
WS19	Canal Sauzal En Puente	34.24	70.55	750	2006-2015
WS20	Rio Pangal En Pangal	34.24	70.32	1500	2002-2015
WS21	Pichidegua	34.28	71.4	110	1996-2015
WS22	Coltauco	34.28	71.08	253	1996-2015
WS23	Rengo	34.42	70.86	310	1996-2015
WS24	Popeta	34.43	70.77	480	1996-2015
WS25	San Fernando	34.59	70.96	350	1996-2015
WS26	Rio Tinguiririca Bajos	34.71	70.82	560	1996-2015
WS27	La Rufina	34.74	70.75	743	1996-2015
WS28	Convento Viejo	34.76	71.13	239	1996-2015
WS29	La candelaria	34.78	71.41	213	1996-2015
WS30	Santa Susana	34.91	71.03	410	1996-2015
WS31	Curico	34.98	71.23	195	1996-2015
WS32	Rio Teno Despues De Junta	34.99	70.82	647	2000-2015
WS33	Los Quees	35	70.81	663	1996-2015
WS34	Lontue	35.04	71.29	199	1996-2015
WS35	Monte Oscuro	35.12	70.97	632	1996-2015
WS36	Potrero Grande	35.18	71.09	445	1996-2015
WS37	El Guindo	35.25	71.32	250	1996-2015
WS38	Agua Fria	35.31	71.09	560	1996-2015
WS39	Fundo El Radal	35.41	71.04	685	1996-2015
WS40	Huapi	35.48	71.29	250	1996-2015
WS41	El Durazno	35.49	71.31	275	1996-2015
WS42	Vilches Alto	35.59	71.08	1058	1996-2015
WS43	Colbun (Maule Sur)	35.62	71.4	280	1996-2015
WS44	Coloroado	35.63	71.26	420	1996-2015
WS45	Armerillo	35.7	71.07	492	1996-2015
WS46	Hornillo	35.86	71.11	810	1996-2015
WS47	Ancoa Embalse	35.91	71.29	421	1996-2015

WS48	Juan Amigo	36.07	71.39	460	1996-2015
WS49	La Remonta	33.71	69.29	1360	1996-2015
WS50	Valle de Uco	33.78	69.27	1199	1996-2015
WS51	Yaucha	34.16	69.17	1471	1996-2015
WS52	Puesto Papagayos	34.23	69.12	1529	1996-2015
WS53	Arroyo Hondo	34.48	69.28	1900	1996-2015
WS54	La Jaula	34.67	69.32	1457	1996-2015
WS55	Las Aucas	34.7	69.54	1800	1996-2015
WS56	Juncalito	34.74	69.21	1593	1996-2015
WS57	Loma Negra	35.26	69.25	1365	2003-2015
WS58	Pincheira	35.52	69.81	1775	1996-2015
WS59	Dique	35.54	69.64	1524	1996-2015
WS60	Los Mayines	35.55	70.29	1663	1996-2015
WS61	Bardas Blancas	35.87	69.81	1445	1996-2015
WS62	Arroyo La Vaina	35.92	69.99	1550	1996-2015

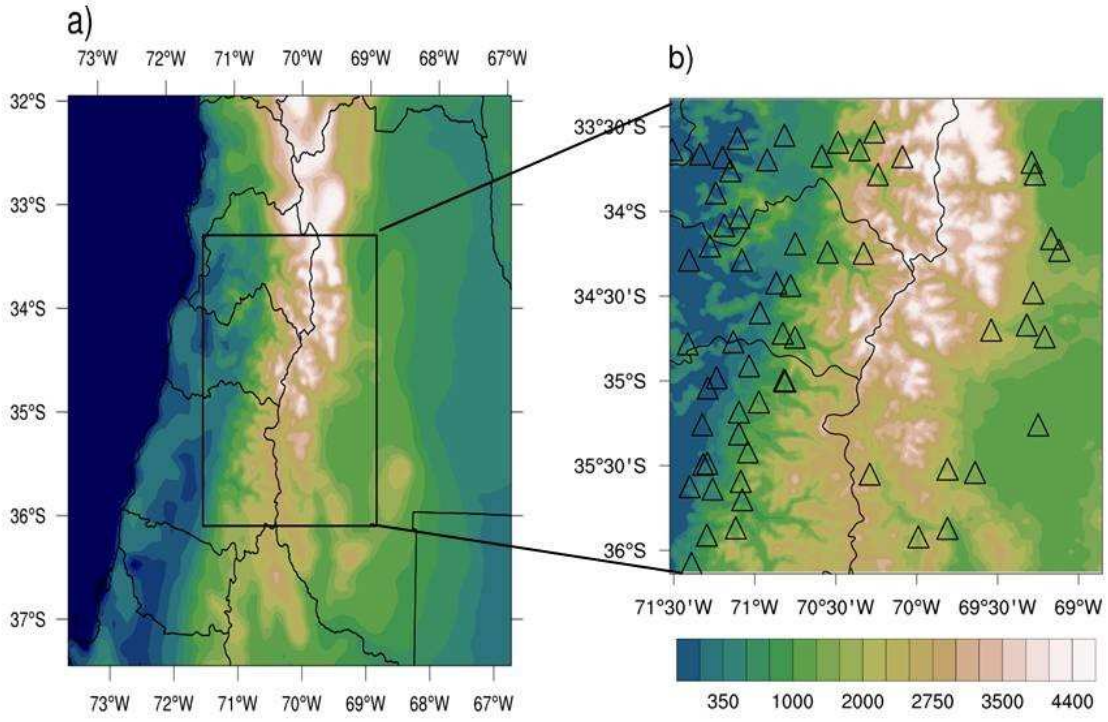

Figure 3.1: (a) WRF model domains, at 9 km (full map) and 3 km (black rectangle), (b) geographic positions of the weather stations located within the 3 km domain, with the main topographic features.

Comparison methods

In order to quantify the WRF ability to represent annual and seasonal precipitation, under distinct resolutions, statistical metrics were computed, namely the percent bias (PB), the mean absolute error (MAE), the Pearson correlation coeficient (PC) and the Willmott index of Agreement (d). Positive values of PB indicate an overestimation of precipitation of the model in relation to observations, whereas negative values indicate underestimation. The MAE provides information on the average magnitude of simulations error, considering both systematic and random errors, where 0 is the perfect match. The PC compute the linear relationship between the model and observations, where 1 is most desirable. Willmott's index is a standardized measure of the degree of model temporal-prediction error and varies between 0 and 1, where value of 1 indicates a perfect match, and 0 indicates no agreement. A more detailed description of these methods can be found in Wilks (2011). Analyses and comparisons are performed using the nearest grid point of the model to observations. Model daily precipitation is computed from 12 to 12 UTC. In this study, the seasonal precipitation was defined according to the characteristics of precipitation in the region, in warm season (October-March) and cold season (April-September).

Results

Annual and seasonal precipitation over Central Andes

The WRF precipitation estimates are compared with each weather station, considering the spatial distribution of the annual and seasonal accumulated precipitation shown in Figure 3.2. The observed annual precipitation pattern is marked by a significant latitudinal gradient with high precipitation values (more than 2000 mm/year) concentrated southward of 35ºS in the Chilean side. On the other hand, observations in Argentina ranges from 500 to less than 200 mm/year, with maximum values in the north of 34ºS and southermost of 35ºS. This difference in precipitation magnitude is characteristic of the Andes shadow effect, translating into an west-east contrast between the Chilean and Argentinian sides.

The variability of seasonal precipitation is also dictated by the contrast be-

tween the two sides of the Andean mountain range. In the warm season, the amount of precipitation along the latitudinal profile shows a decrease of precipitation northward of 35ºS in Chile, whereas a gradual increasis is noted northward of 35ºS in the Argentinian side. The occurrence of precipitation is associated with convective activity in both mountain range side. However, the incursion of warm and moist air from the Amazon basin by the South America Low Level Jet (SALLJ) favors accumulated precipitation in the eastern slopes of the Central Andes (Marengo et al., 2004; Castañeda and Ulke, 2015). On the other hand, in incursion of the winter frontal systems leads to a significant increase in precipitation on the Chilean side. In Argentina, higher precipitation is observed in the north of 35ºS during cold season.

Figure 3.2d-i shows precipitation features based on the WRF simulations. The spatial pattern of annual and seasonal precipitation is well captured by WRF3km as well as the WRF9km. Both simulations are able to capture the latitudinal gradient of precipitation, and the seasonal contrast between warm-cold seasons. Overall, WRF3km and WRF9km present similar pattern, although it is notable that in some regions or some particular points the precipitation is overestimated at 9 km in relation to observations and WRF3km, probably due to topography characteristics in the WRF9km. In mountainous terrain it is known that the smoothing of the topographic features leads to the reduction of the variability of precipitation. Resulting in increase of precipitation displayed in modeling experiments with low resolution (e.g. Soares et al. 2012).

To further illustrate differences in the representation of the annual and seasonal WRF precipitation and observations, Figure 3.3a-f shows the spatial distribution of several metrics statistics used for the validation of WRF simulations. The values of PB show that WRF3km tends to underestimate precipitation in relation to observations over most of Argentina and west of windward stations in Chile, by up to 50%. A wet bias is clearly seen in the nearest locations to windward mountain range, with large bias values to the north of 35ºS depicted by both WRF simulations. This wet bias is extended in almost all locations to windward of the Andes by the WRF9km, and also for some stations in Argentine side. The WRF9km presents 29% of stations with a wet bias, while WRF3km shows approximately 18% based on annual. Seasonal analyses show that in the warm (cold) season, 13% and 32% (19% and 32%) show wet

bias by WRF3km and WRF9km, respectively. The spatial pattern of PB is similar in annual and seasonal scale, although the magnitude of values during the warm season are relatively smaller due to lower precipitation.

Large values of bias (negative or positive) are accompanied by limited performance of the WRF simulations as reproduced by the MAE (Figure 3.3g-l). Higher errors are observed for annual and the cold season analyses, while smaller errors are noticed during warm season and on the Argentine side associated to lower rainfall variability. Considering a threshold for MAE values smaller than 100 mm in the annual and cold season, and smaller than 30 mm during the warm season, it is noticed that WRF3km (WRF9km) presents about 31%, 68%, and 37% (21%, 71%, and 29%) of stations within those categories in the annual, warm and cold season, respectively. An improvement of precipitation at 3 km is highlighted compared to 9 km, seen by the percentage of stations with smaller errors regarding the observed precipitation.

The precipitation amount also changes the level of agreement between WRF simulations and observations as shown by the PC distribution (Figure 3.4a-f), with higher values for annual and cold season in both WRF simulations (>0.7). Low correlations are noted in Argentina during the cold season, especially to the north of 35ºS. Conversely, the spatial distribution of d show a better agreement in the warm season to both Chile and Argentina (Figure 3.4g-l). Poor performance is shown in almost all locations in western Chile, especially insofar as annual and cold season are concerned.

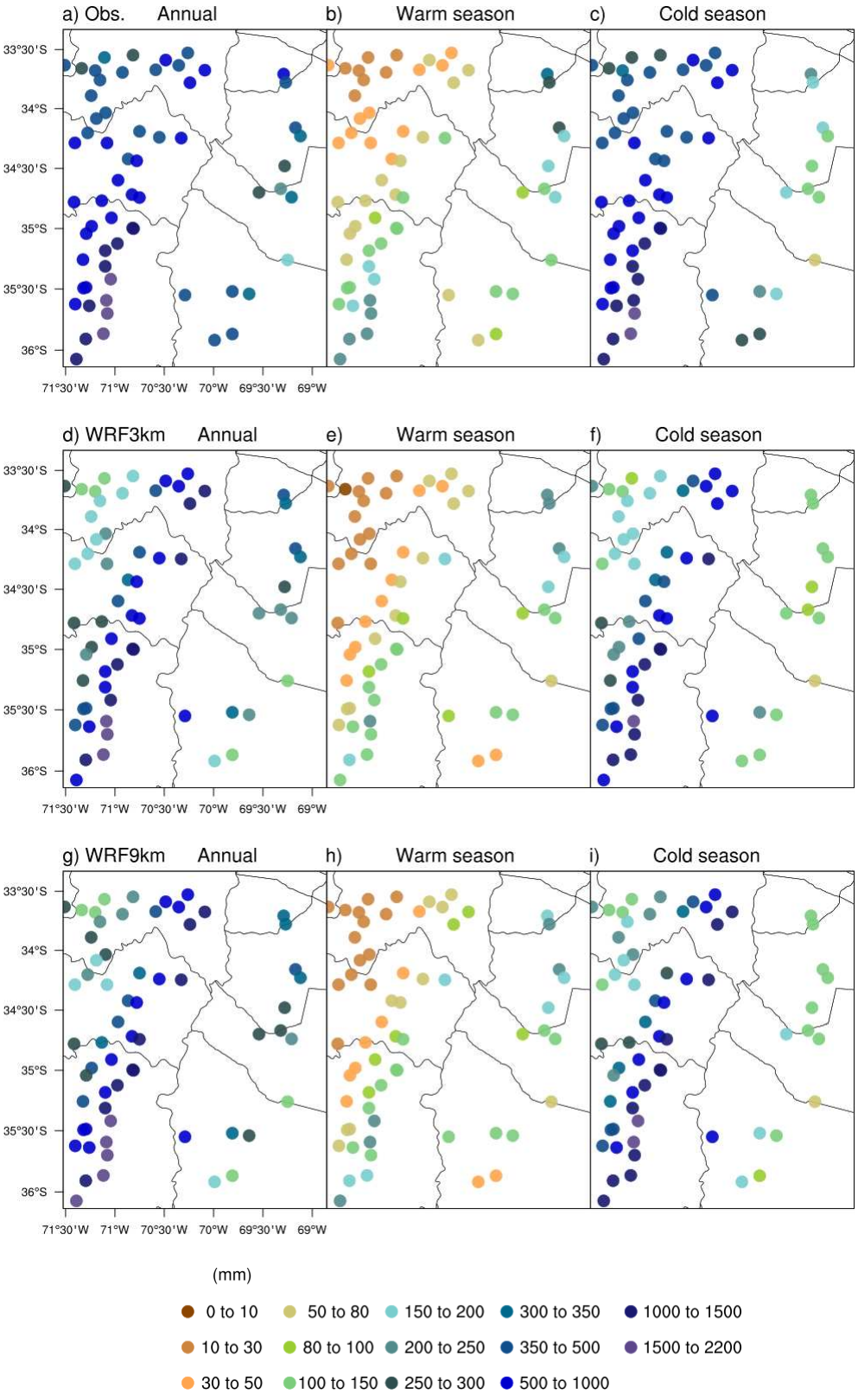

Figure 3.2: Spatial distribution of annual and warm-cold season accumulated precipitation, from (a-c) observations, (d-f) WRF3km, and (g-i) WRF9km.

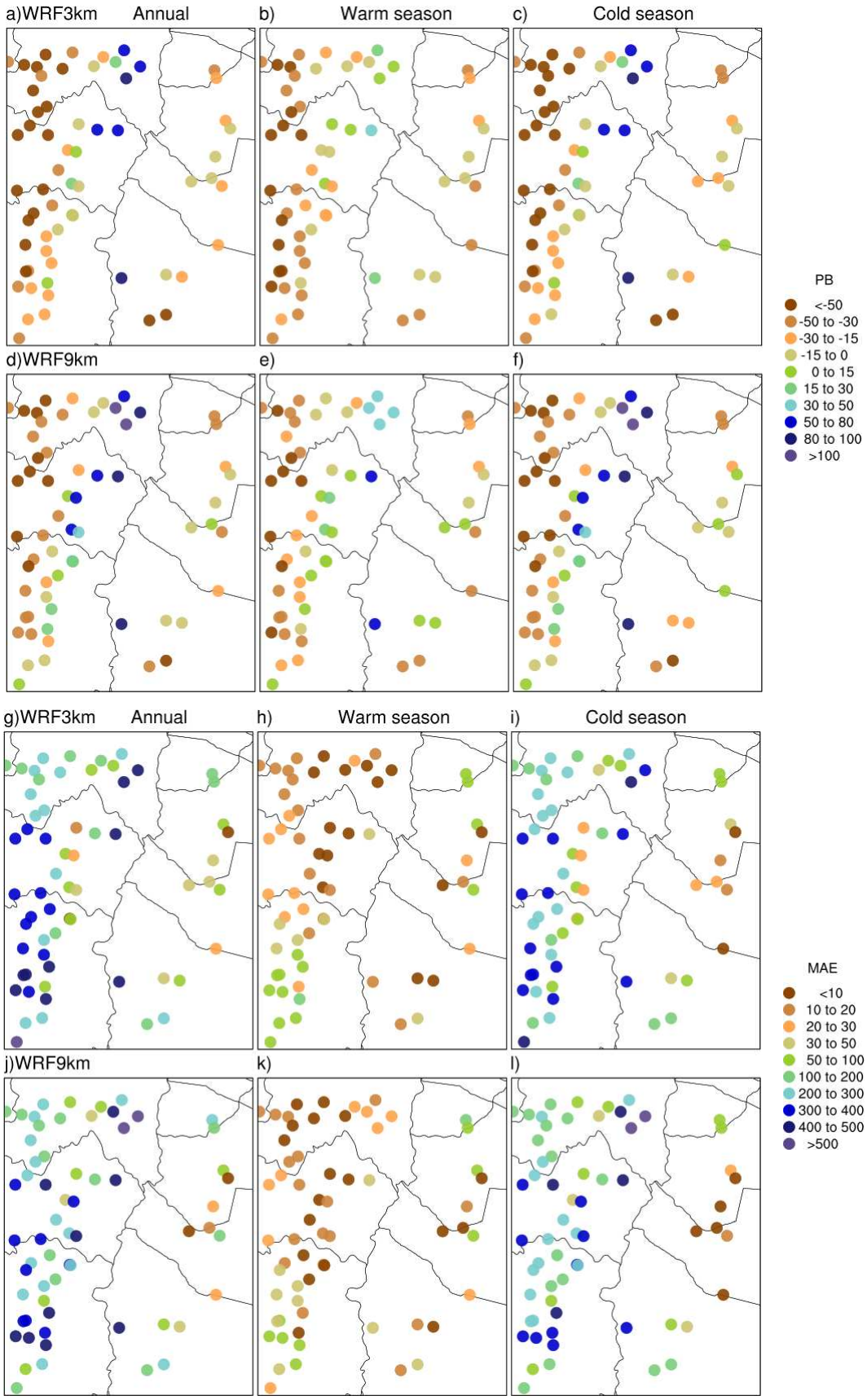

Figure 3.3: Spatial distribution of the (a-f) bias and (g-l) mean absolute error between observations and WRF3km and WRF9km estimations for annual and warm-cold season precipitation.

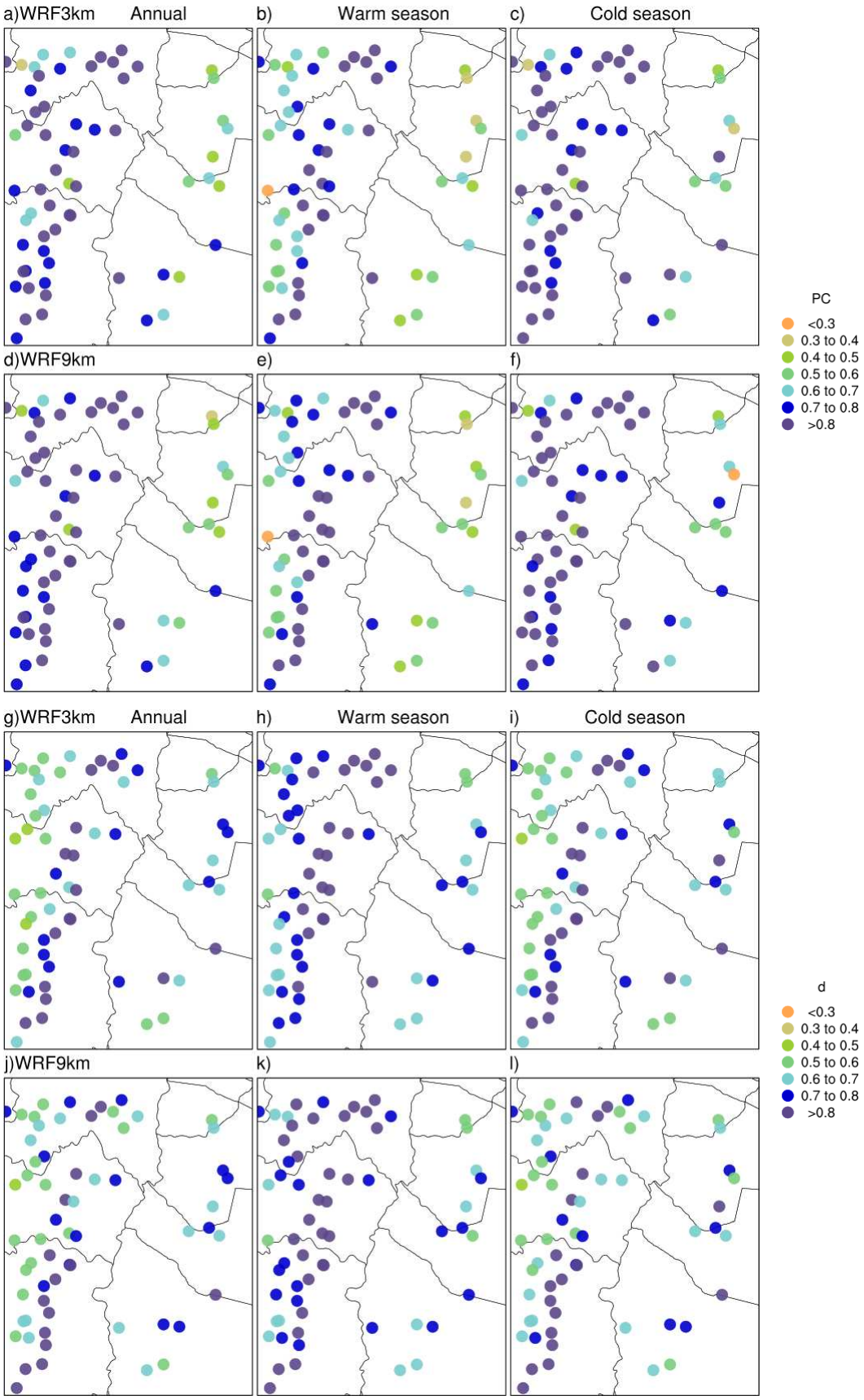

Figure 3.4: As Figure 3, but for (a-f) coefficient correlation and (g-l) the Willmott Index of Agreement.

Annual cycle and extremes precipitation

The annual cycle of precipitation from observational and WRF simulations in the Chile e Argentina are depicted in Figure 3.5. On the Chilean side, the seasonal characteristics of precipitation are clearly seen, with warm months with almost zero precipitation while the maximum values occur during the cold months, especially between May to Ausgust with accumulated precipitation obverved around 300 to 600 mm/month. However, in the Argentine side the seasonal variability is not clearly defined, probaly due to low density stations on this study. However, similar behavior is shown by Rivera et al. (2018) for the central region of Argentina representing by the La Jaula station (34.67ºS, 69.32ºW). Nevertheless, the inter-seasonal variability is noticeable, with maximum values of accumulated precipitation occuring especially in June, July and August.

Chilean seasonality of precipitation is properly reproduced by the WRF3km as well as WRF9km, although variability of precipitation (interquartile range) during the cold months are slightly overestimated by WRF9km whereas WRF3km undestimate in relation to observations, especially during May, July and August. The median and maximum values are also undestimate by both WRF simulations in almost months. Variability of monthly precipitation totals in Argentina is also well represented by the WRF simulations, with slightly underestimated median values during the warm months in relation observations. The maximum values of precipitation are overall underestimated by WRF simulations compared to observation, except to February and October.

In order to illustrate the performance of the WRF model in representing precipitation extremes, daily precipitation percentiles range (10th, 25th, 50th, 75th, 90th, 95th, and 99th) was calculated for each weather stations and compared statistically with the observations (Table 4.2). Many studies have used a combination of percentiles indices, however, this approach lead to misleading conclusions if the percentage of the wet hours-days change, which cannot be directly compared between simulations. Thus, the use the all-day percentiles (wet and dry events) is an alternative (Schär et al., 2016).

In general, both WRF simulations show a good agreement in reproducing precipitation extremes according to the percentiles, with PC values above 0.8. It is

interesting to note that there is no variation in the statistical performance (PB, PC and d) from 10th to 75th percentiles, however, MAE values increases according to the percentile variation. Concerning to moderate precipitation, for percentiles below the 75th, improvement is noticed by WRF3km than WRF9km, especially by lower PB values, from 19.91% to 34.84% respectively. On the other hand, precipitation extremes from 90th, 95th, and 99th percentiles show better performance depicted by WRF9km. This improvement is noted mainly by PB and MAE values, which almost perfect match with observation is shown in relation to 99th percentile, with 0.12% of PB and 0.05 of MAE. However, the 95th percentile shows slightly larger errors compared to the 90th and 99th percentiles in both WRF simulations.

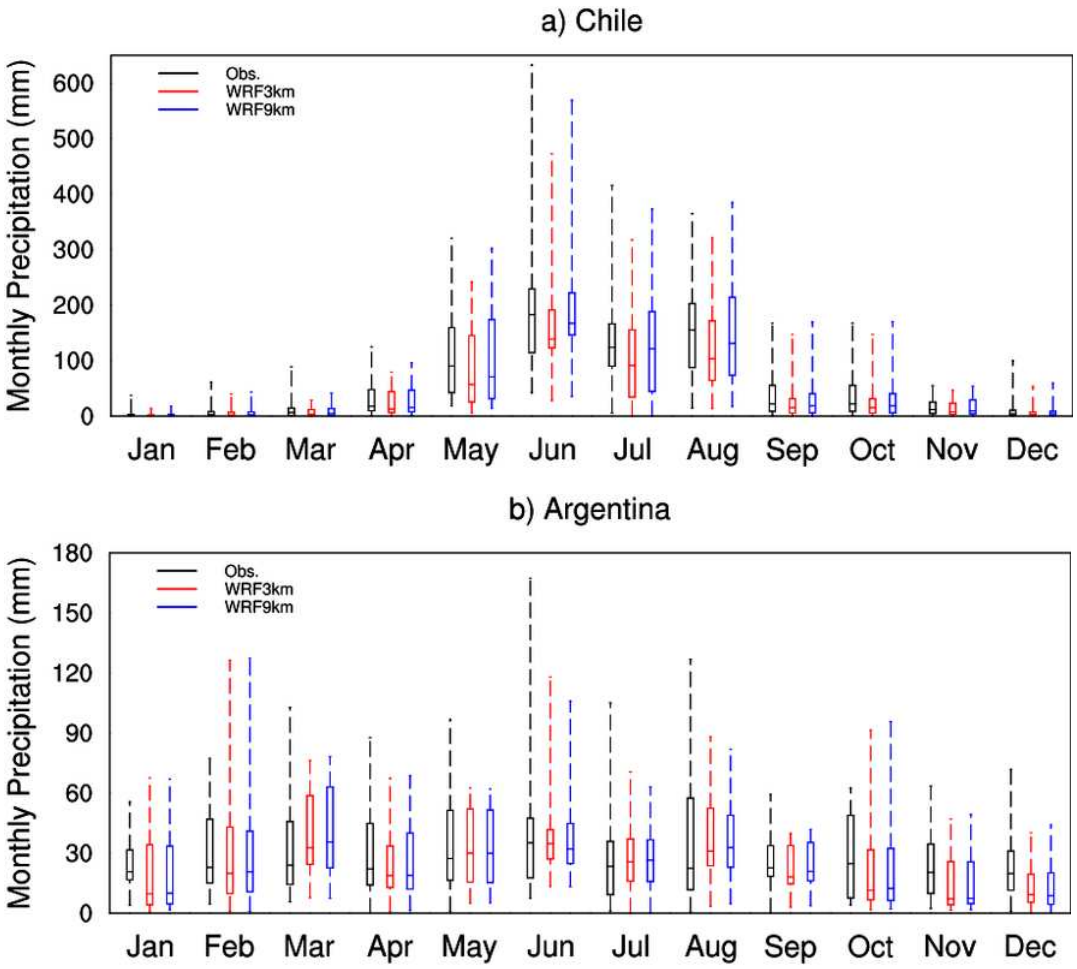

Figure 3.5: Boxplot of the total monthly precipitation from ensemble of the weather stations in the Chile and Argentina. Each boxplot shows the first, median and third quartiles, while the whiskers indicate variability outside the lower and upper quartiles.

Table 3.2: Performance of the WRF3km and WRF9km in relation to percentiles range, 10th, 25th, 50th, 75th, 90th, 95th, and 99th. Asteriscs are significant at the 5% level.

		Percentiles						
Metrics	Model	P10	P25	P50	P75	P90	P95	P99
PB	WRF3km	19.91	19.91	19.91	19.91	34.13	-37.5	-12.5
MAE		0.03	0.07	0.14	0.22	1.04	4.54	5.12
PC		0.82*	0.82*	0.82*	0.82*	0.82*	0.85*	0.85*
d		0.81	0.81	0.81	0.81	0.76	0.85	0.89
PB	WRF9km	34.84	34.84	34.84	34.84	15.08	-20.6	0.12
MAE		0.05	0.12	0.25	0.38	0.46	2.49	0.05
PC		0.80*	0.80*	0.80*	0.80*	0.87*	0.85*	0.84*
d		0.73	0.73	0.73	0.73	0.9	0.91	0.87

WRF performance at different elevation

One of the fundamental aspects in the validation of regional climate models is to understand their performance in complex terrains. In order to add details to the performance of the WRF simulations on elevation, the weather stations were classified in four groups according their elevation, such as 0-300 m (19 stations), 300-600 m (14 stations), 600-1300 m (14 stations) and >1300 (15 stations), statistical evaluation of the WRF at 3 and 9 km with the observations are show in Table 3. From the PB and MAE values is remarkable the best performance of the WRF3km with the elevation increase. The reduction of errors is systematic according to the increase of altitude in daily as well as monthly scale, for example, between 0 and 300 m the PB (MAE) values of -56.27% (26.21) reach -1.42% (0.49) for the stations located above 1300 m. The lower errors are in line with PC and d values as altitude, however, higher values are observed between 600 and 1300 m, and reduced values are noted above 1300 m.

Moreover, it is interesting to note that WRF3km shows a persistent negative bias with increasing altitude. On the other hand, WRF9km shows a dry bias at stations located between 0 and 600 m, whereas a wet bias above 600 m. This induces a poor performance of the WRF model at 9 km between 600 and 1300 m due to the increase of PB and MAE values. Nevertheless, better performance is also achieved at stations above 1300 m, although with larger errors compared to WRF3km. By the ratio of the MAE values between the WRF9km and WRF3km there is a difference of 250% on a daily scale and 314% at monthly above 1300 m, accompanied by slightly lower values of PC and d in relation to high resolution at 3 km.

Table 3.3: Performance of the WRF3km and WRF9km in different elevation levels.

			Elevation (m.a.s.l.)			
Metrics	Model	Time	0-300	300-600	600-1300	> 1300
PB	WRF3km	Monthly	-56.27	-24.13	-2.93	-1.42
		Daily	-56.85	-24.3	-3.38	-1.58
MAE		Monthly	26.21	18.22	2.39	0.49
		Daily	0.88	0.60	0.09	0.02
PC		Monthly	0.91	0.92	0.94	0.83
		Daily	0.80	0.84	0.89	0.61
d		Monthly	0.78	0.93	0.97	0.91
		Daily	0.80	0.91	0.94	0.76
PB	WRF9km	Monthly	-49.79	-9.22	22.51	4.46
		Daily	-50.45	-9.43	21.98	3.31
MAE		Monthly	23.19	6.96	18.33	1.54
		Daily	0.78	0.23	0.59	0.05
PC		Monthly	0.91	0.92	0.93	0.81
		Daily	0.80	0.86	0.88	0.59
d		Monthly	0.82	0.95	0.94	0.90
		Daily	0.82	0.93	0.91	0.75

Synoptic features by WRF simulations

For a better interpretation of the results to be discussed here, Figure 6 shows a climatological analysis; the left panel shows simulations using the 3km x 3km horizontal spacing, while the right panel shows the 9km x 9km horizontal spacing. Figure 6a, b shows surface pressure. It is assumed that the difference in pressure between grids is minimal, because pressure is a large-scale variable with small variations in local scale. During this period, the region of this study is dominated by a low surface pressure area located in the center of the grid. While, highest pressures are located west and east of the grid. In the center of the grid the lowest pressure is followed by the highest wind magnitude from 11 to 15 m/s, with northwest-west flow (Figure 6c, d). In the west and northeast regions there is a higher concentration of humidity up to 8 g/kg, simulated by the 3km x 3km horizontal spacing, and moisture transport to the east. The concentration of humidity has a pronounced orographic dependence, varying between 2 g/kg and 8 g/kg from coastal areas to the cordillera. A marked decline is also observed from the west to the central region. In Figure 6 g,h shows the best represented thermal advection in 3km x 3 km grid with variability from -0.7 to 1 K/s at 850 hPa, the warm air advection creating a convergence zone in at the center

of the grid. The combined flow due to warm advection increases wind speed.

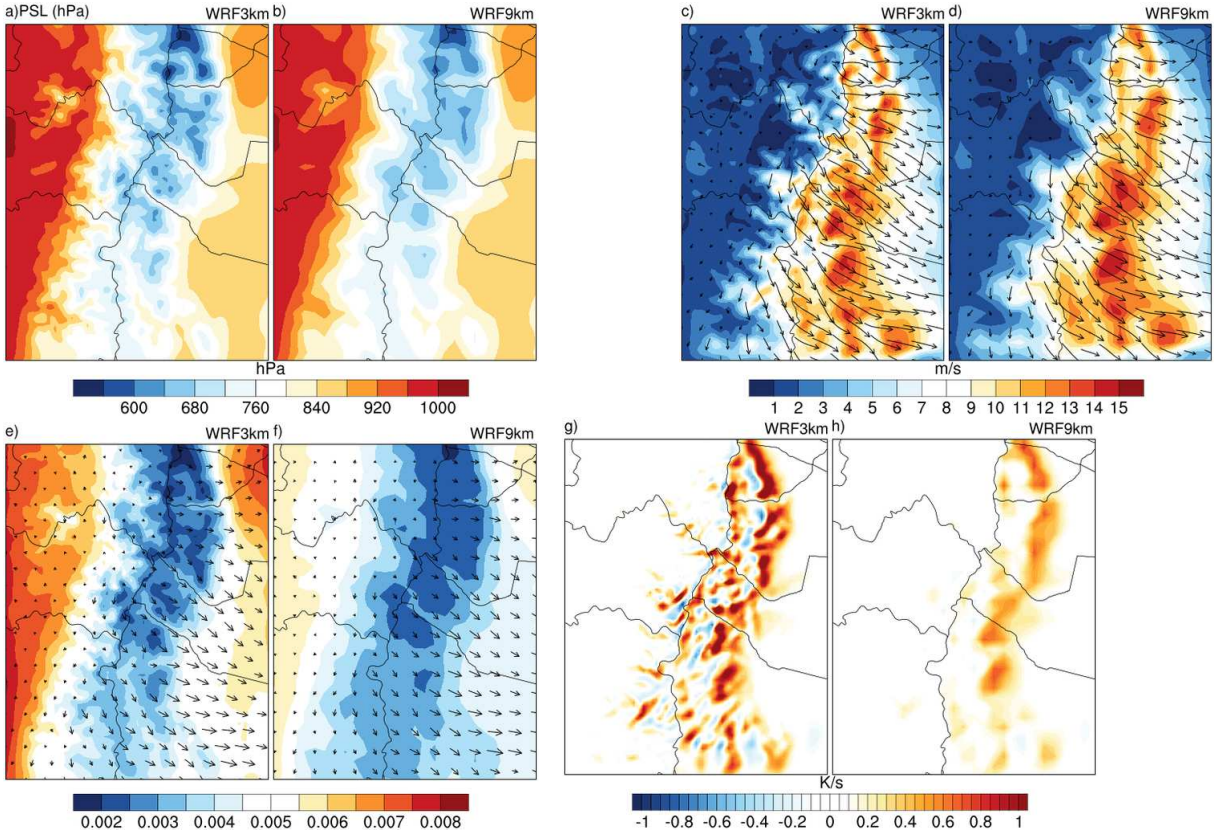

Figure 3.6: Monthly mean of the (a-b) Sea Level Pressure (hPa), (c-d) wind speedy (m s-1; shaded) and wind vector at 850 hPa (e-f) moisture flux convergence (shaded) moisture transport (kg m kg-1 s-1; vector), (g-h) horizontal thermal advection (k s-1) at 850hPa.

Discussion

The WRF simulations biases may result from a variety of sources, such as initial conditions, physical configuration of the model, and terrain complexity among others. Besides, main differences between the two simulations cannot be explained only by statistical error and it is extremely complex to measure.

Substantial differences between WRF simulations can be associated the cumulus scheme. Chawla et al. (2018) has shown that cumulus scheme to modulate the magnitude of simulated precipitation. Sikder and Hossain (2016) also showed that the finer spatial resolution (3 km) without cumulus parameterization schemes did not re-

sult in significant improvements in monsoon precipitation. For instance, the presence of this scheme in the simulation at 9 km could be responsible for the improvement of precipitation extremes in comparison to WRF at 3 km. Argüeso et al. (2011)also demonstrate that physics configuration play an important role in reproducing precipitation extremes in terms of percentiles, through the representation of convective and non-convective processes of precipitation and feedback between cumulus and microphysic scheme. Conversely, Zheng et al. (2015) demonstrated that the explicit treatment of convection, no cumulus parameterization, at 3 km can adequately predict convective systems and precipitation, consistent with many results. However, the influence and connection between the parameterizations used may be a fundamental question, but outside the objectives of this study.

On the other hand, WRF simulation at 3 km has shown better acuracy for precipitation at high elevations. This performance can clearly be associated with better reproduction of the topographic characteristics of the region compared to resolution at 9 km, which it tends smooth the terrain's complexity. In summary, an improvement is highlighted with high resolution in complex terrain in the Central Andes, performing well in all statistical metrics.

Conclusion

The present study contributes to a evaluation of high-resolution precipitation simulations over the Central Andes at 3 and 9 km spatial resolution. A state of the art numerical weather prediction model (WRF) driven by the ERA-Interim reanalysis has been used to downscale precipitation over 20-year long period (1996-2015). The WRF simulations were compared with observations from 62 Chilean and Argentina weather stations carried out at the annual and warm-cold season analysis.

Overall, both WRF simulations reproduce properly several characteristics of precipitation along the Central Andes, although there are some differences among themselves and observations, good performance is obtained in reproducing the spatial variability of annual and seasonal precipitation. The ability of WRF simulations to capture the seasonal accumulated precipitation is higher in the warm season than in the cold season by lower PB and MAE values. Differences between the simulations

are pronounced along windward slopes of the mountain range, in which WRF9km presents a wet bias in relation to observation and WRF3km.

In addition, WRF improvement vary according to precipitation percentiles. WRF3km captures the moderate precipitation (lower-percentiles) more realistically than precipitation extremes. On contrary, WRF9km presents better performance in relation to precipitation extremes, but presents greater errors in moderate precipitation events. Our results also show that the high resolution leads to a better performance of precipitation field as elevation increase, most likely due to the better resolved orography. However, we have shown that both WRF simulations capture precipitation with good accurately, therefore a resolution of 9 km may be a good option when elevation or complex terrain is not relevant, alleviating operating costs.

The analyses presented in current study are subject to a few limitations that could be tested in the future and may vary the results: account a greater number of weather stations expanding the study area and evaluating different physics parameterization schemes from WRF model, in order to better understand the differences between the simulations and errors of the WRF model. Finally, this study presents high resolution and long term datasets that can be a useful tool for understanding the climate in mountainous areas, as well as hydrological studies and extreme events.

References

Ambrizzi, T., Reboita, M. S., da Rocha, R. P., and Llopart, M. (2019). The state of the art and fundamental aspects of regional climate modeling in South America. *Annals of the New York Academy of Sciences*, 1436(1):98–120.

Argüeso, D., Hidalgo-Muñoz, J. M., Gámiz-Fortis, S. R., Esteban-Parra, M. J., Dudhia, J., and Castro-Díez, Y. (2011). Evaluation of WRF parameterizations for climate studies over southern Spain using a multistep regionalization. *Journal of Climate*, 24(21):5633–5651.

Bown, F., Rivera, A., and Acuña, C. (2008). Recent glacier variations at the Aconcagua basin, central Chilean Andes. *Annals of Glaciology*, 48:43–48.

Bravo, C., Loriaux, T., Rivera, A., and Brock, B. W. (2017). Assessing glacier melt

contribution to streamflow at Universidad Glacier, central Andes of Chile. *Hydrology and Earth System Sciences*, 21(7):3249–3266.

Cardoso, R. M., Soares, P. M., Miranda, P. M., and Belo-Pereira, M. (2013). WRF high resolution simulation of Iberian mean and extreme precipitation climate. *International Journal of Climatology*, 33(11):2591–2608.

Castañeda, M. E. and Ulke, A. G. (2015). Analysis of atmospheric conditions associated to CHACO events of the Low Level Jet East of the Andes and their implications for regional transport. *International Journal of Climatology*, 35(14):4126–4138.

Chawla, I., Osuri, K. K., Mujumdar, P. P., and Niyogi, D. (2018). Assessment of the Weather Research and Forecasting (WRF) model for simulation of extreme rainfall events in the upper Ganga Basin. *Hydrology and Earth System Sciences*, 22(2):1095–1117.

Comin, A. N., Schumacher, V., Justino, F., and Fernández, A. (2018). Impact of different microphysical parameterizations on extreme snowfall events in the Southern Andes. *Weather and Climate Extremes*, 21(June):65–75.

Corripio, J. G. and Purves, R. S. (2005). *Surface Energy Balance of High Altitude Glaciers in the Central Andes: the Effect of Snow Penitentes*. Wiley \& Sons: London.

Dudhia, J. (1989). Numerical study of convection observed during the winter monsoon experiment using a mesoscale two-dimensional model. *Journal of the Atmospheric Sciences*, 46:3077–3107.

Falvey, M. and Garreaud, R. (2007). Wintertime Precipitation Episodes in Central Chile: Associated Meteorological Conditions and Orographic Influences. *Journal of Hydrometeorology*, 8(1991):171–193.

Fathalli, B., Pohl, B., Castel, T., and Safi, M. J. (2016). Dynamical downscaling of temperature variability over Tunisia: evaluation a 21-year-long simulation performed with the WRF model. *Journal of Climatology & Weather Forecasting*, 4(2):1–8.

Hong, S. and Lim, J. (2006). The WRF single-moment 6-class microphysics scheme (WSM6).

Hong, S.-Y., Noh, Y., and Dudhia, J. (2006). A new vertical diffusion package with an explicit treatment of entrainment processes. *Monthly Weather Review*, 134:2318–2341.

Kain, J. S. (2004). The Kain–Fritsch Convective Parameterization: An Update. *Journal of Applied Meteorology*, 43:170–181.

Malmros, J. K., Mernild, S. H., Wilson, R., Tagesson, T., and Fensholt, R. (2018). Snow cover and snow albedo changes in the central Andes of Chile and Argentina from daily MODIS observations (2000–2016). *Remote Sensing of Environment*, 209(February 2017):240–252.

Marengo, J. a., Soares, W. R., Saulo, C., and Nicolini, M. (2004). Climatology of the low-level jet east of the Andes as derived from the NCEP-NCAR reanalyses: Characteristics and temporal variability. *Journal of Climate*, 17:2261–2280.

Masiokas, M. H., Rivera, A., Espizua, L. E., Villalba, R., Delgado, S., and Aravena, J. C. (2009). Glacier fluctuations in extratropical South America during the past 1000years. *Palaeogeography, Palaeoclimatology, Palaeoecology*, 281(3-4):242–268.

Mlawer, E. J., Taubman, J., Brown, P. D., Iacono, M. J., and Clough, S. A. (1997). Radiative transfer for inhomogeneous atmospheres: RRTM, a validated correlatedk model for the longwave. *Journal of Geophysical Research*, 102:16663–16682.

Mög, T. and Kaser, G. (2011). A new approach to resolving climate-cryosphere relations: Downscaling climate dynamics to glacier-scale mass and energy balance without statistical scale linking. *Journal of Geophysical Research Atmospheres*, 116(16):1–13.

Paulson, C. A. (1970). The Mathematical Representation of Wind Speed and Temperature Profiles in the Unstable Atmospheric Surface Layer. *Journal of Applied Meteorology*, 9:857–861.

Pellicciotti, F., Helbing, J., Rivera, A., Favier, V., Corripio, J., Araos, J., Sicart, J.-E., and Carenzo, M. (2008). A study of the energy balance and melt regime on Juncal Norte Glacier, semi-arid Andes of central Chile, using melt models of different complexity. *Hydrological Processes*, 22(19):3980–3997.

Posada-Marín, J. A., Rendón, A. M., Salazar, J. F., Mejía, J. F., and Villegas, J. C. (2019). WRF downscaling improves ERA-Interim representation of precipitation around a tropical Andean valley during El Niño: implications for GCM-scale simulation of precipitation over complex terrain. *Climate Dynamics*, 52(5-6):3609–3629.

Rivera, J. A., Marianetti, G., and Hinrichs, S. (2018). Validation of CHIRPS precipitation dataset along the Central Andes of Argentina. *Atmospheric Research*, 213:437–449.

Schär, C., Ban, N., Fischer, E. M., Rajczak, J., Schmidli, J., Frei, C., Giorgi, F., Karl, T. R., Kendon, E. J., Tank, A. M., O'Gorman, P. A., Sillmann, J., Zhang, X., and Zwiers, F. W. (2016). Percentile indices for assessing changes in heavy precipitation events. *Climatic Change*, 137(1-2):201–216.

Skamarock, W. C., Klemp, J. B., Dudhia, J., Gill, D. O., Barker, D. M., Duda, M. G., Huang, X.-Y., Wang, W., and Powers, J. G. (2008). A Description of the Advanced Research WRF Version 3. *NCAR Tech. Note NCAR TN- 475_STR*, page 113.

Soares, P. M., Cardoso, R. M., Miranda, P. M., de Medeiros, J., Belo-Pereira, M., and Espirito-Santo, F. (2012). WRF high resolution dynamical downscaling of ERA-Interim for Portugal. *Climate Dynamics*, 39(9-10):2497–2522.

Viale, M. and Nuñez, M. N. (2011). Climatology of Winter Orographic Precipitation over the Subtropical Central Andes and Associated Synoptic and Regional Characteristics. *JOURNAL OF HYDROMETEOROLOGY*, 12:481–507.

Ward, E., Buytaert, W., Peaver, L., and Wheater, H. (2011). Evaluation of precipitation products over complex mountainous terrain: A water resources perspective. *Advances in Water Resources*, 34(10):1222–1231.

Wilks, D. S. (2011). *Statistical Methods in the Atmospheric Sciences*, volume 100. Academic Press.

Zheng, Y., Alapaty, K., Herwehe, J. A., Del Genio, A. D., and Niyogi, D. (2015). Improving High-Resolution Weather Forecasts Using the Weather Research and Forecasting (WRF) Model with an Updated Kain–Fritsch Scheme. *Monthly Weather Review*, 144(3):833–860.

Chapter 4

Modeling glacier surface mass balance in complex terrain on Chilean Central Andes

Introduction

The Andes concentrate the largest glacierized area in the Southern Hemisphere outside Antarctica (Mark and Fernández, 2017). In several Andean regions, glaciers are the main source of local water supply, in particular to communities living close to the mountain range (Mark et al., 2015). Seasonal variation of glaciers also plays a role in nourishing the hydrological regime of important rivers, essential for water consumption as well as economic activities such as agriculture, mining, hydroelectric, wine industry and tourism (Vergara et al., 2007; Masiokas et al., 2012; Valdés-Pineda et al., 2014). Indeed, water availability along the Andes is related to the local climate variability, where the glaciers retreat in response to temperature and precipitation change may affect future water resources in most Andean countries (Le Quesne et al., 2009; Bradley, 2006).

Retreat of Andean glaciers impacts the economic growth and development mainly in semi-arid regions such as in Central Chile, which includes densely populated cities and strong dependence on glacial melt, especially during scarcity of rainfall in summer season (Pellicciotti et al., 2014; Le Quesne et al., 2009). In addition to the impact on human lives and livelihoods, Andean glaciers mass loss in response to climate change also contributes to natural hazards and rising sea levels (Marzeion et al., 2014; Mernild et al., 2016). Glaciers fluctuation are strong indicators of climate change due to high sensitivity to small variations in the climate system (Kaser et al.,

2010; Mark and Fernández, 2017). This highlights the importance of glaciers in society.

Currently, studies indicate that the glaciers recession is happening in all territorial extension of the Andes Cordillera, from north to south, encompassing glaciers from Venezuela to Patagonia (Barcaza et al., 2017; Braun and Bezada, 2013; Masiokas et al., 2016a; Basantes-Serrano et al., 2016). For instance, the total glacierized area in the tropical Andes has decreased by about 15% since 1970 (Kaser and Osmaston 2002), whereas in the Central Andes of Chile it has decreased 20% on average since 1955 (Bown et al., 2008). This recession affects mainly small glaciers at low altitudes, which may disappear in the next decades (Rabatel et al., 2013).

The heterogeneity of climate regimes along the Andes makes it difficult to understand mechanisms responsible for triggering glacier melting, since local factors may also impact the observed changes (Garreaud, 2009). Additionally, the behavior of glaciers in their variation of volume and mass balance has not only resulted from global trends of temperature increase, but also to other drivers such as albedo, cloudiness, shortwave radiation, precipitation, topography, among others (Francou, 2003; Mög and Kaser, 2011; Pedersen and Egholm, 2013). This shows the complexity of climate interaction on glaciers, which requires more studies dealing with the impact of climatic variability and global warming on the dynamics of glacier expansion and shrinkage.

The Andes are one of world's least studied glacierized regions, specifically in terms of mass balance. In particular, the semi-arid Andes of Chile have received little attention as compared to others Andean regions, such as Cordillera Blanca in the Peruvian Andes and glaciers in the Patagonia (Fernández and Mark, 2016; Veettil et al., 2017). One reason for this lack of research is due to the scarcity of continuous climatic and hydrological datasets in this region, especially in the glacierized mountains around Central Chile. Additionally, finding accurate weather information in the Andes Cordillera is a challenge due to sparse and incomplete networks of surface stations and high elevation climate records (Masiokas et al., 2016a; Manz et al., 2016). The Andean complex terrain makes it difficult to maintain and expand the network of meteorological stations and also the development of reliable measurements of the spatial and long-term historical observations. Furthermore, there is a large discontinuity of mass balance monitoring programs along the mountain range, in which only

one glacier across the Andes has been monitored for more than 30 years (Fernández and Mark, 2016).

Remote sensing techniques and different modeling approaches have been used as alternative to overcome this limitation in glacier monitoring along the Andes (e.g. Veettil et al. 2017; López-Moreno et al. 2016; Mernild et al. 2016). In addition, climatic downscaling techniques in combination with glacier modeling have been useful tools to fill gaps in mass balance observations. This combination is valid to quantify the mass balance in response to large-scale circulation (Mög and Kaser, 2011). However, the success of this type of strategy linked to glacier mass balance modeling depends on high resolution of input-output datasets to improve the ability to reproduce local climatic features, especially in mountain areas, where complex terrain induces large biases in the assessment of essential drivers such as temperature and precipitation (Silva et al., 2011; Schauwecker et al., 2014).

Despite these efforts, there are still many gaps in large glacierized areas that need to be analyzed in detail to understand the dynamics of glaciers. This study, we provide the first comprehensive long-term analysis of Universidad Glacier in Central Chile from 1996 to 2015, in which a high-resolution dynamical downscaling and a mass balance model are utilized, provides new insights into glaciers mass balance behavior along Central Andes and helps expands current understanding in research of modeling of the Andean cryosphere.

Data and Methods

Study area

The Central Andes of Chile (32-36° S) contains several large glacierized subregions, nourishing a number of watersheds which provide water resources for more than 10 million of people, such as Aconcagua (33°00'S), Mendoza (32°07'S), Maipo (33°50'S), and Tinguirica (34°45'S). The specific study area corresponds to Universidad Glacier (Fig. 4.1b). This glacier is part of the third glaciological zone that extends from the Aconcagua River basin to the Maule River, located in the O'Higgins region of Chile, next to the Chilean-Argentinean border.

The glacier mean elevation is around 3500 m a.s.l, with minimum of 2463

m a.s.l at the Universidad glacier (Le Quesne et al., 2009). The 0ºC isotherm altitude ranges between 4000 to 3000 m a.s.l at 32ºS to 36ºS, respectively (Carrasco et al., 2005). A recent study of glaciers fluctuations in Central Andes noticed that positive mass balance ocurred until the beginning of the millennium, thereafter strongly negative mass balance is widespread in this region (Braun et al., 2019). Glaciar Universidad a front receded about 2 km between 1945 and 2004 (Rivera et al., 2002; Le Quesne et al., 2009).

The Central Andes are characterized by a Mediterranean climate type, with semi-arid and temperate conditions. The precipitation is marked by high inter-annual variability, generally associated with the El Niño-Southern Oscillation (ENSO), with wet winters (April-September) and dry summers (October-March). Winter precipitation is associated with predominance of westerly winds and orographic effects of the Andes (Montecinos and Aceituno, 2003; Bown et al., 2008; Garreaud, 2009; Viale and Garreaud, 2015). At high altitudes, annual precipitation reaches less than 500 mm in the semi-arid region (32ºS) in contrast to southward 36ºS with 2500 mm (Pellicciotti et al., 2014). In this region, glacial meltwater plays a fundamental role in feed rivers Cachapoal and Tinguiririca, major streams in the region, providing water resources to supply the main sectors that drive the economy in the region, which is led by local agriculture and industry.

Automatic weather stations

The data for validation of mass balance model included meteorological observations at two automatic weather stations (AWS) located at Universidad Glacier (Fig. 4.1b). One in the eastern basin (AWS1E, 34.64ºS, 70.32ºW, 3629 m a.s.l.), covering from 01 December 2012 to 15 May 2013. This AWS was moved to the western basin (AWS1W, 34.68ºS, 70.36ºW, 3724 m a.s.l) for the time period 01 November 2013 to 22 April 2014. The lower station (AWS2, 34.69ºS, 70.33ºW, 2790 m a.s.l.) located on the ablation zone at glacier tongue, operated continuously between 01 December 2012 and 24 April 2014. The datasets have been provided and previously analyzed by Kinnard et al. (2018).

Mesoscale atmospheric model

The regional climate model used to dynamical downscaling scheme is the non-hydrostatic Weather Research and Forecasting (WRF) model (Skamarock et al., 2008) version 3.5.1. A high resolution is achieved by using three nested domains, with 9, 3 and 1 km resolution, respectively. Both grids are centered in the Central Chile, and have, respectively, 70 x 70, 82 x 106 and 130 x 157 grid points, the innermost domain covers the study area of glacier (Fig. 4.1a).

The physical parameterizations used include the WRF Single Moment 6-class (WSM6, Hong et al. 2010). In recent analysis this parameterization has been highlighted in complex terrain of the Andes (Comin et al., 2018). Radiation schemes of Rapid Radiative Transfer Model (RRTP, Mlawer et al. 1997) for longwave and Dudhia scheme (Dudhia, 2013) for shortwave. The MM5 similarity surface layer scheme (Paulson, 1970). The Yonsei University parameterization of the planetary Boundary Layer (Hong and Lim, 2006) and the Kain-Fritch scheme to atmospheric convection (Kain, 2004) used for outer domain and turned off for the inner domain (3 and 1 km) in order to explicitly resolve the precipitation processes. All three model domains used the same vertical resolution (28 layers up to a model top of 50 hPa) and physical parameterizations.

The present study is based on present day climate using the initial and lateral conditions for the outer domain derived from the European Centre for Medium-Range Weather Forecasts (ECMWF) ERA-Interim reanalysis (ERA) (Dee et al., 2011), with 0.75º horizontal resolution, 17 pressure levels, lateral forcing updated every 6 hour for the time period of 20 years, 1996-2015.

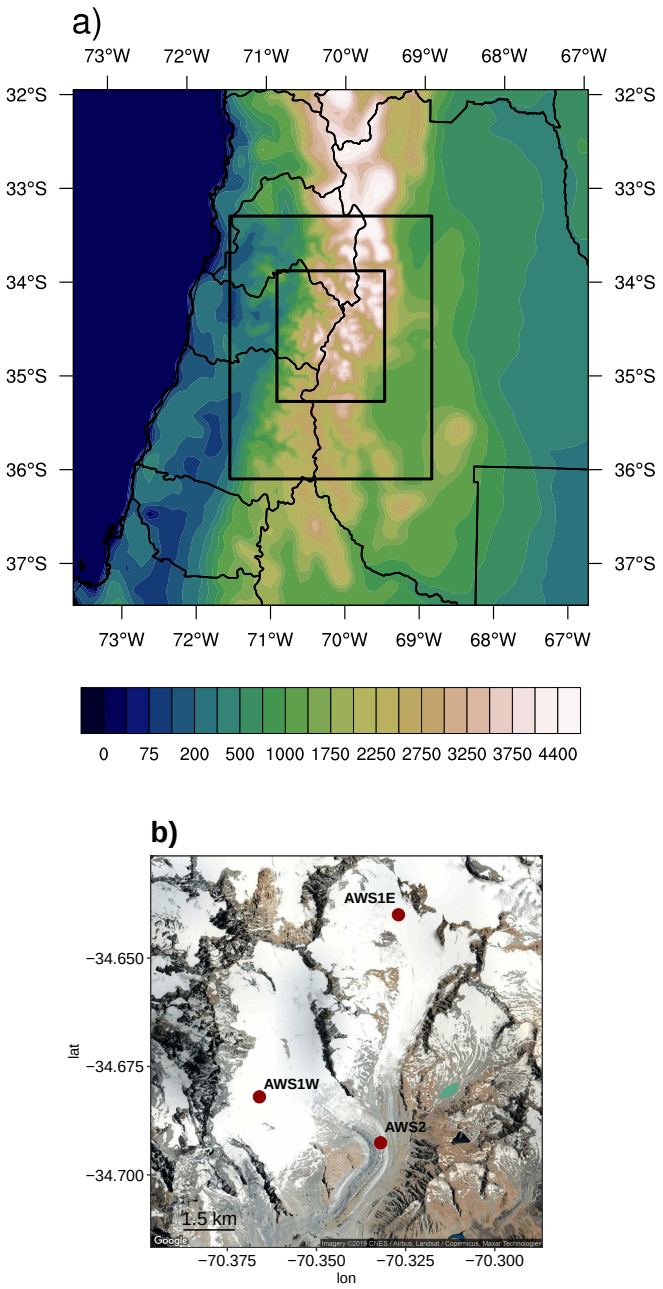

Figure 4.1: (a) Study area represented by the WRF domains and topography, at 9 km (full map), 3 km (first black retangle) and 1 km represented by the smallest nest, where the analysis of this work is performed. (b) Location of Universidad Glacier in central Chile and automatic weather stations (AWS).

Surface energy and mass balance model (SEB)

The distributed mass balance model is a simplified version of most relevant components of surface energy balance, of medium complexity and forced with high resolution from the WRF model output (1 km). Fields of downscaled incoming solar radiation, precipitation, near surface air temperature, specific humidity and wind

speed are used. The model is an improved version from Fernández (2014) following a structure based on previous approaches glaciers modeling such as Rupper and Roe (2008); Plummer and Phillips (2003); Arnold et al. (1996); Paul et al. (2008).

Commonly, annual mass balance is measured or modeled considering the hydrological year, i.e. from the beginning of winter until the end of summer. In this study, the hydrological year spans from the 1st of April to the 31st of March, with accumulation and ablation periods defined from April to September and October to March, respectively. Mass or energy loss from the surface is defined as negative while gain is defined as positive. The glacier-wide, specific surface mass balance is usually given in metres water equivalent per year (B_a, in m w.e. yr^{-1}), obtained by subtracting the ablation (Q_a) from the accumulation (Q_c), and integrating to the whole glacier area (A):

$$B_\mathrm{a} = \frac{1}{A}\int_A b dA \tag{4.1}$$

The accumulation term is defined as the solid part of the precipitation (P_r) based on air temperature (T_a), according to the critical temperature threshold, one for rainfall (liquid precipitation) (T_r) and another for snowfall (solid precipitation) (T_{sf}):

$$\begin{aligned} Q_\mathrm{c} &= 0 \;\; if \;\; T_\mathrm{a} \geq T_\mathrm{r} \\ Q_\mathrm{c} &= P_\mathrm{r}\left[\left(\frac{T_\mathrm{r}T_\mathrm{a}}{T_\mathrm{r}T_\mathrm{sf}}\right)\right] \;\; if \;\; T_\mathrm{sf} < T_\mathrm{a} < T_\mathrm{r} \\ Q_\mathrm{c} &= P_\mathrm{r} \;\; if \;\; T_\mathrm{a} \leq T_\mathrm{sf} \end{aligned} \tag{4.2}$$

Ablation is calculated according to a basic surface energy balance (Wm^{-2}):

$$Q_\mathrm{a} + Q_\mathrm{N} + Q_\mathrm{S} + Q_\mathrm{L} = 0 \tag{4.3}$$

where Q_N is the net radiation, Q_S is the turbulent sensible heat flux, and Q_L is the turbulent latent heat flux. The Q_N is the sum of shortwave (S_W) and longwave radiation (L_W), with S_W calculated as:

$$S_\mathrm{W} = l_\mathrm{SW}(1-\alpha) \tag{4.4}$$

where l_{SW} is the incoming solar radiation and α the albedo.

The albedo estimate includes a time-varying albedo model, which decreases from a maximum value for snow to a minimum value corresponding for ice, following a logarithmic and exponential relation with the T_a, according to a threshold of significant snowfall (Brock et al., 2000). The parameters values for albedo of snow, firn and ice are determined during calibration (Sect.1.3.2).

when accumulation $\geq$ threshold:

$$\alpha = 0.713 - 0.112 log_{10} T_a \tag{4.5}$$

when accumulation $<$ threshold:

$$\alpha = \alpha_{ice} + 0.442 e^{-0.058 T_a} \tag{4.6}$$

The L_W is defined by the difference between incoming radiation and the outgoing energy from the glacier surface, defined as:

$$L_W = (\epsilon_{atm} \sigma {T_a}^4) - (\epsilon_{gl} \sigma {T_s}^4) \tag{4.7}$$

where the σ is the Stefan-Boltzmann constant, ϵ_{gl} is the emissivity from the glacier surface, and ϵ_{atm} the atmospheric emissivity defined according to Arnold et al. (1996):

$$\epsilon_{atm} = 8.733.10^{-3} {T_a}^{0.788} (1 + kn) \tag{4.8}$$

where n is defined by the cloud fraction at the time step, and k is a coefficient about cloud type (Hock, 2005). The surface temperature (T_S) is calculated follows similar approach of DeWalle and Rango (2008):

$$T_S = T_{S1} + TSF(T_a - T_{s1}) \tag{4.9}$$

with T_{s1} being T_s at the previous time-step, and TSF a dimensionless factor that accounts for the total change of T_s. Assuming T_S to be 0ºC and TSF as 1.

The turbulent fluxes of latent and sensible heat are estimate by bulk aerodynamic method, commonly used to estimate turbulent fluxes for glacier studies (Oke, 2002; Cuffey and Paterson, 2010).

$$Q_S = \rho_a c_p \tau_c u (T_a - T_s) \tag{4.10}$$

$$Q_L = (\rho_a 0.622 L_{v,s}) \tau_c u (q_a - q_s) \tag{4.11}$$

where ρ_a is air density, c_p is the specific heat of air at constant pressure, τ_c the turbulent transfer coefficient, u is wind speed. The terms, L_v and L_s corresponds to the latent heat of vaporization and sublimation. The right-hand term is the difference between specific humidity of air (q_a) and ice surface (q_s).

The estimate of the τ_c, the same for transfer of either heat or water vapor, depend of wind speed, surface roughness and atmospheric stability, included in the following equations:

$$\tau_d = \frac{v^2}{\left[ln\left(\frac{Z_u}{Z_0}\right)\right]^2} \tag{4.12}$$

$$Ri = \left(g\left(\frac{T_a + T_s}{2}\right)\right) Z_t \left(\frac{T_a + T_s}{u^2}\right) \tag{4.13}$$

where τ_d is the coefficient for neutral stability, Ri the Richardson number; u the wind speed; Z_u and Z_t are the measurement level above the ground for wind and temperature, respectively. Z_0 the roughness length (for temperature and vapor pressure), v the von Kármán constant; and g the gravitational acceleration.

The mass balance model considers a criterion to determine that stable and unstable conditions occur instead of neutral conditions, where stable conditions are defined when Ri is larger than 0.01, while unstable correspond to values smaller than -0.01 (Oke, 2002). Thus, for stable conditions:

$$\frac{\tau_c}{\tau_d} = (1 - 5Ri)^2 \tag{4.14}$$

and for unstable:

$$\frac{\tau_c}{\tau_d} = (1 - 16Ri)^{0.75} \tag{4.15}$$

Finally, the model calculates Q_a by determining if that mass loss is due to melt (melt), evaporation (evap) or sublimation (subl):

$$Q_a = melt = \frac{Q_a {L_f}^{-1}}{\rho_{ice}} \quad if \quad T_s = 0C$$

$$Q_a = evap = \frac{Q_a {L_v}^{-1}}{\rho_{ice}} \quad if \quad T_s = 0C \quad and \quad e_a < e_i$$

$$Q_a = subl = \frac{Q_a {L_s}^{-1}}{\rho_{ice}} \quad if \quad T_s < 0C \quad and \quad e_a < e_i$$

where e_i and e_a are the vapor pressure on the ice surface (assumed in saturation (Rupper and Roe, 2008) and above the surface, respectively. The parameterizations and the constant values are summarized in Table 4.1.

Table 4.1: Parameters and constants.*NU: No unit.

Parameter	Value	Unit
Freshsnow albedo (α_{frsnow})	0.85	NU*
Firn albedo (α_{firn})	0.50	NU*
Ice albedo (α_{ice})	0.30	NU*
Ice surface temperature (Ts)	273.15	K
Ice emissivity (ϵ_{gl})	1	NU*
Cloud type coefficient (k)	0.26	NU*
Critical temperature for snowfall (T_{sf})	0	ºC
Critical temperature for rainfall (T_r)	2	ºC
Threshold of a significant snowfall	5	mm
Stefan-Boltzmann constant (σ)	5.67E-08	Wm^{-2} K^{-4}
Von Kárman constant (v)	0.4	NU*
Gravitacional acceleration (g)	9.8	m/s2
Measurement level (z_t)	2	m
Measurement level (z_u)	10	m
Roughness lenght (z_0)	0.001	m
Ice density (ρ_{ice})	916	kg/m3
Specific heat of air (c_p)	1005	J/Kg K
Latent heat of vaporization (L_v)	2.50E+06	J/kg
Latent heat of sublimation (L_s)	2.80E+06	J/kg
Latent heat of fusion (L_f)	334000	J/kg

Limitations of the SEB model

The mass balance model used in this study includes main processes of energy balance components, such as shortwave radiation, turbulent heat fluxes and longwave radiation, which they present an important contribution to surface melt energy. The model also accounts for the ablation term in melt, sublimation, and evaporation. This is an relevant feature since sublimation also plays an important role in the semiarid

Andean glaciers due to the combination of high altitude and hot and dry atmosphere (Ayala et al., 2017).

For simplicity, some terms were neglected in this model approach, such as topographic factors, heat transferred from rain, and heat conduction through the ice. Another limitation in this model is not taken into account the debris-covered effect, which may lead to limitations of mass balance accuracy for some types of glaciers. For instance, Andes of Central Chile approximately 36% corresponds to rock and debris covered glaciers (Janke et al., 2015). Although most modeling approaches in Central Chile not account debris cover (e.g. Bravo et al. 2016; Kinnard et al. 2018; Ragettli and Pellicciotti 2012), it would be expected that the presence of debris on snow or glacier ice may influences surface energy balance and ablation rates (Benn and Evans, 2014).

However, limitations and simplifications are found in entire glacier energy balance modeling approaches, mainly by scarcity of observed data for validation. In particular, estimates of mass balance in which they involve different processes of gain and mass loss on the surface, within the glacier, or at the base. For instance, refreezing of meltwater and thermal erosion are internally important processes, as well as geothermal heat and sliding friction at the base (Bishop et al. 2014). However, most modeling studies do not account the subsurface processes. Although, these processes tend to have a small magnitude relative to the surface mass balance, but can be more representative than sublimation in some glaciers (e.g. Kinnard et al. 2018). The limitations in detail on the main glaciers modeling approaches are highlighted by Hock (2005); Fernández and Mark (2016).

Results and discussion

WRF performance assessement

The capability of the WRF model in simulating climatic variables in the glacier area is evaluated by comparing with observations localized in the domain, using the nearest grid-point of the model to observations, and assessed through the use of Taylor Diagrams (Taylor, 2001). The Taylor Diagram provides a summary of statistical parameters, such as the linear correlation coefficients (CCs), root-mean-square error (RMSE), bias and the simulated to observed ratio of their variances. The distance from the origin correspond to the standard deviation (SD) of the model, normalized by the observation. Therefore, CC, RMSE and SD close to the observation point indicates a perfect match over the considered domain.

The performance of dynamical downscaling of main meteorological variables used as imput in the SEB model against observations are shown in Figure 4.2 and 4.3. In general, WRF output is able to reproduce the observed behavior of the variables, although there are some mismatches. Better performance is remarkable in relation to shortwave radiation and near-surface temperature. Conversely, poor performance is noticed for relative humidity and wind speed.

The comparison of daily mean incoming shortwave radiation to observation show generally good agreement, mainly at AWS1E and AWS2, whereas at AWS1W the WRF output overestimates (underestimates) the maximum (minimum) values in relation to observation (Fig. 4.2a-c). In fact, in this location high variance and large positive bias (72 Wm^2-25%) are noticed in comparison, for example the lower bias (27 Wm^2-9%) at AWS1E (Fig. 4.3). This high bias may be associated with

slope effect or cloud reduction in the WRF input. However, high correlations are shown at all locations, above 0.79 statiscally significant (Fig. 4.3). It is important to note that the WRF output represents very well the annual cycle of the incoming radiation represented by Figure 4.2c.

Simulated temperature matches closely to observations pattern for near surface temperature at 2 m (T2) as well as surface skin temperature (TSK) (Figure 4.2d-f). However, a cold bias is noticed at AWS1E (-3.56 ºC) and AWS2 (-2.61 ºC) in relation to T2, whereas for TSK there is a reduction of cold bias in theses localities, -0.62 ºC and -0.73 ºC, respectively. Conversely, at AWS1W a warm bias is displayed by both T2 (2 ºC) and TSK (5.86 ºC). The Taylor Diagram also depicts high correlation at all locations, above 0.88 and better performance for T2 as verified through the smaller NSD and RMSE (Fig. 4.3).

Insofar relative humidity the WRF skill is reduced, with a high daily variability and large negative biases at AWS1W (-18%) and AWS2 (-13%) while at AWS1E positive bias is found of 6 % (Fig. 4.2g-i, Fig. 4.3). Lower correlations and higher variance variability are also noticed compared the good ability of the WRF to simulate incomimg radiation and temperature. Large biases are also noted for wind speed, however a positive bias is actually expected due to the logarithmic expression of the wind with altitude. The observed wind speed are measured at approximately 2 m while the WRF output at 10 m with smoother topography. Better performance is obtained at AWS1W with a statistically significant correlation of 0.70 and a bias of 5.54 m/s (Fig. 4.3b).

In terms of precipitation, there is available observed dataset only at glacier tongue (AWS2). There are no measurements of snowfall. The WRF shows a good

performance, with a bias of -0.09 and correlation of 0.75 in this locality. However, we need to keep in mind that the comparison period is very short in both weather stations.

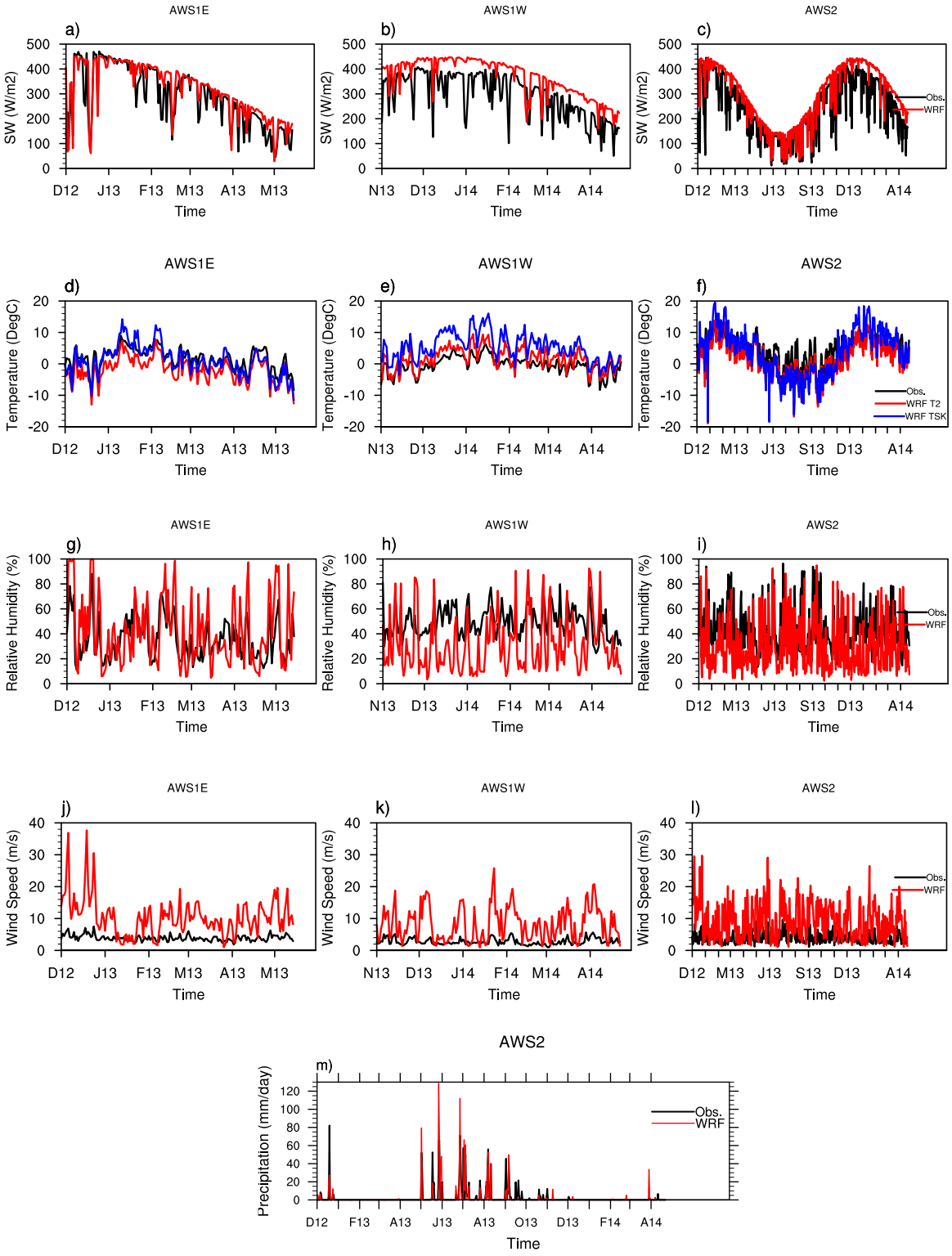

Figure 4.2: Comparison between WRF input and observations for the daily average of shortwave solar radiation (SW), near surface temperature at 2m (T2) and skin (TSK), relative humidity, wind speed and precipitation* at (a-c) AWS1E, (d-f) AWS1W, and (g-i) AWS2.*Precipitation data is available only at AWS2.

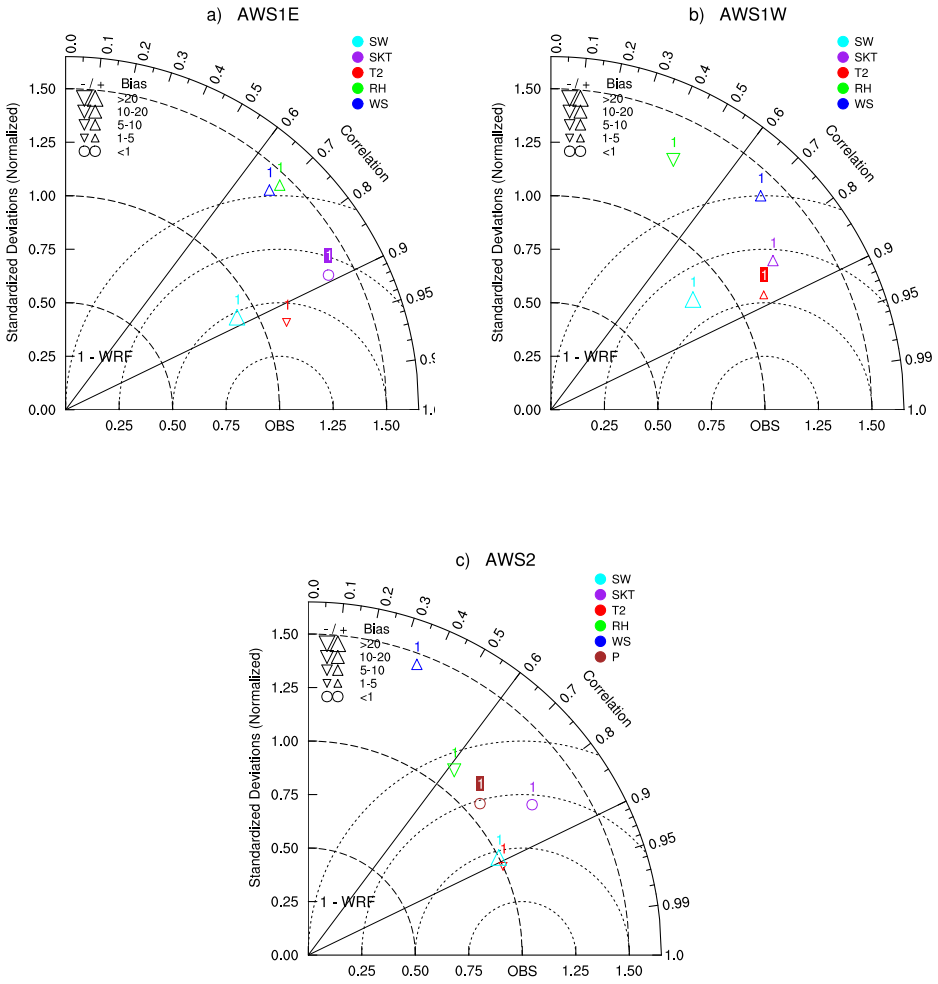

Figure 4.3: Taylor Diagram for shortwave radiation (SW), surface temperature at 2 m (T2), surface skin temperature (SKT), relative humidity (RH) and wind speed (WS) from WRF model over (a) AWS1E, (b)AWS1W, and (c)AWS2. The radial distance from the zero point represents the standard deviation, the angular axes show correlation between each model and the reanalyses and centered root mean square difference between each model and reanalyses is their distance apart.

Calibration of the SEB model and parameters sensitivity

The SEB model contains some parameters in order to simplify atmospheric processes on the glacier surface. Therefore, it is important a calibration and sensitivity analysis of the model. There are three main parameters in which they influence the energy fluxes and accumuation, and consequently the correct reproduction of the mass balance: albedo variation for freshsnow ($\alpha_{freshsnow}$), firn (α_{firn}) and ice (α_{ice}), significant snowfall threshold (SnT) based on temperature threshold for rainfall (T_r) and snowfall (T_{sf}), and temperature surface factor (TSF). In order to obtain an improvement of the performance of the SEB model in relation to calibration of these parameters and to illustrate the sensitivity regarding the mass balance, three experiments were performed by modifying the initial conditions for each parameter. A brief description of parameters sensitivity experiments are provided in Table 4.2.

To evaluate the performance of calibration of parameters, the results of each simulation were compared with observations by percent bias (PBIAS). The experiments based on albedo and SnT were compared with the albedo output and observation for each weather station. The SnT parameter directly affect the accumulation, which consequently reaches the albedo. However, in the absence of observed accumulation data, the results of this test were also compared with the albedo observed, whereas the TSF parameter was compared with the glacier surface temperature observed. The parameters sensitivity is also showed by mass balance in response to changes parameters. Table 4.3 summarize the results.

About the albedo experiments, a first approach considered the minimum values (see Cuffey and Paterson 2010) for each albedo parameters, one control (A1) followed by the perturbation of these parameters (A2-A4). The sensitivity of the mass

balance to these parameters is high for firn albedo, with a positive increment of 130 mm w.e.q yr^1 in both hydrological years, whereas snow albedo presents a low response and ice albedo no variation in mass balance. This is characteristic of temperate glaciers, which have no superimposed ice. Similar results are founded by Østby et al. (2017) and pointed out as the short exposure of ice on the surface.

From the experiments of A5 to A7, an improvement using the last sets of albedo parameterizations is remarkable, especially at AWS1W with PB of 0.69 (Table 4.3). Although the A4 experiment also shows a good calibration with low PB values, these parameter values are very low for the study region and do not match the maximum and minimum in situ values of the albedo shown in the Figure 4.4a-c. Therefore, the set of albedo parameters refers to experiment A7 will be used as control for the other experiments.

The sensitivity of the model seems to be more robust to the choice of SnT parameterization, since it show low variation in the mass balance with the perturbation of the snowfall temperature, ranges between 0 to 3.6 ºC. In addition, the T5 experiment performed best in comparison to sets experiments. Conversely, TSF performance shows large differences between three tests, with an improvement using the TSF as 1.

Figure 4.4 shows the comparison between albedo and glacier surface temperature modeled and observed from the improved calibration of the parameters discussed. Overall, SEB model is able to represent the albedo observed pattern, although it does not reproduce accurately the variability, featuring a fast decay of snow to ice albedo. In line with PB low (Table 4.3), there are good correlations, statistically significant in all weather stations, with better fit at AWS2, with CC of 0.78 followed by a

smaller error 0.16. This good match is very interesting because the AWS2 represents the glacier tongue in which it is covered by debris. The decrease in albedo values measured in the summer months is clearly due to the effect of debris (Fig. 4.4c). Furthermore, the glacier surface temperature modeleded closely match to observation (Fig. 4.4d-e), showing a great performance by high correlations, ranging 0.81, 0.73 and 0.85 at AWS1E, AWS1W and AWS2, respectively.

Table 4.2: Description of parameter sensitivity experiments.

Parameter	Experiment	Conditions
Albedo	A1	α_{frsnow} = 0.75, α_{firn} = 0.15, α_{ice} = 0.06
	A2	α_{frsnow} = 0.95, α_{firn} = 0.15, α_{ice} = 0.06
	A3	α_{frsnow} = 0.75, α_{firn} = 0.50, α_{ice} = 0.06
	A4	α_{frsnow} = 0.75, α_{firn} = 0.15, α_{ice} = 0.30
	A5	α_{frsnow} = 0.85, α_{firn} = 0.52, α_{ice} = 0.34
	A6	α_{frsnow} = 0.95, α_{firn} = 0.50, α_{ice} = 0.30
	A7	α_{frsnow} = 0.85, α_{firn} = 0.50, α_{ice} = 0.30
SnT	T1	T_{sf} = 0.0, T_r = 0
	T2	T_{sf} = 0.0, T_r = 1.5
	T3	T_{sf} = 0.0, T_r = 3
	T4	T_{sf} = 0.6, T_r = 3.6
	T5	T_{sf} = 0.0, T_r = 2
TSF	TSF1	TSF = 0.5
	TSF2	TSF = 1.0
	TSF3	TSF = 1.5

Table 4.3: Percent bias (PBIAS) for each experiment and parameters sensitivity in response to mass balance.

Experiment	PBIAS (%)			Mass Balance	
	AWS1E	AWS1W	AWS2	$b_{2012-2013}$	$b_{2013-2014}$
A1	-6.12	-41	-43	-0.81	-1.41
A2	8.22	-35	-43	-0.80	-1.40
A3	-6.12	-41	-43	-0.81	-1.41
A4	19	-3.96	2	-0.68	-1.28
A5	33	6.76	13.5	-0.65	-1.24
A6	37	4.29	9	-0.66	-1.26
A7	29	0.69	6	-0.67	-1.26
T1	29	5.14	6	-0.68	-1.26
T2	29	5.31	5	-0.67	-1.26
T3	29	5.30	6.5	-0.66	-1.27
T4	29	5.30	6	-0.66	-1.26
T5	29	0.69	6	-0.67	-1.26
TSF1	-36	-63	-45	-0.67	-1.26
TSF2	-0.64	-27	8.75	-0.66	-1.26
TSF3	92	9	62	-0.74	-1.29

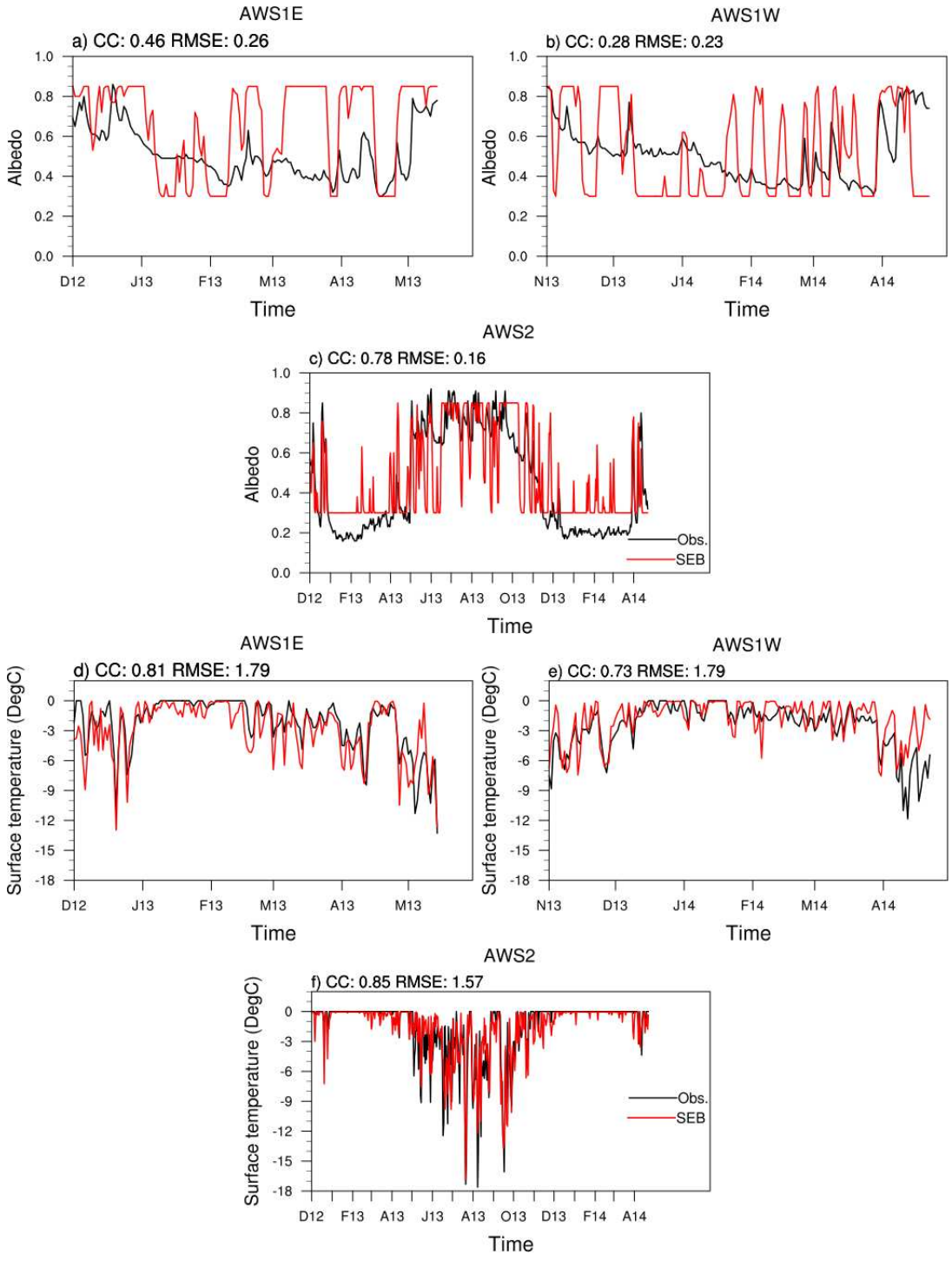

Figure 4.4: Comparison between SEB model and observations in relation to daily average (a-c) albedo and (d-f) glacier surface temperature at AWS1E, AWS1W, and AWS2.

SEB model performance

An assessment of the quality and long term of the SEB model is almost impossible because data available is very scarce. However, an effort is made by comparing the performance of the SEB model in simulating surface energy fluxes observed at weather stations. Figure 4.5 shows the mean monthly energy fluxes of incoming shortwave (SW), longwave (LW) and net radiation (QN), latent (QL) and sensible (QS) heat, and resulting energy available for melt (QM) for observed and modeleded. In general, the SEB model is able to simulate the main characteristics and behavior of energy fluxes, such as the response of dominant fluxes that lead to gain and loss of energy.

At both stations, the incoming shortwave corresponds to the main energy input to the glacier surface followed by sensible heat flux, whereas longwave radiation and latent heat flux represent the larger lost energy, respectively. The SEB model responds well to incoming shortwave behavior, with the maximum occurring in January decreasing gradually. The sensible heat term has a smaller magnitude, implying lower energy released for melting. On the other hand, the latent heat indicates mass loss by evaporation or sublimation, which the SEB model overestimates in comparison with the observations. This mismatch can be associated with the positive bias of humidity and wind speed by the WRF input (Fig. 4.2).

In addition, the available energy to melt is driven by the net radiation at almost period, thereby melt decreases significantly when net radiation is also reduced. This pattern is reproduced by the SEB model, however, it drastically reduces the amount of energy to melt in the winter months. Negative values of available melt energy occur due to shortwave energy decrease, in association with longwave energy

flux more negative than observations, probably resulting from cold bias from WRF input. This behavior is in line with other results in alpine glaciers (e.g. Collier et al. 2013). Conversely, SEB model closely matches energy available for melt observed through months with high net radiation.

To exemplify the relationship of mass balance with elevation, Figure 4.6 shows annual and seasonal distribution at Universidad Glacier for the hydrological years 2012/13 and 2013/14. This modeled pattern allows an assessment visually from know features on the glacier. The typical pattern of surface mass balance with altitude is reproduced by the SEB model, with decrease of gradient with altitude, characteristic of most mountain temperate glaciers. It is expected that during winter the predominance is accumulation, thereby the mass balance profile is positive with elevation. Additionally, we compared our results to mass balance estimates by Kinnard et al. (2018), although a direct comparison is not realistic, due to the inherent differences of each method and areal coverage. Table 4.4 summarizes the results, in general, there is a good agreement between the SEB model and observed values, mainly during the hydrological year 2012-2013. The main difference is observed during the winter, which the SEB model estimates are less positive compared to the observed. This may be due to less precipitation or higher air temperature than the observed.

In general, one should not expect the model to accurately reproduce all aspects of observations because both the observations are too few and the both models (WRF and SEB) have their own uncertainties. In modeling approaches it is expected that several inconsistencies will be added from the input data of the simulation to the differences due to the observed and modeled methods used.

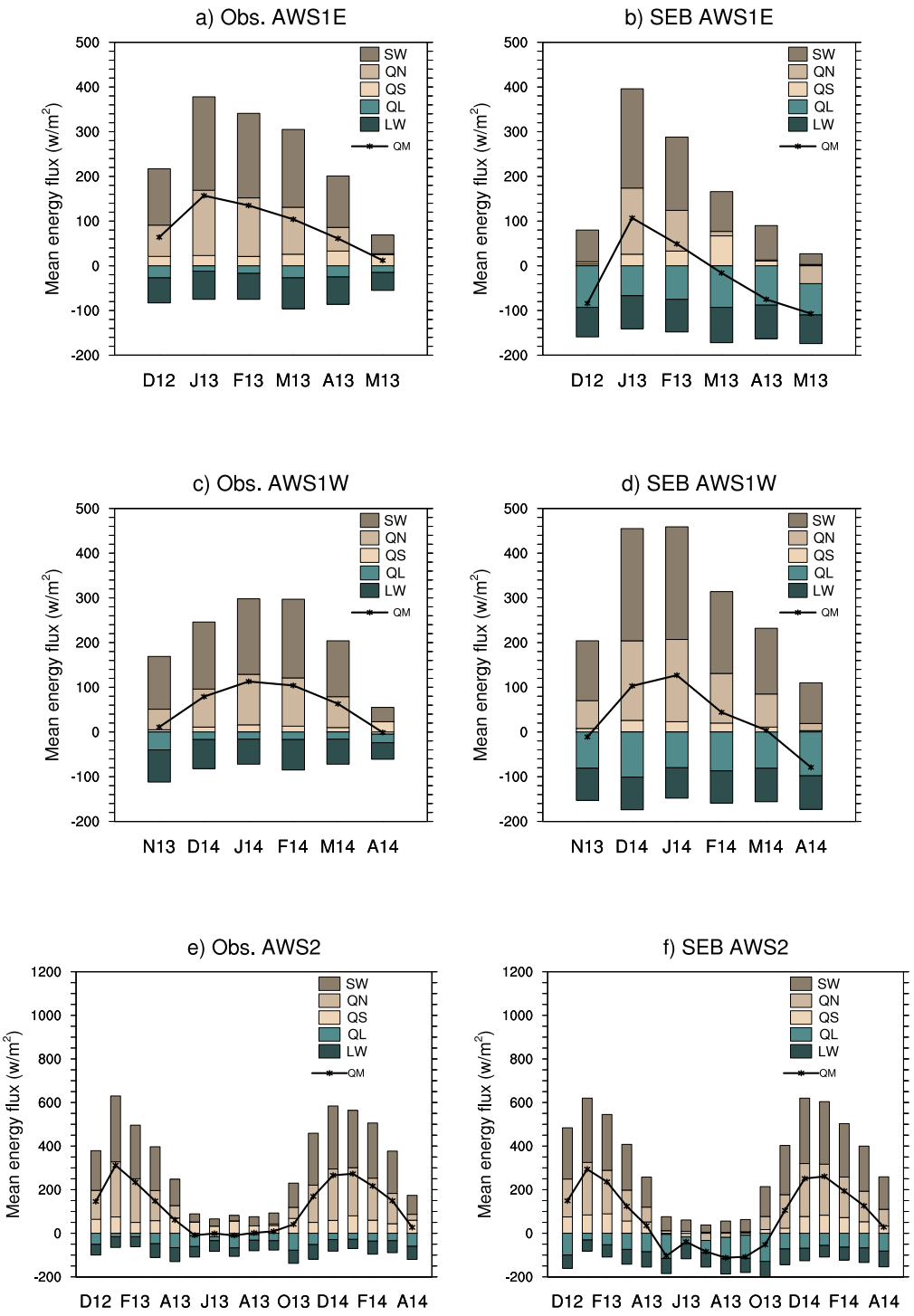

Figure 4.5: Comparison between monthly mean energy fluxes from (a,c,e) observations and (b,d,f) SEB model at AWS1E, AWS1W, and AWS2.

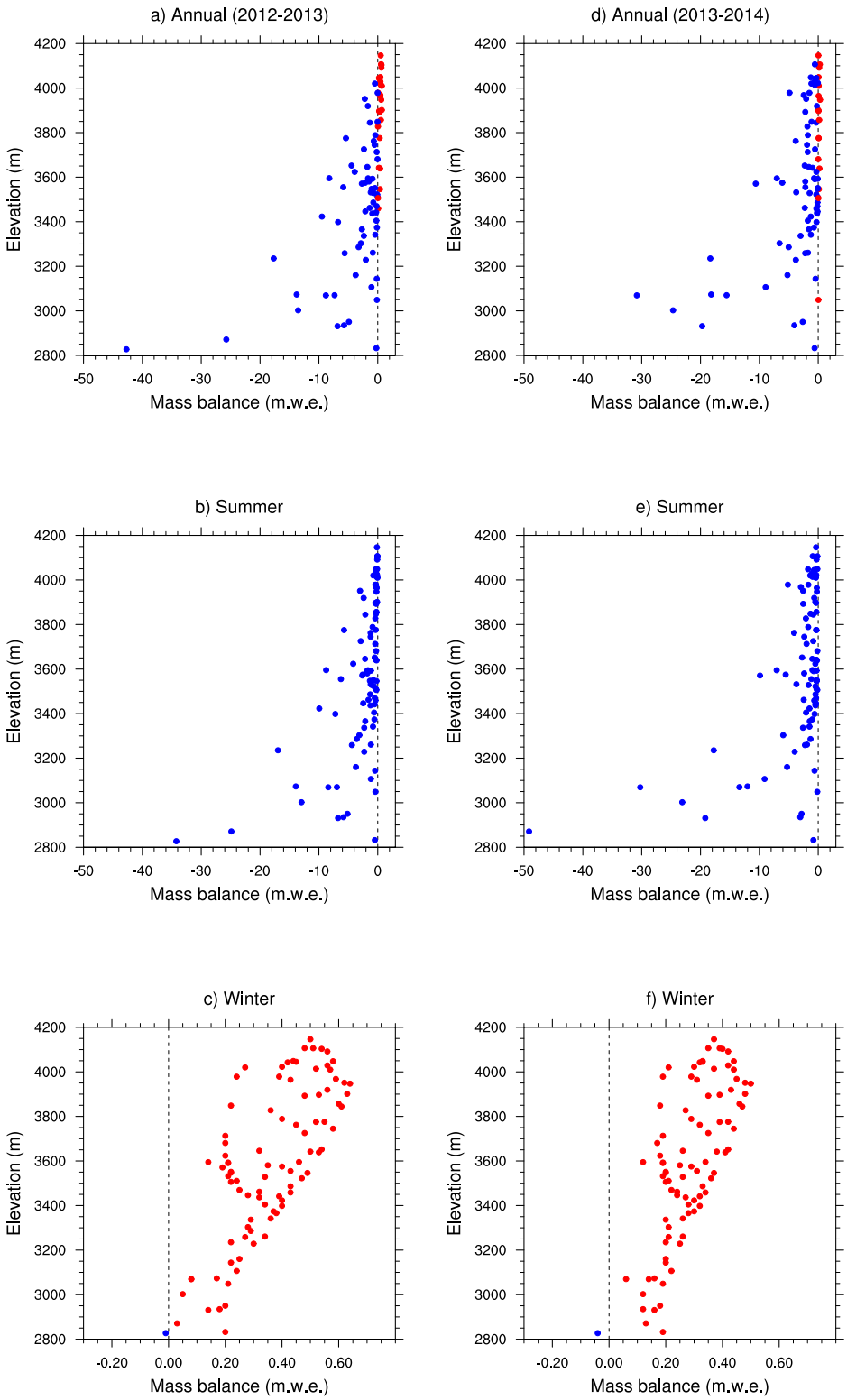

Figure 4.6: Surface mass balance distributed according to the elevation of each grid-cell, for (a,d) annual, (b,e) summer (DJFMA) and (c,f) winter (MJJAS) from the hydrological year 2012-2013 and 2013-2014.

Table 4.4: Mass balance and standard deviation for Universidad Glacier, where Bw for winter (MJJASO), Bs for summer (NDJFMA) and Ba for annual.

	Year	Bw (m w.e.)	Bs (m w.e.)	Ba (m w.e.)
SEB model	2012-2013	0.57 +- 0.07	-1.24 +- 0.16	-0.67 +- 0.13
Kinnard et al. (2018)		1.43 +- 0.06	-1.75 +- 0.38	-0.32 +- 0.40
SEB model	2013-2014	0.37 +- 0.09	-1.63 +- 0.17	-1.26 +- 0.14
Kinnard et al. (2018)		1.48 +- 0.15	-4.01 +- 0.56	-2.53 +- 0.57

Modeled mass balance and energy fluxes

Figure 4.7 shows the spatial distribution of the annual accumulation, ablation and specific mass balance over the Universidad Glacier, average between the hydrological years 1996/97 to 2015/16. Maximum accumulation values are distributed in the upper zone, mainly in the eastern basin, between 50 and 70 cm w.e. Very small accumulation values are confined on the glacier tongue associated with precipitation falling as rain. In contrast, ablation is highest on the glacier tongue, it reaches 1500 cm w.e. due to ice exposure during most of the ablation season, increasing its sensitivity to radiation fluxes. Hence, the mass balance values is in line with maximum and minimum exhibited by accumulation and ablation. On the eastern glacier, positive mass balance is dominating up to 39 cm e.w., whereas very negative values of -1500 cm w.e. are located on the lower glacier tongue. This mass changes indicates the typical pattern mass balance features.

The glacier-wide mass balance averaged over the entire Universidad glacier between 1996 to 2015 is negative (-82 cm w.e.yr^{-1}), which corresponds to a loss mass with a negative trend of -2.2 cm w.e.yr^{-1} (not significant at 95% level) (Table 4.5). Net

mass balance components show that melting largely predominates the ablation (84%) with a significant trend of 2.5 cm w.e.yr^{-1}. The proportion of ablation occurring by sublimation is about 10% while evaporation is a smaller component (6%), but shows significant trend over entire period (0.17 cm w.e.yr^{-1}). The accumulation has a small decrease, although not significant. Melt and accumulation are well correlated with mass balance (CC of 0.72 and 0.63, respectively) and melt is the main ablation drivers on the Universidad Glacier (Table 4.5).

The temporal variability of the glacier-wide annual mass balance and their components are shown in Figure 4.8a. High interannual variability of mass balance is remarkable, with almost all years spanning negative values. In general, the mass balance behavior coincides with melt change, and low accumulation agrees with high melt. Table 4.6 summarizes the annual and seasonal variability of the cumulative mass balance throughout each balance year. In general, during winter (April-September) the total accumulation is smaller than what is melting during summer (October-March), reproducing negative mass balance almost every year. However, Sagredo and Lowell (2012) showed that glacier in the dry Andes there is very low precipitation, mean about 0.3 m w.e.yr^{-1}.

One exception is noted in the hydrological year 1999/2000, with positive mass balance. In this year, the accumulation is higher than all components for ablation compared to other years. These years are recognized by strong La Niña years, which are associated with precipitation suppression in Central Chile. However, La Niña usually leads to air temperatures lower than normal (average) (Quintana, 2000). This is worth mentioning that in this particular year, net radiation and sensible heat flux was 74% and 65% lower than the average for entire period, respectively. Hence,

these conditions lead to decreased heat transfer to air, reducing the available melt anergy. Similar condition is shown by Schaefer et al. (2013) in the Northern Patagonia Icefield during 2000 year, associated with high accumulation feedback, where increased albedo and cloudiness reduces incoming radiation, taking longer to melt.

Mean annual and monthly energy fluxes are shown in Figure 4.8b,c. As expected, the incoming radiation largely dominates the energy input to the glacier in entire years, mean annual between 92 and 115 wm^{-2}, while sensible heat flux is smaller component, minimum is show during 1999/00 (13 wm^{-2}) and maximum in 2014/15 (25 wm^{-2}), with significant trend over the period (0.17 wm^{-2}, Table 4.5). Conversely, longwave radiation and latent heat flux presented similar magnitudes (negative) throughout the period. This leads to a reduction in the energy flux for melt. The widespread negative values associated with latent heat flux indicates that vapour pressure in air is lower than ice, thereby induces the evaporation or sublimation, as shown by Figure 4.8a, these terms occurred in all years, although they are the smallest energy loss terms.

In terms of energy fluxes in annual cycle, incoming shortwave radiation predominates the energy gains in summer season, in particular between November and March. Energy available for melt is in line with incoming shortwave radiation and net radiation, with maximum values during summer. During winter (May-October) radiation fluxes are reduced, associated with higher accumulation and albedo (Fig. 4.8c). It is interesting to note that warmer air temperature in summer reflects in the variability of sensible heat flux, while latent heat flux shows no seasonal variation, even during winter as humidity increases. In general, mass balance is well correlated with incoming shortwave and net radiation, energy melt and sensible heat flux over

the entire period, while the energy flux for melt shows good agreement with almost all energy fluxes, except to longwave radiation (Table 4.5).

Table 4.5: Summary of modeled mass balance components and energy fluxes averaged over Universidad Glacier for the period 1996-2015. SD is standard deviation of the remporal variability, Trend is the estimate of a linear trend by Sen Slope and the Mann-Kendall, and CC is coefficient correlation with mass balance (melt).

Variable	Unit	Mean	SD	Trend	CC
Mass Balance	(cm w.e.)	-81.50	18.62	-2.2	1
Snowfall	(cm w.e.)	49.92	6.7	-1.1	-0.63*
Melt	(cm w.e.)	113.7	13.57	2.55**	0.72*
Sublimation	(cm w.e.)	-12.97	0.57	0.02	0.17
Evaporation	(cm w.e.)	8.7	1.15	0.17*	-0.35
Incoming radiation	(wm^{-2})	109	7.27	0.34	-0.89* (0.81*)
Longwave radiation	(wm^{-2})	-66	2.46	0.07	0.32 (0.08)
Net radiation	(wm^{-2})	42.54	6.62	0.36	-0.76* (0.95*)
Sensible heat	(wm^{-2})	20.11	2.5	0.17*	-0.48* (0.55*)
Latent heat	(wm^{-2})	-75.28	4.76	0.16	-0.27 (0.65*)
Energy for Melt	(wm^{-2})	-12.66	11	0.54	-0.73* (1)

*Significant at the 95% level **Significant at the 90% level

Table 4.6: Modeleded cumulative total mass balance for Universidad Glacier. SD is standard deviation, CC is coeficient correlation between mass balance and altitude. ELA: equilibrium line altitude. AAR: accumulation area ratio.

Year	Parameter	Bw	Bs	Ba	ELA	AAR
			(m w.e.)		(m)	
1996-1997	B +- SD	0.15 +- 0.13	-1.56 +- 0.13	-1.41 +-0.13	3873	0.18
	CC	0.74	0.73	0.66		
1997-1998	B +- SD	0.41 +- 0.10	-0.44 +- 0.09	-0.02 +- 0.10	3763	0.69
	CC	0.8	0.88	0.85		
1998-1999	B +- SD	0.13 +- 0.10	-1.21 +- 0.10	-1.07 +- 0.10	3822	0.16
	CC	0.71	0.60	0.67		
1999-2000	B +- SD	0.88 +- 0.11	-0.16 +- 0.10	0.71 +- 0.11	3699	0.82
	CC	0.69	0.91	0.75		
2000-2001	B +- SD	0.56 +- 0.11	-1.02 +- 0.11	-0.46 +- 0.11	3787	0.58
	CC	0.71	0.81	0.79		
2001-2002	B +- SD	0.46 +- 0.12	-1.29 +- 0.13	-0.83 +- 0.12	3752	0.29
	CC	0.67	0.52	0.44		
2002-2003	B +- SD	0.68 +- 0.12	-1.24 +- 0.12	-0.56 +- 0.12	3817	0.44
	CC	0.72	0.73	0.74		
2003-2004	B +- SD	-0.09 +- 0.13	-1.25 +- 0.13	-1.34 +- 0.13	3851	0.29
	CC	0.74	0.72	0.69		
2004-2005	B +- SD	0.30 +- 0.12	-1.16 +- 0.12	-0.85 +- 0.12	3860	0.4
	CC	0.79	0.79	0.77		
2005-2006	B +- SD	0.57 +- 0.17	-1.63 +- 0.17	-1.06 +- 0.17	3840	0.44
	CC	0.69	0.82	0.75		
2006-2007	B +- SD	-0.01 +- 0.14	-0.93 +- 0.14	-0.95 +- 0.14	3836	0.49
	CC	0.72	0.82	0.81		
2007-2008	B +- SD	0.22 +- 0.08	-1.17 +- 0.09	-0.95 +- 0.09	3819	0.16
	CC	0.77	0.76	0.74		
2008-2009	B +- SD	0.28 +- 0.12	-1.64 +- 0.12	-1.36 +- 0.12	3808	0.07
	CC	0.72	0.80	0.79		
2009-2010	B +- SD	0.07 +- 0.09	-0.74 +- 0.10	-0.67 +- 0.10	3781	0.31
	CC	0.63	0.80	0.67		
2010-2011	B +- SD	0.04 +- 0.10	-1.26 +- 0.10	-1.22 +- 0.10	3833	0.13
	CC	0.71	0.70	0.68		
2011-2012	B +- SD	0.09 +- 0.11	-1.27 +- 0.11	-1.17 +- 0.11	3797	0.16
	CC	0.73	0.75	0.64		
2012-2013	B +- SD	0.44 +- 0.12	-0.92 +- 0.12	-0.48 +- 0.12	3795	0.42
	CC	0.81	0.81	0.71		
2013-2014	B +- SD	0.15 +- 0.14	-1.47 +- 0.14	-1.32 +- 0.14	3853	0.27
	CC	0.68	0.64	0.60		
2014-2015	B +- SD	0.21 +- 0.12	-1.45 +- 0.12	-1.24 +- 0.12	3797	0.31
	CC	0.67	0.78	0.72		
2015-2016	B +- SD	0.28 +- 0.05	-0.33 +- 0.05	-0.05 +- 0.05	3732	0.64
	CC	0.77	0.91	0.85		

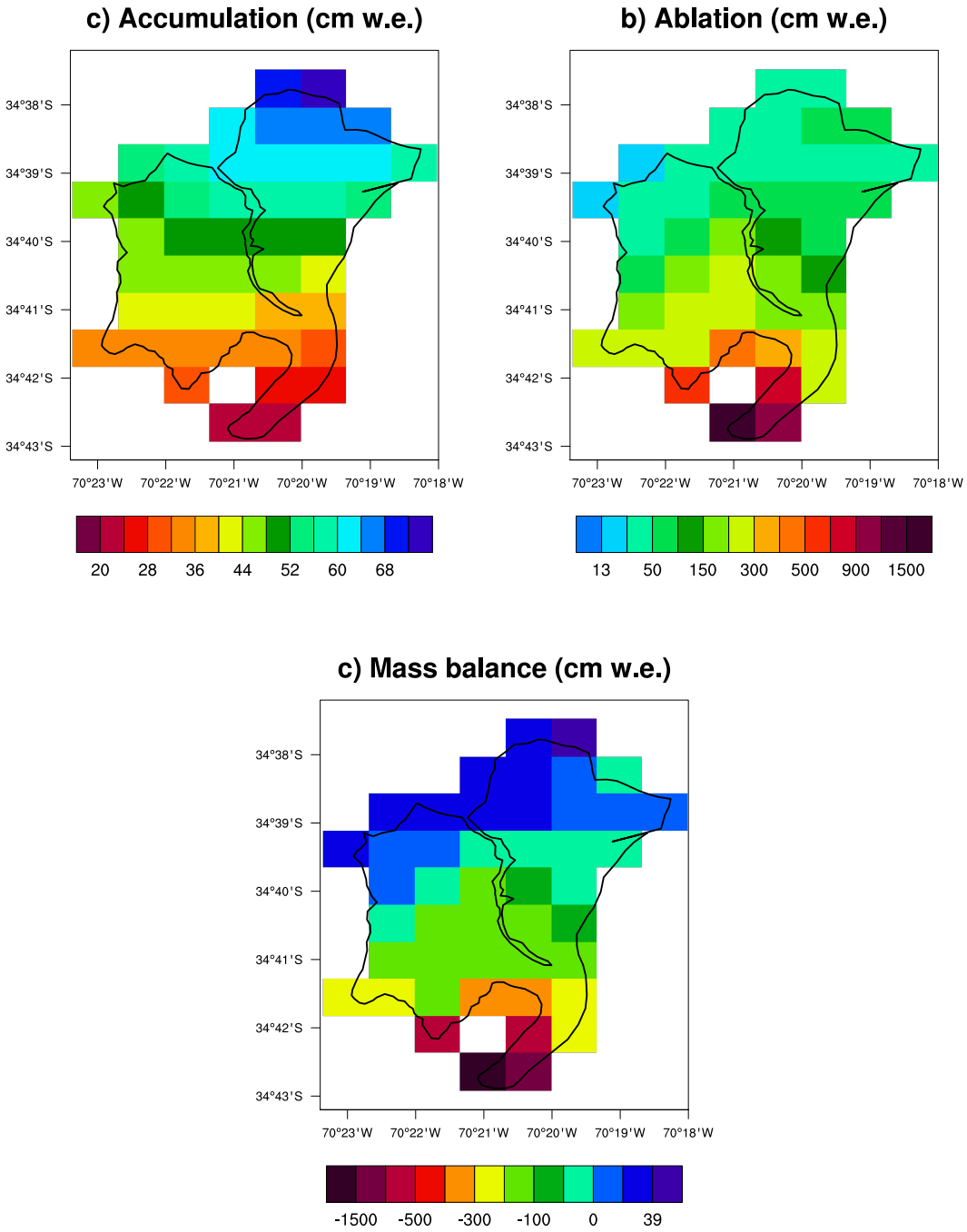

Figure 4.7: Spatial distribution of simulated a) accumulation, b) ablation and c) specific climatic mass balance, averaged for the period 1996-2015 in cm w.e. yr^{-1}.

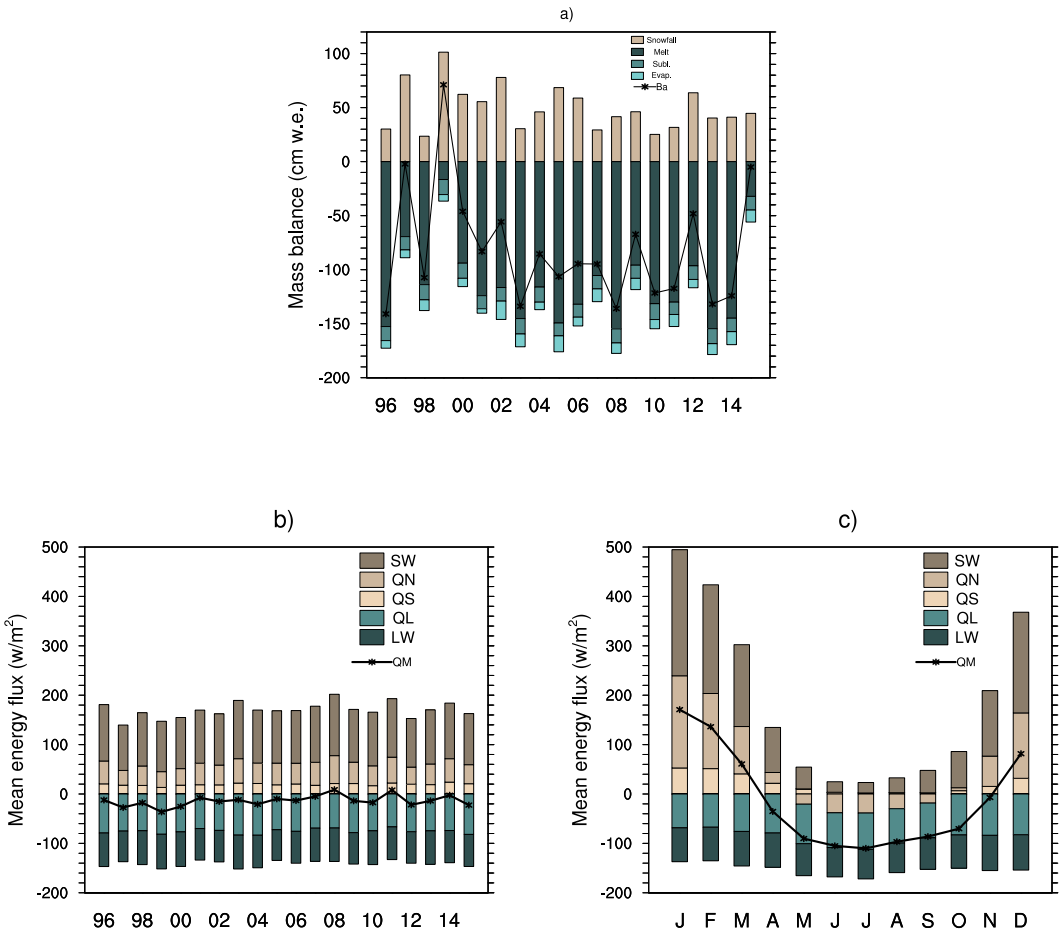

Figure 4.8: Time serie a) annual surface mass balance and its components, b) annual and c) monthly energy fluxes over Universidad Glacier for the period 1996 to 2015.

Elevation dependence and Equilibrium-line altitudes

Universidad Glacier is a typical valley glacier with strong relationship with altitude. In order to illustrate the mass changes gradient, Figure 4.9 shows the elevational distribution of specific mass balance, sublimation ratio and evaporation ratio averaged over entire period. Mass balance distribution shows higher variability and sparser grid-cells in lower elevations, located on the tongue glacier. The gradient decrease with altitude, which negative and positive mass balance occurs near the equilibrium-line altitude (ELA), about 3800 m (averaged over period). This mass bal-

ance behavior with altitude is associated with increased albedo in the accumulation zone in contrast to the ablation area. Simulated mass balance shows strong relationship with altitude, with correlation of 0.75 statistically significant and about 60% of the variance over period. Table 4.6 also shows strong elevation dependence of mass balance throughout glacier over each balance years, with correlations of 0.60 to 0.85 in annual estimates, 0.63 to 0.81 in winter and 0.52 to 0.91 in summer.

Typically, sublimation and evaporation requires about eight time more energy to occurs than melt, therefore, the ratio between sublimation and evaporation terms and melt plays an important driver to ablation process. The sublimation ratio shows a linear increase with altitude, with almost no influence of sublimation below 3000 m. Above this, most grid-cells account for up to 30% melt (65% of the grid-cells). The greatest contribution of sublimation occurs in the high glacier zone (above the ELA) where the surface temperature is below freezing and the air is drier than the ice almost all the time. On the other hand, evaporation ratio shows an elevational distribution with mostly grid-cells concentrated around 3600 m. Most grid-cells accounts for less than 15% of melt over period, about 75%. Sublimation ratio shows strong influence with altitude, with significant correlaion of 0.82, whereas evaporation ratio shows no relationship with altitude.

ELA represents the elevation on a glacier which defines the boundary between accumulation and ablation area, where accumulation of snow is balanced by ablation over the hydrological year, i.e. mass balance is null (Braithwaite and Raper, 2009). ELA is closely related to changes in temperature (ablation) and precipitation (accumulation) (Sagredo et al., 2014). This strong relationship drive the mass balance behavior at the ELA, where negative mass balance the ELA rise whereas positive mass

balance implies in the decrease ELA. Figure 4.10 shows the SEB model captures this variability between the ELA and mass balance. The accumulation-area ratio (AAR) is defined as the ratio between the accumulatin area and the total glacier area, allows to estimate the total accumulated area on the glacier each year. AAR is inversely proportional to ELA and well correlated with mass balance. AAR averaged for entire period corresponds to 36% of the surface of Universidad Glacier accumulated, with maximum in 1999/00 of 82% and minimum in 2008/09 (7%). Moreover, ELA, ARR and mass balance shows a similar trend, with a slight declining over period, although not statistically significant. Table 4.6 summarizes the ELA and ARR values for each hydrological year. Monthly ELA variability ranges from a minimum in June (2832 m) to a maximum in January (4146 m) on the Universidad Glacier averaged over entire period.

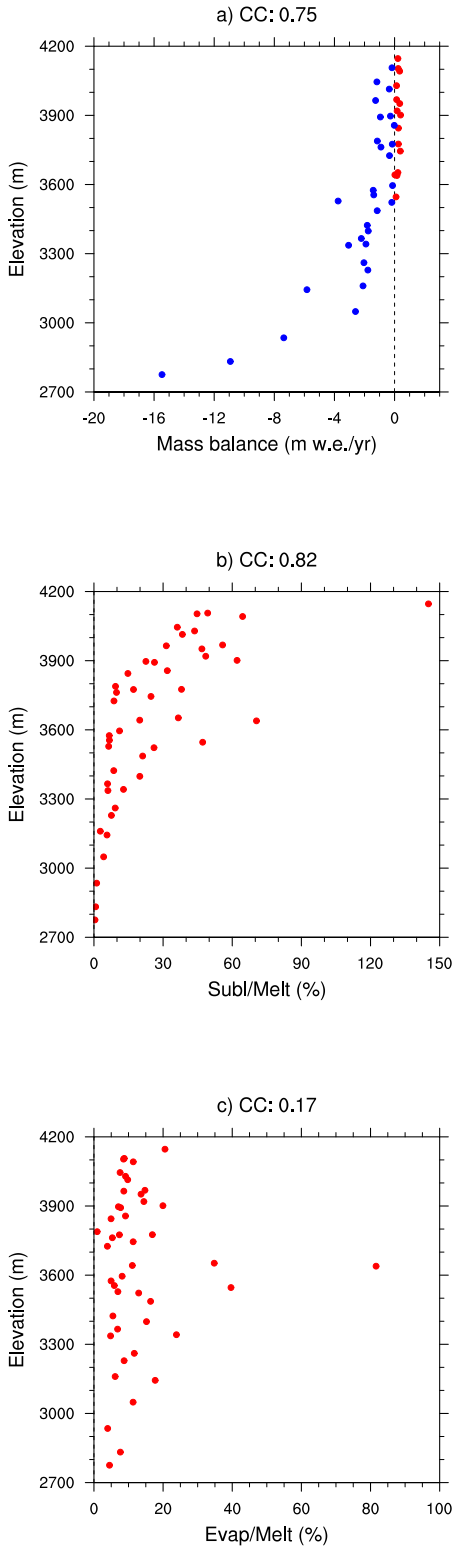

Figure 4.9: a)Surface mass balance, b)ratio of sublimation versus melt and c) ratio of evaporation versus melt distributed according to the elevation of each grid-cell. CC values refers to coeficient correlation.

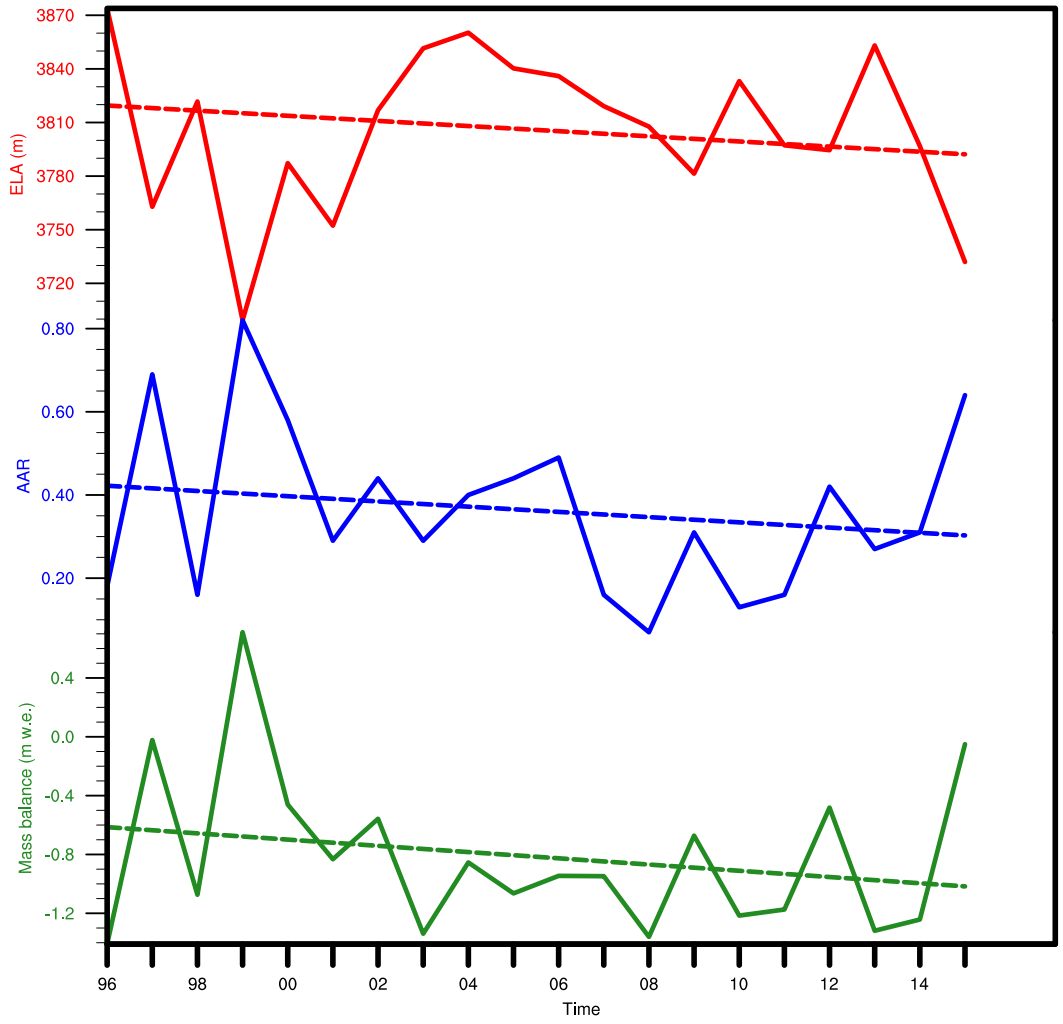

Figure 4.10: Temporal variation of the ELA, AAR and mass balance. Dashed line is the linear ELA trend of -1.44 m, AAR trend of -0.006 and mass balance trend of -0.02 m w.e.yr^{-1}. Trends not significant at 95% level.

Conclusion and Outlook

This study presents long-term modeled mass balance for Universidad Glacier in Central Chile for the period 1996 to 2015. We used a distributed mass balance model forced with high resolution from the ERA-Interim downscalling (1 km). The results of this study are innovative in terms of modelling glacier in this particular

region, contributing to filling the gap related to the investigation of changes in the Andean glaciers. The following conclusions are drawn.

The results indicated a mean cumulative glacier wide mass loss of -82 cm w.e.yr^{-1} over the period with a negative trend of -2.2 cm w.e.yr^{-1}, but it is not significant at 95% level. The interannual variability is controlled mainly by summer melt. The sublimation accounts about 10% of ablation while evaporation is a smaller component, corresponding to 6%. Overall there is a good agreeement with mass and energy fluxes presented by Kinnard et al. (2018) over Universidad Glacier.

In general, our mass balance simulations are in line with others studies in Central Chilean Andes. The long-term, modeled mass balance between 1955 and 2013 over the Echaurren Norte glacier was similar magnitude, with -63 cm w.e.yr^{-1} (Masiokas et al., 2016b), more recent study also showed a negative mass balance (-68 cm w.e.yr^{-1}) between 1955 and 2015 for this glacier in the Central Andes, calculated by differencing digitial elevation models (Farías-Barahona et al., 2019).

Several uncertainties are introduced along with this study by a combined effect from the climate forcing by ERA-interim, WRF parameterizations, smooth topographic, SEB simplifications, and uncertainties of the observations used for comparisons. These systematic shifts are common about glacier modeling and extremely hard to quantify the individual sources of errors (Østby et al., 2017; Machguth et al., 2009).

The main uncertainties are associated with WRF input from climate dynamical downscaling. We have noted that the effect of over predicting wind speed leads to impact of the latent and sensible heat fluxes and ablation process by calculating turbulent transfer coefficient. Moreover, WRF has a slight cold bias, which induces

to low net radiation as consequence to more negative longwave radiation. This effects associated with increase of latent flux should leading to less energy for melt at times.

It is important to emphasize that our results are mostly based on simulations, which comprises several uncertainties difficult to quantify overall. Hence, more observations are essential for better evaluation of the modeling studies for future improvements. Moreover, the simulations provides several nested domains, they will support further studies of water resources, climate and cryosphere in the larger area of the Central Andes of Chile and Argentina. Besides contributing with understand the role of the main climatic variables in the glaciers mass balance in present day and future conditions under global warming, providing a deeper understanding of climate-glacier feedback.

In the future study, the SEB model will be used for several purposes. The modeled turbulent heat fluxes should be improvement by wind speed correction. The analyzes will be expanded to the whole Sierra del Brujo, a glacierized massif containing at least 4 relatively large and important glaciers: Cipreses, Cortaderal, Palomo, and Universidad. The sensitivity of mass balance to climate changes will be assessed in more details, with additional simulation under global warming conditions, derived from the Community Earth System Model (CESM) spans the historical period (1986-2005) and for the projected simulation (2081-2100). Remote sensing should be used as a future tool for the model validation.

References

Arnold, N. S., Willis, I. C., Sharp, M. J., Richards, K. S., and Lawson, W. J. (1996). A distributed surface energy-balance tnodel for a small valley glacier . I . Developtnent

and testing for. *Journal of Glaciology*, 42(240):77–89.

Ayala, A., Pellicciotti, F., Peleg, N., and Burlando, P. (2017). Melt and surface sublimation across a glacier in a dry environment: Distributed energy-balance modelling of Juncal Norte Glacier, Chile. *Journal of Glaciology*, 63(241):803–822.

Barcaza, G., Nussbaumer, S. U., Tapia, G., Valdés, J., García, J. L., Videla, Y., Albornoz, A., and Arias, V. (2017). Glacier inventory and recent glacier variations in the Andes of Chile, South America. *Annals of Glaciology*, 58(75):166–180.

Basantes-Serrano, R., Rabatel, A., Francou, B., Vincent, C., Maisincho, L., Cáceres, B., Galarraga, R., and Alvarez, D. (2016). Slight mass loss revealed by reanalyzing glacier mass-balance observations on Glaciar Antisana 15α (inner tropics) during the 1995–2012 period. *Journal of Glaciology*, 62(231):124–136.

Benn, D. and Evans, D. J. (2014). *Glaciers and Glaciation*, volume 36. Routledge.

Bown, F., Rivera, A., and Acuña, C. (2008). Recent glacier variations at the Aconcagua basin, central Chilean Andes. *Annals of Glaciology*, 48:43–48.

Bradley, R. S. (2006). CLIMATE CHANGE: Threats to Water Supplies in the Tropical Andes. *Science*, 312(5781):1755–1756.

Braithwaite, R. J. and Raper, S. C. (2009). Estimating equilibrium-line altitude (ELA) from glacier inventory data. *Annals of Glaciology*, 50(53):127–132.

Braun, C. and Bezada, M. (2013). The History and Disappearance of Glaciers in Venezuela. *Journal of Latin American Geography*, 12(2):85–124.

Braun, M. H., Malz, P., Sommer, C., Farías-Barahona, D., Sauter, T., Casassa, G.,

Soruco, A., Skvarca, P., and Seehaus, T. C. (2019). Constraining glacier elevation and mass changes in South America. *Nature Climate Change*, 9(2):130–136.

Bravo, C., Loriaux, T., Rivera, A., and Brock, B. W. (2016). Assessing glacier contribution to river runoff in the Andes of central Chile: Analysis of in situ weather station data, runoff measurements and melt modelling at Universidad glacier (34°40' S, 70°20' W. *Hydrology and Earth System Sciences Discussions*, (October):1–32.

Brock, B., Willis, I. C., and Sharp, M. J. (2000). Measurement and parameterization of albedo variations at Haut Glacier d'Arolla, Switzerland. *Journal of Glaciology*, 46(155):675–688.

Carrasco, J. F., Casassa, G., and Quintana, J. (2005). Changes of the 0°C isotherm and the equilibrium line altitude in central Chile during the last quarter of the 20th century / Changements de l'isotherme 0°C et de la ligne d'équilibre des neiges dans le Chili central durant le dernier quart du 20ème siècle. *Hydrological Sciences Journal*, 50(6).

Collier, E., Mölg, T., Maussion, F., Scherer, D., Mayer, C., and Bush, A. B. G. (2013). High-resolution interactive modelling of the mountain glacier-atmosphere interface: An application over the Karakoram. *Cryosphere*, 7(3):779–795.

Comin, A. N., Schumacher, V., Justino, F., and Fernández, A. (2018). Impact of different microphysical parameterizations on extreme snowfall events in the Southern Andes. *Weather and Climate Extremes*, 21(June):65–75.

Cuffey, K. M. and Paterson, W. S. B. (2010). *The Physics of Glaciers*, volume 14. Academic Press, 4 edition.

Dee, D. P., Uppala, S. M., Simmons, a. J., Berrisford, P., Poli, P., Kobayashi, S., Andrae, U., Balmaseda, M. a., Balsamo, G., Bauer, P., Bechtold, P., Beljaars, a. C. M., van de Berg, L., Bidlot, J., Bormann, N., Delsol, C., Dragani, R., Fuentes, M., Geer, a. J., Haimberger, L., Healy, S. B., Hersbach, H., Hólm, E. V., Isaksen, L., Kållberg, P., Köhler, M., Matricardi, M., Mcnally, a. P., Monge-Sanz, B. M., Morcrette, J. J., Park, B. K., Peubey, C., de Rosnay, P., Tavolato, C., Thépaut, J. N., and Vitart, F. (2011). The ERA-Interim reanalysis: Configuration and performance of the data assimilation system. *Quarterly Journal of the Royal Meteorological Society*, 137(April):553–597.

DeWalle, D. R. and Rango, A. (2008). *Principles of snow hydrology*, volume 9780521823. Cambridge University Press.

Dudhia, J. (2013). Overview of WRF physics. *WRF Workshop 2013*, pages 1–207.

Farías-Barahona, D., Vivero, S., Casassa, G., Schaefer, M., Burger, F., Seehaus, T., Iribarren-Anacona, P., Escobar, F., and Braun, M. (2019). Geodetic Mass Balances and Area Changes of Echaurren Norte Glacier (Central Andes, Chile) between 1955 and 2015. *Remote Sensing*, 11(3):260.

Fernández, A. and Mark, B. G. (2016). Modeling modern glacier response to climate changes along the Andes Cordillera: A multiscale review. *Journal of Advances in Modeling Earth Systems*, 8:467–495.

Fernández, A. R. A. (2014). Waning and Waxing of Mountain Glaciers in South America: A Modeling Approach over Multiple Spatial and Temporal Scales. *The Ohio State University Dissertation*, 53(9):1–363.

Francou, B. (2003). Tropical climate change recorded by a glacier in the central Andes

during the last decades of the twentieth century: Chacaltaya, Bolivia, 16°S. *Journal of Geophysical Research*, 108(D5):1–12.

Garreaud, R. D. (2009). The Andes climate and weather. *Advances in Geosciences*, 22:3–11.

Hock, R. (2005). Glacier melt: a review of processes and their modelling. *Progress in Physical Geography*, 29(3):362–391.

Hong, S. and Lim, J. (2006). The WRF single-moment 6-class microphysics scheme (WSM6).

Hong, S.-Y., Lim, K.-S. S., Lee, Y.-H., Ha, J.-C., Kim, H.-W., Ham, S.-J., and Dudhia, J. (2010). Evaluation of the WRF Double-Moment 6-Class Microphysics Scheme for Precipitating Convection. *Advances in Meteorology*, 2010:1–10.

Janke, J. R., Bellisario, A. C., and Ferrando, F. A. (2015). Classification of debris-covered glaciers and rock glaciers in the Andes of central Chile. *Geomorphology*, 241:98–121.

Kain, J. S. (2004). The Kain–Fritsch Convective Parameterization: An Update. *Journal of Applied Meteorology*, 43:170–181.

Kaser, G., Großhauser, M., Marzeion, B., and Barry, R. G. (2010). Contribution potential of glaciers to water availability in different climate regimes. *Proceedings of the National Academy of Sciences of the United States of America*, 107(47):21300–21305.

Kinnard, C., Macdonell, S., Petlicki, M., Martinez, M., Abermann, J., and Urrutia, R. (2018). *Mass Balance and Meteorological Conditions at Universidad Glacier, Central Chile*. CRC Press.

Le Quesne, C., Acuña, C., Boninsegna, J. A., Rivera, A., and Barichivich, J. (2009). Long-term glacier variations in the Central Andes of Argentina and Chile, inferred from historical records and tree-ring reconstructed precipitation. *Palaeogeography, Palaeoclimatology, Palaeoecology*, 281(3-4):334–344.

López-Moreno, J. I., Valero-Garcés, B., Mark, B., Condom, T., Revuelto, J., Azorín-Molina, C., Bazo, J., Frugone, M., Vicente-Serrano, S. M., and Alejo-Cochachin, J. (2016). Hydrological and depositional processes associated with recent glacier recession in Yanamarey catchment, Cordillera Blanca (Peru). *Science of the Total Environment*, 579:272–282.

Machguth, H., Paul, F., Kotlarski, S., and Hoelzle, M. (2009). Calculating distributed glacier mass balance for the Swiss Alps from regional climate model output: A methodical description and interpretation of the results. *Journal of Geophysical Research Atmospheres*, 114(19):1–19.

Manz, B., Buytaert, W., Zulkafli, Z., Lavado, W., Willems, B., Robles, L. A., and Rodríguez-Sánchez, J. P. (2016). High-resolution satellite-gauge merged precipitation climatologies of the Tropical Andes. *Journal of Geophysical Research: Atmospheres*, 121(3):1190–1207.

Mark, B. G., Baraer, M., Fernandez, A., Immerzeel, W., Moore, R. D., and Weingartner, R. (2015). Glaciers as water resources. In Huggel, C., Carey, M., Clague, J. J., and Kaab, A., editors, *The High-Mountain Cryosphere: Environmental Changes and Human Risks*, pages 184–203. Cambridge University Press, Cambridge.

Mark, B. G. and Fernández, A. (2017). The significance of mountain glaciers as sentinels of climate and environmental change. *Geography Compass*, 11(6):1–16.

Marzeion, B., Jarosch, A. H., and Gregory, J. M. (2014). Feedbacks and mechanisms affecting the global sensitivity of glaciers to climate change. *Cryosphere*, 8(1):59–71.

Masiokas, M. H., Christie, D. A., Le Quesne, C., Pitte, P., Ruiz, L., Villalba, R., Luckman, B. H., Berthier, E., Nussbaumer, S. U., González-Reyes, Á., McPhee, J., and Barcaza, G. (2016a). Reconstructing the annual mass balance of the Echaurren Norte glacier (Central Andes, 33.5° S) using local and regional hydroclimatic data. *The Cryosphere*, 10(2):927–940.

Masiokas, M. H., Christie, D. A., Le Quesne, C., Pitte, P., Ruiz, L., Villalba, R., Luckman, B. H., Berthier, E., Nussbaumer, S. U., González-Reyes, Á., McPhee, J., and Barcaza, G. (2016b). Reconstructing the annual mass balance of the Echaurren Norte glacier (Central Andes, 33.5° S) using local and regional hydroclimatic data. *The Cryosphere*, 10(2):927–940.

Masiokas, M. H., Villalba, R., Christie, D. a., Betman, E., Luckman, B. H., Le Quesne, C., Prieto, M. R., and Mauget, S. (2012). Snowpack variations since AD 1150 in the Andes of Chile and Argentina (30°-37°S) inferred from rainfall, tree-ring and documentary records. *Journal of Geophysical Research: Atmospheres*, 117:1–11.

Mernild, S. H., Liston, G. E., Hiemstra, C. A., Yde, J. C., Mcphee, J., and Malmros, J. K. (2016). The Andes Cordillera. Part II: Rio Olivares Basin snow conditions (1979-2014), central Chile. *International Journal of Climatology*.

Mlawer, E. J., Taubman, J., Brown, P. D., Iacono, M. J., and Clough, S. A. (1997). Radiative transfer for inhomogeneous atmospheres: RRTM, a validated correlatedk model for the longwave. *Journal of Geophysical Research*, 102:16663–16682.

Mög, T. and Kaser, G. (2011). A new approach to resolving climate-cryosphere relations: Downscaling climate dynamics to glacier-scale mass and energy balance without statistical scale linking. *Journal of Geophysical Research Atmospheres*, 116(16):1–13.

Montecinos, A. and Aceituno, P. (2003). Seasonality of the ENSO-related rainfall variability in central Chile and associated circulation anomalies. *Journal of Climate*, 16(2):281–296.

Oke, T. R. (2002). *Boundary Layer Climates.*, volume 17. Routledge, 2 edition.

Østby, T. I., Vikhamar Schuler, T., Ove Hagen, J., Hock, R., Kohler, J., and Reijmer, C. H. (2017). Diagnosing the decline in climatic mass balance of glaciers in Svalbard over 1957-2014. *Cryosphere*, 11(1):191–215.

Paul, F., Machguth, H., Hoelzle, M., Salzmann, N., and Haeberli, W. (2008). Alpinewide distributed glacier mass balance modeling: a tool for assessing future glacier change? *In: Orlove, B [et al.]. Darkening Peaks: Glacier Retreat, Science, and Society*, Berkeley,:111–125.

Paulson, C. A. (1970). The Mathematical Representation of Wind Speed and Temperature Profiles in the Unstable Atmospheric Surface Layer. *Journal of Applied Meteorology*, 9:857–861.

Pedersen, V. K. and Egholm, D. L. (2013). Glaciations in response to climate variations preconditioned by evolving topography. *Nature*, 493(7431):206–10.

Pellicciotti, F., Ragettli, S., Carenzo, M., and McPhee, J. (2014). Changes of glaciers in

the Andes of Chile and priorities for future work. *The Science of the total environment*, 493C:1197–1210.

Plummer, M. A. and Phillips, F. M. (2003). A 2-D numerical model of snow/ice energy balance and ice flow for paleoclimatic interpretation of glacial geomorphic features. *Quaternary Science Reviews*, 22(14):1389–1406.

Quintana, J. (2000). The drought in Chile and la Niña. *Drought Network News*, (12):3–6.

Rabatel, A., Francou, B., Soruco, A., Gomez, J., Caceres, B., Ceballos, J., Basantes, R., Vuille, M., Sicart, J.-E., Huggel, C., Scheel, M., Lejeune, Y., Arnaud, Y., Collet, M., Condom, T., Consoli, G., Favier, V., Jomelli, V., Galarraga, R., Ginot, P., Maisincho, L., Mendoza, J., Menegoz, M., Ramirez, E., Ribstein, P., Suarez15, W., Villacis, M., and Wagnon, P. (2013). Current state of glaciers in the tropical Andes: a multi-century perspective on glacierevolution and climate change. *The Cryosphere*, 7(1):81–102.

Ragettli, S. and Pellicciotti, F. (2012). Calibration of a physically based, spatially distributed hydrological model in a glacierized basin: On the use of knowledge from glaciometeorological processes to constrain model parameters. *Water Resources Research*, 48(3):W03509.

Rivera, A., Acuña, C., Casassa, G., and Bown, F. (2002). Use of remote sensing and field data to estimate the contribution of Chilean glaciers to the sea level rise. *Annals of Glaciology*, 34:367–372.

Rupper, S. and Roe, G. (2008). Glacier changes and regional climate: A mass and energy balance approach. *Journal of Climate*, 21(20):5384–5401.

Sagredo, E. A. and Lowell, T. V. (2012). Climatology of Andean glaciers: A framework to understand glacier response to climate change. *Global and Planetary Change*, 86-87(August):101–109.

Sagredo, E. A., Rupper, S., and Lowell, T. V. (2014). Sensitivities of the equilibrium line altitude to temperature and precipitation changes along the Andes. *Quaternary Research (United States)*, 81(2):355–366.

Schaefer, M., Machguth, H., Falvey, M., and Casassa, G. (2013). Modeling past and future surface mass balance of the Northern Patagonia Icefield. *Journal of Geophysical Research: Earth Surface*, 118(2):571–588.

Schauwecker, S., Rohrer, M., Acuña, D., Cochachin, A., Dávila, L., Frey, H., Giráldez, C., Gómez, J., Huggel, C., Jacques-Coper, M., Loarte, E., Salzmann, N., and Vuille, M. (2014). Climate trends and glacier retreat in the Cordillera Blanca, Peru, revisited. *Global and Planetary Change*, 119:85–97.

Silva, V. B. S., Kousky, V. E., and Higgins, R. W. (2011). Daily Precipitation Statistics for South America: An Intercomparison between NCEP Reanalyses and Observations. *Journal of Hydrometeorology*, 12(1):101–117.

Skamarock, W. C., Klemp, J. B., Dudhia, J., Gill, D. O., Barker, D. M., Duda, M. G., Huang, X.-Y., Wang, W., and Powers, J. G. (2008). A Description of the Advanced Research WRF Version 3. *NCAR Tech. Note NCAR TN- 475_STR*, page 113.

Taylor, K. E. (2001). Summarizing multiple aspects of model performance in a single diagram. *Journal of Geophysical Research*, 106(D7):7183.

Valdés-Pineda, R., Pizarro, R., García-Chevesich, P., Valdés, J. B., Olivares, C., Vera,

M., Balocchi, F., Pérez, F., Vallejos, C., Fuentes, R., Abarza, A., and Helwig, B. (2014). Water governance in Chile: Availability, management and climate change. *Journal of Hydrology*, 519(PC):2538–2567.

Veettil, B. K., Wang, S., Florêncio de Souza, S., Bremer, U. F., and Simões, J. C. (2017). Glacier monitoring and glacier-climate interactions in the tropical Andes: A review. *Journal of South American Earth Sciences*, 77:218–246.

Vergara, W., Deeb, A. M., Valencia, A. M., Bradley, R. S., Francou, B., Zarzar, A., Grünwaldt, A., and Haeussling, S. M. (2007). Economic impacts of rapid glacier retreat in the Andes. *Eos*, 88(25):2–4.

Viale, M. and Garreaud, R. (2015). Orographic effects of the subtropical and extra-tropical Andes on upwind precipitating clouds. *Journal of Geophysical Research : Atmospheres*, 120:4962–4974.